

How unstable was the environment during the Penultimate Glacial in the South-Western Mediterranean? Vegetation, climate and human dynamics during MIS 6.

Liz Charton^{1,2}, Nathalie Combourieu-Nebout¹, Adele Bertini², Odile Peyron³, Mary Robles³, Vincent Lebreton¹, Marie-Hélène Moncel,¹.

1 : UMR 7194 HNHP- « Histoire Naturelle des Humanités Préhistoriques », MNHN / CNRS / UPVD, Paris, France.
liz.charton@mnhn.fr

2 : Dipartimento di Scienze della Terra, Università degli Studi di Firenze, Florence, Italy.

3: UMR 5554, ISEM-Institut des Sciences de l'Evolution de Montpellier, CNRS, Université de Montpellier, Montpellier, France.

Correspondance : Liz charton (liz.charton@mnhn.fr)

Abstract

The impact of rapid climate variability on Neanderthal population in Europe during the Last Glacial (Marine Isotope Stages 4-2), including Dansgaard-Oeschger cycles and Heinrich stadials, has been the subject of a long-standing debate. However, few studies have focused on the nature and impact of such rapid variations on human population during earlier periods. A growing number of high-resolution paleoclimatic archives supports the persistence of rapid oscillations during the penultimate glaciation (Marine Isotope Stage - MIS 6), and the close response of Mediterranean ecosystems to these. Still, few palynological sequences in the Mediterranean region offer sufficient resolution to document vegetation dynamics during this time. Pollen records are especially lacking in the western Mediterranean, a key region to understand the connection between North Atlantic and Mediterranean climatic influences. This region is also traditionally considered a climatic refugium for human population during unfavourable periods. We provide new palynological data covering MIS 6 from the long and continuous marine record of the ODP site 976 in the Alboran Sea. A total of 200 samples, spanning the interval from 196 to 127 ka Before Present (BP), reveals both long-term trends and rapid fluctuations in the regional vegetation composition. A multi-method approach, including modern analogues, regression, and machine learning approaches, was applied to the ODP 976 pollen assemblages to reconstruct the annual/seasonal temperatures and precipitation. Results show that three phases can be identified. The first phase (187-166 ka BP) is characterized by significant oscillations of temperate trees and rather cool and humid conditions during early MIS 6, coincident with a sapropel layer deposition in both the western and eastern Mediterranean. In the second phase (165-144 ka BP), arid herbaceous vegetation is dominant, marking the main imprint of glacial maxima

34 conditions and reduced climate variability. The third phase (144-129 ka BP) is marked by the
35 development of Ericaceae and increased annual precipitation. At the end of MIS 6 glaciation, an
36 episode of strong cooling and steppe and semi-desert expansion is identified as Heinrich Stadial 11
37 (135-129 ka BP), marking a distinct pattern for Termination II in the Western Mediterranean. Rapid
38 oscillations appear like a pervasive feature of the Penultimate glacial in the SW Mediterranean, though
39 they present reduced amplitude and frequency compared to the Last Glacial. A synthesis of human
40 occupation during MIS 6 shows that a mosaic of traditional (Mode 2) and innovative (Mode 3) lithic
41 technological features is observed in the archaeological record. Although the data are scarce,
42 Neanderthals seem to have continuously inhabited Western Mediterranean regions across the
43 penultimate glacial. The severe climate conditions during Heinrich Stadial 11 (~133-129 ka BP) might
44 have played a role in the apparent population contraction at the end of MIS 6, and perhaps also in the
45 definitive abandonment of Lower Palaeolithic industries.

46 1. Introduction

47 Rapid climate oscillations occurred during the last Glacial period (MIS 4-2). Dansgaard-
48 Oeschger (DO) cycles have been well identified in ice-core records (Bond et al., 1999; Dansgaard et al.,
49 1993; Johnsen et al., 1992; Rasmussen et al., 2014) and recognized in Atlantic sedimentary cores (e.g.
50 Bond et al., 1993, 1997; Roucoux et al., 2005; Sánchez Goñi et al., 2002; Shackleton et al., 2000,
51 Zumaque et al., 2025). Short periods of intense cold named Heinrich Stadials (HS) and linked with
52 intense iceberg discharges were also evidenced in Atlantic sediments (Bond et al., 1992; Heinrich,
53 1988; Hemming, 2004; Rasmussen et al., 2003; Ruddiman, 1977; Shackleton et al., 2004). Major cooling
54 events also occurred during MIS 5 and the penultimate deglaciation (e.g. Chapman & Shackleton, 1999;
55 Oppo et al., 2001). These high-frequency oscillations reflect major changes at global scale in the
56 oceanic circulation and the Atlantic Meridional Overturning Circulation (AMOC), that are important
57 features particularly during glacial terminations (Barker and Knorr, 2021). The Mediterranean region
58 has been very sensitive to the rapid climate oscillations of MIS 5 to MIS 1, with changes recorded in
59 both marine and continental environments (Cacho et al., 1999, 2006; Combourieu-Nebout et al., 2002,
60 2009; Fletcher et al., 2010; Martrat et al., 2007; Penaud et al., 2016; Sánchez Goñi et al., 2002, 2022).

61 The penultimate glacial (MIS 6) took place between ~185 and 130 ka BP and presented a
62 different ice-sheet and global climate configuration compared to the last glacial (MIS 4-2). It is
63 considered among the coldest glacial periods of the past 800 ka BP (Masson-Delmotte et al., 2010),
64 characterized by larger European Ice-Sheet and smaller Laurentide ice-sheet extension (Colleoni et al.,
65 2016; Ehlers et al., 2018; Ehlers & Gibbard, 2007; Rohling et al., 2017). In Europe, it corresponds to the
66 Riss glaciation in the Alpine area, and to the late Saalian glaciation complex in northern and central

67 Europe, with two major ice-sheet advances identified in Germany: the Drenthe advance (~170-155 ka
68 BP) characterized by the maximum ice extent in Europe, and the less extensive Warthe advance during
69 the younger stage of MIS 6 (Ehlers et al., 2011). The exact chronology of the Penultimate Glacial
70 Maximum (i.e. the maximum extension of the northern hemisphere ice-sheet) is still not well
71 constrained (Svendsen et al., 2004), but is usually considered around 140 ka BP (Colleoni et al., 2016).
72 Five marine isotopic substages were identified from MIS 6e to 6a, reflecting variations of global sea
73 temperatures : three cold substages (6e : ~180 ka BP, 6c : ~160 ka BP, 6a : ~136 ka BP) with increasing
74 cold intensity, and two warm substages (6d : ~170 ka BP and 6b : ~149 ka BP) (Railsback et al., 2015).
75 Different speleothem records revealed that MIS 6 glaciation in Europe, including the Mediterranean
76 region, was characterized by wetter conditions in comparison with the last glacial (Ayalon et al., 2002;
77 Koltai et al., 2017; Nehme et al., 2018; Regattieri et al., 2014). Furthermore, various studies highlighted
78 the apparent higher stability of the Laurentide ice-sheets during the penultimate glacial, leading to the
79 absence of typical “Heinrich layers” in the North Atlantic sediments, with the exception of the large
80 event recorded at the MIS 6 to MIS 5 transition, HS11 (~135-129 ka BP) (de Abreu et al., 2003;
81 McCarron et al., 2021; McManus et al., 1999; Obrochta et al., 2014; Ovsepyan and Murdmaa, 2017;
82 Shackleton et al., 2003).

83 Human Palaeolithic groups in Europe were likely affected by rapid climate changes
84 (Bradtmöller et al., 2012; Dennell et al., 2011; Raia et al., 2020; Willis et al., 2004). The South-Western
85 Mediterranean probably played a major role as one of the climate refugia areas around the
86 Mediterranean Basin during the most unfavourable climatic periods, permitting the persistence of
87 “source” population able to recolonize the northernmost areas during more favourable periods (Bailey
88 et al., 2008; Bicho & Carvalho, 2022). Neanderthal presence in very distinct ecotones in Eurasia proves
89 they could adapt to a very wide range of environments. However, recent niche modelling approaches
90 together with palaeoecological data from archaeological sites strengthened the view that warm
91 forested landscapes like the MIS 5e environments represented the most suitable habitats for
92 Neanderthals, where they could persist during colder periods (Carrión et al., 2026; Ochando et al.,
93 2019; Stewart et al., 2019; Trájer, 2023). This conception leads to the overlap of the notions of
94 refugium for vegetation and human populations, despite the greatest adaptability and niche extension
95 of humans. Many studies focused on the potential impact of abrupt environmental changes on
96 Neanderthal populations, especially those associated with Heinrich Stadials during MIS 3 (e.g. Charton
97 et al., 2025; D’Errico & Sánchez Goñi, 2003; Finlayson & Carrión, 2007; Melchionna et al., 2018). During
98 the previous climatic cycles of the Middle Pleistocene, when Early to Middle Palaeolithic cultures
99 developed, repeated climate instability has been brought forward as an explanation for the large
100 variability in the lithic production (Dennell et al., 2011; Foerster et al., 2022; Sánchez-Yustos and Diez-

101 Martín, 2015), and the non-linearity of Neanderthal biological evolution (Bermúdez de Castro &
102 Martín-Torres, 2013; Hublin, 2009). Still, the short and long-term resilience of human populations
103 in a globally unstable environment is poorly understood, and partially hindered by our limited
104 knowledge of fast millennial-scale climate oscillations in older glaciations prior to MIS 4-2.

105 While the Greenland ice does not provide an adequate record for periods older than 123 ka BP
106 (Chappellaz et al., 1997), the description of a precise stratigraphy of climatic events at sub millennial
107 scale for the previous glacial/interglacial cycles remains complex, and relies on the Antarctic isotope
108 record (Bazin et al., 2013; Jouzel et al., 2007), the study of marine sediments (de Abreu et al., 2003;
109 Lisiecki & Raymo, 2005; Margari et al., 2010, 2014; McManus et al., 1999; Obrochta et al., 2014) and
110 high-resolution continental archives such as speleothems (Burns et al., 2019; Held et al., 2024; Hodge
111 et al., 2008; Wainer et al., 2013; Wang et al., 2018; Wang et al., 2001). Benthic and planktonic isotopic
112 ratios together with Sea Surface Temperatures (SSTs) reconstructions in the North Atlantic and the
113 Western Mediterranean showcased the persistence of millennial-scale events and interhemispheric
114 bipolar see-saw heat transport during MIS 6, in addition to important reorganization of the water
115 circulation during sapropel S6 deposition ~175 ka BP (Margari et al., 2010, 2014; Martrat et al., 2004,
116 2007, 2014; Rousseau et al., 2020; Siirro & Andersen, 2022). Nevertheless, MIS 6 is much less well
117 documented than the last glacial in Mediterranean Europe. Few palynological sequences are available
118 to document the vegetation changes across this interval (Camuera et al., 2019, 2022; Follieri et al.,
119 1988; Margari et al., 2010; Okuda et al., 2001; Roucoux et al., 2011; Sadori et al., 2016; Sinopoli et al.,
120 2019; Tzedakis et al., 2006; Wilson et al., 2021). Among them, only one in SW Europe provides
121 sufficient resolution to document high-frequency changes (Margari et al., 2010, 2014). This record
122 from the deep-sea core MD01-2444 showed that several millennial-scale climatic events impacted the
123 vegetation during the lower part of MIS 6 (Margari et al., 2010). The core is located out of the
124 Mediterranean Sea, along the Portuguese margin in the Atlantic Ocean. Therefore, questions remain
125 open concerning the impact of such rapid events on the Western Mediterranean region, considered a
126 Pleistocene refugium for human populations.

127 To fill this gap, our study provides high-resolution pollen data and quantitative climate
128 reconstructions from ODP site 976 in south-western Mediterranean focusing on MIS 6. We aim to (i)
129 reconstruct the vegetation and climate changes in the SW Mediterranean during the penultimate
130 glacial, (ii) identify millennial-scale climatic changes and correlate them with other Atlantic and
131 Mediterranean paleoenvironmental records, (iii) compare the nature of millennial-scale climate and
132 vegetation dynamics during the last glacial period and the penultimate glacial using a single,
133 continuous pollen record and (iv) explore the potential impact of these climatic changes for Early

134 Middle Palaeolithic human groups, with particular attention to the presence of climate refugia during
135 the most extreme glacial phases.

136 2. Study site

137 Ocean Drilling Program (ODP) Site 976 (36°12 N, 4°18W, 1108 m depth) core was retrieved in
138 1995 in the Alboran Sea (Zahn et al., 1999). The site is located about 110 km east of the Gibraltar Strait,
139 70 km south of the Spanish coast, and 100 km north of Morocco (Fig. 1).

140 The Alboran Sea is the westernmost extensional basin of the Mediterranean Sea, bordered to
141 the north by the Betic Cordillera and to the south by the Moroccan Rif mountains. Oceanic currents
142 result from the water masses exchanges between the Atlantic Ocean and the Mediterranean Sea
143 through the Gibraltar Strait. The surface currents are governed by the inflow of low-salinity Atlantic
144 waters (Atlantic Jet) forming two anticyclonic gyres named Western and Eastern Alboran Gyres (WAG
145 and EAG) (Renault et al., 2012) (Fig. 1). The Mediterranean high-salinity water masses flow out in the
146 Atlantic basin through the intermediate depth currents.

147 The modern climate in the Alboran Sea region is typically Mediterranean, defined by long, hot,
148 dry summers and mild and cool winters (Lionello et al., 2006; Sánchez-Laulhé et al., 2021). Atlantic
149 westerlies dominate during winter, while subtropical high pressure masses generate intense drought
150 during summer (Sumner et al., 2001). The current vegetation distribution on the Alboran borderlands
151 follows a strong altitudinal climatic gradient : dry steppe elements such as *Artemisia* and *Lygeum* grow
152 in the most arid lowlands along the coast, sclerophyllous evergreen taxa, including *Quercus ilex*, *Olea*
153 and *Pistacia* are the main representatives of the thermo-to meso-Mediterranean belts, while
154 temperate vegetation with deciduous trees constitutes the overlying supra-Mediterranean belt
155 (Quézel, 2000). Finally, coniferous forests of *Abies* and *Pinus* grow in the oro-Mediterranean belt
156 (above approximately 1200 m), with the presence of *Cedrus* in altitudinal vegetation of the Moroccan
157 Rif mountains.

158 The main sedimentation processes in the area originate from the strong erosion in the Betic
159 Cordillera (Alonso et al., 1999; Liqueste et al., 2005; Lobo et al., 2006) and the material transported by
160 the surface Atlantic waters (Auffret et al., 1974), although a significant but unknown proportion of
161 particles including pollen was transported by African winds as evidenced by the presence of Saharan
162 clay particles and *Cedrus* pollen across the Pleistocene (Bout-Roumazielles et al., 2007; Jiménez-
163 Moreno et al., 2020; Magri & Parra, 2002). Therefore, the pollen assemblage is interpreted as reflecting
164 the regional vegetation of the southern Iberian Peninsula, with smaller but variable contribution from
165 Northern Africa. Previous studies have shown that the Alboran Sea palynological record displays close
166 similarities with the Padul record in SE Spain (Camuera et al., 2019), indicating that ODP 976 is a valid

167 archive to reconstruct the southern Iberian Peninsula vegetation changes (Fletcher & Sánchez Goñi,
 168 2008; Charton et al., 2025).

169 Two Organic-Rich Layers (ORLs) were identified in ODP 976 core during the MIS 6 interval, bed
 170 607 (50.43-49.93 m), and bed 606 (41.6-40.4 m) (Murat, 1999). The ages were recalculated based on
 171 the updated age model for MIS 6 presented here, giving 178.07-174.53 ka BP for bed 607, and 132.64-
 172 129.16 ka BP for bed 606. With a Total Organic Carbon (TOC) of 1.18% and 1.85% respectively, these
 173 layers have been described as “ghost sapropels”, as they present a lower organic matter content than
 174 the Eastern Mediterranean sapropels (Rogerson et al., 2008). Their relevance for hydrological and
 175 climatic inferences in the Alboran Sea will be discussed in the light of the vegetation dynamics.



Fig. 1. Map showing the location of ODP 976 core together with other paleoenvironmental and paleoclimate records covering part or all of MIS 6, as discussed in the text.

176

177 3. Methods

178 3.1. Age Model

179 The age model for the study interval uses three previously published tie-points between ODP
180 976 Mg/Ca-derived SST (Jiménez-Amat and Zahn, 2015) and the speleothem temperature records from
181 Dongge cave in China (Kelly et al., 2006, see Supplement Fig. S1). Several other marine records covering
182 MIS 6 in the region are chronologically tuned to speleothems (e.g. Sierro & Anderson, 2022; Tzedakis
183 et al., 2018). For the lower interval, the low resolution of planktonic isotopic data available for ODP
184 976 did not allow direct correlation to global temperature stacks or orbital configuration (von
185 Grafenstein et al., 1999). Instead, we chose to align the higher-resolution pollen record produced in
186 this study with the one from MD01-2444 core on the Portuguese margin (Margari et al., 2010, 2014;
187 Tzedakis et al., 2018). Previous studies highlighted the strong similarities between pollen records on
188 the Atlantic margin and the Alboran Sea during the last glacial period (Fletcher et al., 2010; Fletcher &
189 Sánchez Goñi, 2008; Sánchez Goñi et al., 2002), supporting this approach. MD01-2444 chronology is
190 based on the alignment of benthic isotopic events with the Antarctic temperature record, on AICC2012
191 timescale (Jouzel et al., 2007; Margari et al., 2010; Shin et al., 2020). The eleven tie-points between
192 MD01-2444 core and EPICA Dome C can be found in Supplement (Table S1). Five peaks of temperate
193 forest in MD01-2444 were used as control-points for ODP 976 (Table 1). The main assumptions of these
194 tuning approaches to the Dongge cave speleothem and the Antarctic record are discussed in detail in
195 Jiménez-Amat and Zahn (2015) and Margari et al. (2010) respectively. The obtained chronology for
196 ODP 976 core for MIS 6 prevents any assessment of the southwestern Mediterranean vegetation
197 response to global climatic events.

Event type	ODP 976 meters composite depth (mcd)	Age (ka BP)	References
Dongge cave speleothem D3	40.25	128.73	Jiménez-Amat and Zahn, 2015; Kelly et al., 2006
Dongge cave speleothem D2	42.61	135.57	Jiménez-Amat and Zahn, 2015; Kelly et al., 2006
Dongge cave speleothem D1	44.14	142.09	Jiménez-Amat and Zahn, 2015; Kelly et al., 2006
Temperate pollen peak in MD01-2444	46.4	149.43	(Margari et al., 2010; Shin et al., 2020)
Temperate pollen peak in MD01-2444	48.5	160.00	(Margari et al., 2010; Shin et al., 2020)
Temperate pollen peak in MD01-2444	49.3	170.07	(Margari et al., 2010; Shin et al., 2020)
Temperate pollen peak in MD01-2444	50.48	178.42	(Margari et al., 2010; Shin et al., 2020)
Temperate pollen peak in MD01-2444	53.2	193.758	(Margari et al., 2010; Shin et al., 2020)

198 **Table 1. List of control points used to calibrate the ODP 976 record for the MIS 6 interval.** The tie-
199 points on MD01-2444 temperate pollen curve are on AICC2012 timescale.

200 A linear regression was applied to obtain a continuous age for the study interval, spanning from
201 126.4 to 196.6 ka BP, with a mean resolution of about 350 years for the record (Fig. 2).

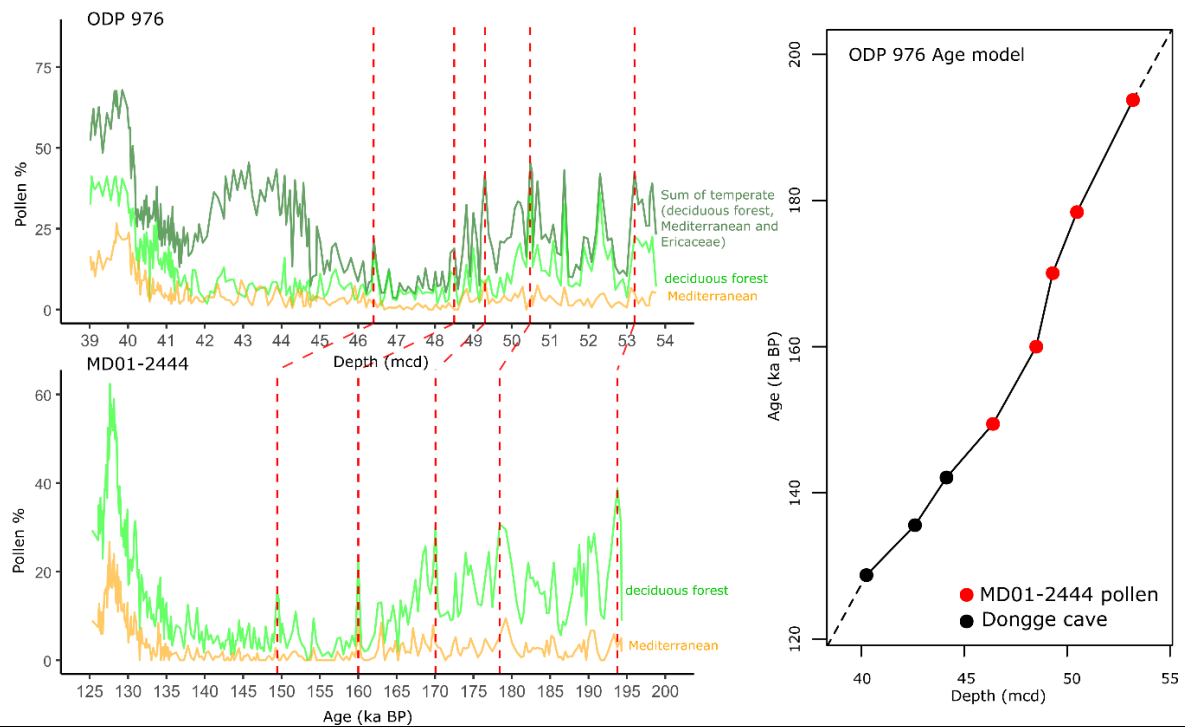


Fig. 2. Age versus depth model for the MIS 6 part of ODP 976 record, based on correlation between the Mg/Ca-based SST curve (Jiménez-Amat and Zahn, 2015) and the Dongge cave speleothem temperature record (Kelly et al., 2006) (black dots), and graphical correlation of the temperate pollen curve with the MD01-2444 palynological record (red dots and dotted lines) on AICC2012 timescale (Margari et al., 2010; Shin et al., 2020).

202

203 3.2. Pollen analyses

204 Two hundred samples have been analysed in this study, between 40 and 54 m (mcd) depth.
205 The sample processing followed the traditional steps used for pollen extraction (Faegri and Iversen,
206 1964) and previously applied to the ODP 976 core (Combourieu-Nebout et al., 2002; 2009; Sassoon et
207 al., 2023, Charton et al., 2025). It included sample weighing between 5 and 10 g of sediments, a 150
208 μm sieving for retrieving macrofossils and macroparticles, followed by 10% HCl, 40% HF, 20% HCl and
209 a final 10 μm sieving.

210 A minimum of 150 pollen grains were counted for each sample, excluding *Pinus* as it is usually
211 overrepresented in marine sequences (e.g. Combourieu-Nebout et al., 2002; Fletcher et al., 2010b;
212 Mudie, 2011 and references therein), and represents often more than 50% of the total pollen sum in
213 the study interval (see Fig. 3).

214 Ecological groups of pollen taxa were defined following previous studies of the ODP 976 record
215 (Charton et al., 2025; Combourieu-Nebout et al., 2009; Sassoon et al., 2023). The percentage pollen

216 diagram was constructed using the *rioja* R package (Juggins, 2023). Constrained Incremental Sum-of-
217 Squares (CONISS) cluster analysis was applied for pollen zonation, using the *vegan* package on R
218 (Oksanen et al., 2024).

219 3.3. Pollen-inferred climate reconstructions: a multi-method approach

220 Four methods were applied to the ODP 976 record to reconstruct past climate changes during
221 MIS 6. This is the first time this approach is used for the entire MIS 6 interval (Sinopoli et al., 2019).
222 The multi-method approach allows for a more accurate climate reconstruction (trends and rapid
223 events) compared to the traditional single-method approach (Chevalier et al., 2020; Peyron et al.,
224 2011, 2013; Salonen et al., 2019; Sassoon et al., 2025). It also allows us to compare the reliability and
225 biases of the different methods, which are based on different ecological principles and mathematical
226 algorithms. Four methods were used in this study.

227 The Modern Analogue Technique (MAT) is the first “assemblage” method ever developed to
228 estimate climate parameters based on pollen assemblages, and is still the most widely used (Guiot,
229 1990). It is based on the calculation of a dissimilarity index between the fossil samples and samples
230 from a modern pollen dataset. The values of the closest modern analogues selected (here, 4) are
231 averaged to reconstruct the climate parameters for each fossil sample. Weighted-Averaging Partial
232 Least Squares (WA-PLS) (ter Braak and Juggins, 1993) is the second most widely used method, and is
233 based on a different mathematical approach using non-linear regression. Assuming that taxa are most
234 abundant where they find their optimum climatic conditions, WA-PLS models the plant/climate
235 relationships from the modern calibration dataset, weighing the climatic values based on the pollen
236 taxa percentage. These plant pollen abundance / climate transfer functions are then used to calculate
237 the climate parameters of the fossil samples. The last two methods, Random Forest (RF) and Boosted
238 Regression Trees (BRT), rely on a completely different approach using machine learning: they generate
239 a large set of regression trees based on a randomised pollen dataset by bootstrapping (with pollen
240 taxa selected randomly). Contrary to RF (Prasad et al., 2006), BRT (Salonen et al., 2012) assigns a higher
241 probability to select samples that have not been selected before (boosting), increasing the
242 performance of the model for elements that are less well predicted (Chevalier et al., 2020). The
243 application of these machine learning methodologies in paleoclimatology is very promising, especially
244 for BRT, and they have already been validated through different European and Mediterranean pollen
245 records, for different time periods (Charton et al, 2025; D’Oliveira et al., 2023; Robles et al., 2022,
246 2023; Salonen et al., 2019; Sassoon et al., 2025).

247 The four methods were run on R using the *Rioja* package for MAT and WA-PLS (Juggins, 2024),
248 *dismo* for BRT (Hijmans et al., 2023) and *randomForest* for RF (Liaw and Wiener, 2022).

249 We used the modern pollen dataset compiled by Peyron et al. (2013, 2017) and updated by
250 Dugerdil et al. (2021a) and Robles et al. (2023). Samples belonging to non-relevant biomes for this
251 study were excluded (Taiga, Tundra, Pioneer Forest, warm steppe and hot desert), resulting in 2373
252 samples for calibration dataset spanning Eurasia and NW Africa (see Supplement, Fig. S2). A total of
253 103 harmonized pollen taxa are included in the dataset, excluding *Pinus* and aquatic taxa.

254 Six climate variables were reconstructed: PANN (annual precipitation), MAAT (annual
255 temperatures), SUMMERPR (summer precipitation), WINTERPR (winter precipitation), MTWA (mean
256 temperature of the warmest month) and MTCO (mean temperature of the coldest month). The
257 climatic tolerance spectra of the ten most abundant pollen taxa in the ODP 976 record have been
258 reconstructed based on the modern dataset (Supplement, Fig. S3). They show that steppe and semi-
259 desert taxa display the highest tolerance to low winter temperature and precipitation, while
260 Mediterranean taxa (*Olea* and *Quercus ilex*-type) are the most tolerant taxa to high annual and summer
261 temperature, and *Cedrus* and Ericaceae to higher annual and seasonal precipitation. SUMMERPR was
262 poorly reconstructed according to the accuracy indicators (Table 2). This is in agreement with previous
263 studies showing the poor reliability of summer parameters (e.g. Camuera et al., 2022). Therefore, we
264 chose to represent seasonal parameters as contrast values for a better visualization: TCON
265 (temperature contrast) = MTCO - MTWA, and PCON (precipitation contrast) = WINTERPR -
266 SUMMERPR. The MTWA and SUMMERPR results can be found in Supplement (Fig. S4).

267 For comparison with the present-day climate, and the calculation of anomalies, the modern
268 values were extracted from ERA 5 reanalysis of the ECMWF (European Centre for Medium-Range
269 Weather Forecasts), based on data assimilation into meteorological modelling from 1960 to 2022
270 (Hersbach et al., 2020). Pollen dispersal is reduced beyond a radius of 175 km (Rojo et al., 2016).
271 However, other studies suggest that pollen can be transported up to distances of 200-300 km
272 (Fernández-Rodríguez et al., 2014) and even over distances greater than 500 km (Bayr et al., 2023;
273 Damialis et al., 2017). Sediments from marine cores such as ODP 976 can therefore include close and
274 long-distance pollen. To account for these observations, an averaged value of the climate parameters
275 on a 400 km radius around the ODP 976 site was extracted (Supplement, Fig. S5), giving MAP = 478
276 mm, MAAT = 16.78°C, MTCO = 13.78 °C, WINTERPR = 172 mm, TCON = -9.59, PCON = 141.5 mm. These
277 values for modern climate, averaged temporally and spatially, provide a better basis for understanding
278 the nature of the climate signal extracted from a marine palynological sequence at a regional pluri-
279 annual scale.

280 The reliability of the different methods and climate parameters reconstructed is evaluated with
281 bootstrapping cross-validation through two indicators: the correlation coefficient between the
282 variables (R^2) and the root mean square error (RMSE).

283 4. Results

284 4.1. Pollen record

285 The pollen diagram shows the vegetation dynamics between 196.6 and 127.5 ka BP, spanning
286 late MIS 7 to early MIS 5 (Fig. 3). Five pollen zones were separated by CONISS cluster analysis, with
287 zone 4 being divided in three subzones (Table 2).

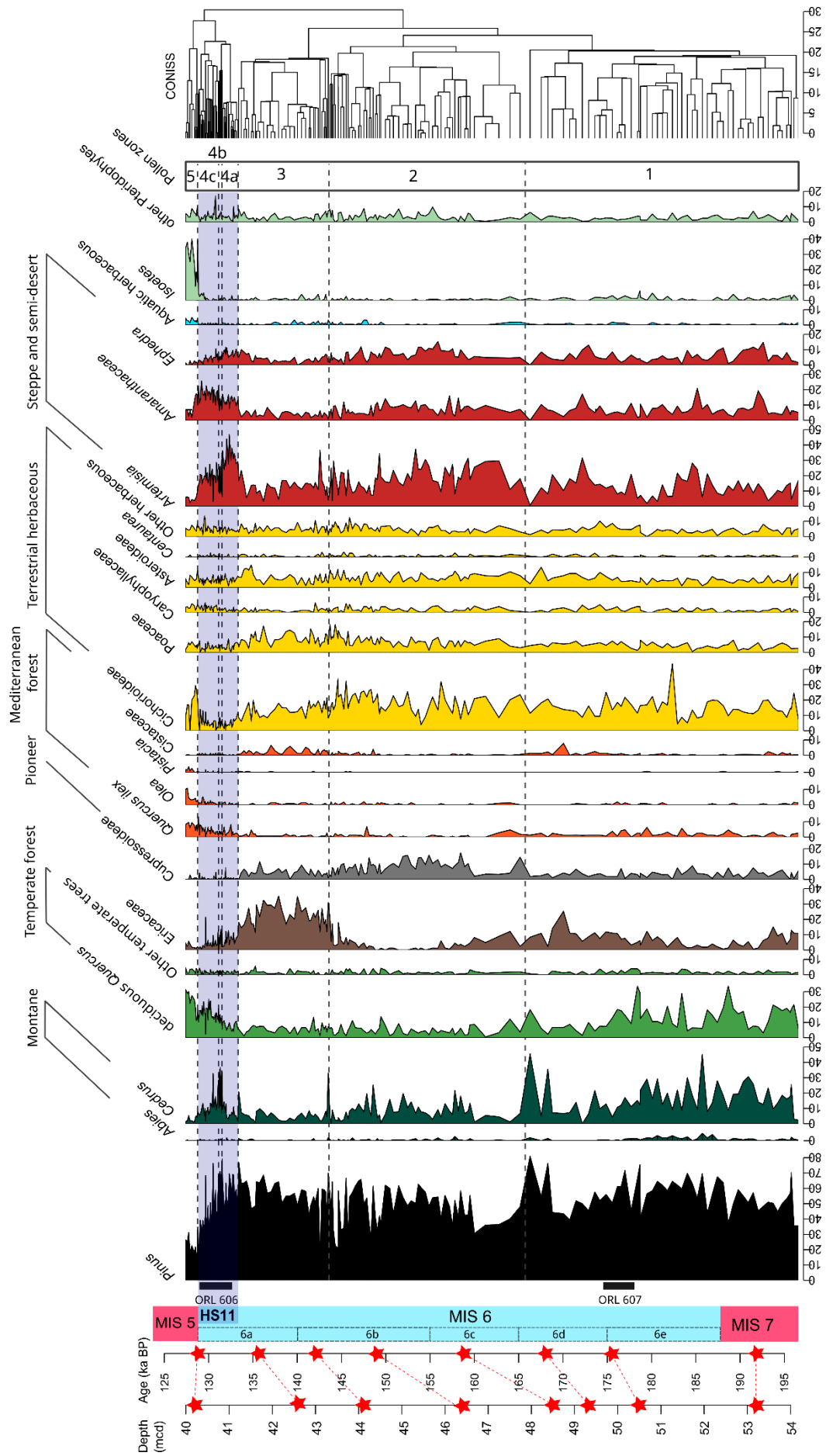


Fig. 3. Pollen diagram of selected taxa for MIS 6 interval in the ODP 976 record, plotted against age. Taxa are grouped by ecological groups (see Table 2). Red stars indicate control points used for the age calibration, and their correspondence with mcd (meters composite depth) (see Table 1). The blue bar indicates Heinrich Stadial 11. ORL : Organic Rich Layers from ODP 976 (Murat, 1999).

288

289 Zone 1 most represented taxa are deciduous *Quercus* and *Cedrus*, with important abundance
290 variability showing an unstable phase at the transition from MIS 7 to MIS 6e and 6d. Zone 2 displays
291 the maximum expansion of steppe and semi-desert vegetation together with other open vegetation
292 taxa and Cupressoideae during the MIS 6b and 6c. An additional noteworthy observation within this
293 interval is the presence of gastropod shells identified as *Limacina retroversa* (Jeanne Rampal, personal
294 communication, 2023), recovered during sieving of a sample at 46.4 m, corresponding to around
295 155.5 ka BP (Fig. 4). This species is usually most abundant in temperate to subpolar waters in the
296 North-Atlantic (Thabet et al., 2015). Zone 3 is mainly characterized by the abundance of Ericaceae at
297 the final stage of MIS 6 (6b and 6a). Zone 4, at the end of MIS 6a, is divided into 3 subzones which
298 display fast vegetation changes during the transition from MIS 6 to MIS 5 (Termination II), and Heinrich
299 Stadial 11. The fast expansion of steppe and semi-desert taxa (*Artemisia*, *Amaranthaceae*, *Ephedra*)
300 occurs simultaneously with the first increase of deciduous temperate and Mediterranean forest
301 indicative of the initialization of interglacial conditions (zone 4a). This episode of arid vegetation
302 dominance is interrupted in zone 4b by the fast expansion of montane vegetation mainly represented
303 by *Cedrus*. A new steppe and semi-desert vegetation increase is observed in zone 4c, while the
304 deciduous temperate forest and the Mediterranean vegetation continue to expand. Finally, zone 5 is
305 characterized by the maximum abundance of mesophilous and thermophilous elements, mainly
306 represented by deciduous *Quercus* and *Quercus ilex*, typical of the MIS 5 interglacial.

307

308

309

310

311

312

313

314

315

316

317

318

Pollen zone	Depth (mcd) and Age (ka BP)	Description of the pollen assemblage (Fig. 3)	Climate reconstructions (Fig. 5)
5	40.25-39.98 m 128.73-127.47 ka BP	Peak abundance of deciduous <i>Quercus</i> (up to 32%), <i>Quercus ilex</i> (4-10%), <i>Olea</i> (2-11%), <i>Pistacia</i> (up to 4%), aquatic herbaceous (up to 5%) and <i>Isoetes</i> (up to 38%). High values of Cichorioideae (up to 30%). Low percentages of <i>Pinus</i> (<35%), <i>Artemisia</i> (<11%), Amaranthaceae (<18%) and <i>Ephedra</i> (<3%).	Rapid increase of temperature, precipitation and seasonal contrast close to the modern value
4c	41.08-40.28 m 131.13-128.81 ka BP	New increase of <i>Artemisia</i> (up to 29%) and Amaranthaceae (up to 26%). High values of <i>Cedrus</i> (5-28%), and increasing percentages of deciduous <i>Quercus</i> (10-23%), Cichorioideae (0-14%) and <i>Quercus ilex</i> (1-13%). Decrease of Ericaceae (13-0%). Increasing percentages of <i>Isoetes</i> (0-5%) and Pteridophytes spores (0-17%).	First decrease, and then increase in temperatures and precipitation, with low PCON.
4b	41.21-41.09 m 131.51-131.16 ka BP	Peak abundance of <i>Cedrus</i> (up to 37%). Decrease of <i>Artemisia</i> (30-7%), Amaranthaceae (6-13%) and <i>Ephedra</i> (6-4%). Notable abundance of deciduous <i>Quercus</i> (6-15%) and <i>Quercus ilex</i> (1-3%).	Abrupt rise in precipitation contrast, but still cold conditions.
4a	41.82-41.22 m 133.28-131.54 ka BP	Peak abundance of <i>Artemisia</i> , (24-47%), Amaranthaceae (14-6%) and <i>Ephedra</i> (5-11%). Decreasing trend of Ericaceae percentages (12-2%), and progressive increasing of deciduous <i>Quercus</i> (4-11%) and <i>Quercus ilex</i> (1-8%). Decrease of Cichorioideae (<11%) and Cupressoideae (<8%).	Rapid decrease in temperature, precipitation and seasonal contrast.
3	44.57-41.85 m 143.49-133.37 ka BP	Peak abundance of Ericaceae (12-35 %), and high values of Cichorioideae (8-22%). Notable presence of Cupressoideae (2-11%). Peak abundance of <i>Artemisia</i> (37%) at 44.28 m / 142.54 ka BP and <i>Cedrus</i> (33%) at 44.57 m/143.49 ka BP.	Increase of temperatures (but still lower than present), and important precipitation rise until values higher-than-present. Seasonal contrast close to present-day.

2	48.91-44.63 m 165.16-143.68 ka BP	High percentages of Cichorioideae (11-34 %), Poaceae (4-18%), <i>Artemisia</i> (4-37%), Amaranthaceae (3-16%) and <i>Ephedra</i> (3-12%). Cupressoideae maximum between 150-160 ka BP (up to 17%), and abundant <i>Cedrus</i> (up to 25%). Very low values of deciduous <i>Quercus</i> (<10%), Mediterranean taxa (<4%) and Ericaceae (<12%), with minimum values between 150 and 158 ka BP.	Decline of temperatures and precipitation, both lower than the modern values, reaching a minimum between ~164-155 ka BP. Afterwards, progressive rise in temperature, precipitation and seasonal contrast.
1	53.76-49 m 196.15-166.29 ka BP	High percentages of <i>Cedrus</i> (8 to 45%) and deciduous <i>Quercus</i> (4 to 34%), with important variations. Abundant Cichorioideae (up to 43%) and Ericaceae (up to 25%), with notable presence of <i>Abies</i> (up to 5%), <i>Quercus ilex</i> (up to 6%) and <i>Isoetes</i> (up to 6%). Relatively low values of semi-desert elements (<i>Artemisia</i> , Amaranthaceae, <i>Ephedra</i>) but with two increases at 49.6 m / 172 ka BP and at 51.6 m / 185 ka BP.	Rather stable conditions expressed by the smoothed lines, but important and numerous rapid oscillations. In general, values of precipitation and seasonal contrast are close or higher than the modern value, while temperature is cooler than present.

321

322

323

Table 2. Description of the pollen zones identified through CONISS cluster analysis, including the main characteristics of their pollen assemblage and associated climate reconstructions.

324

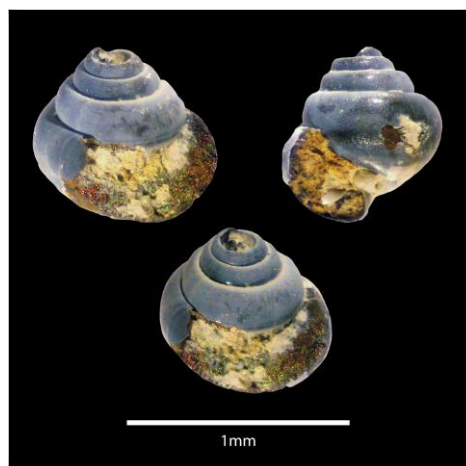


Fig. 4. *Limacina retroversa* specimen found in sample B6H4 130-132 (identification: Jeanne Rampal personal communication, 2023). Photo: Dael Sassoon.

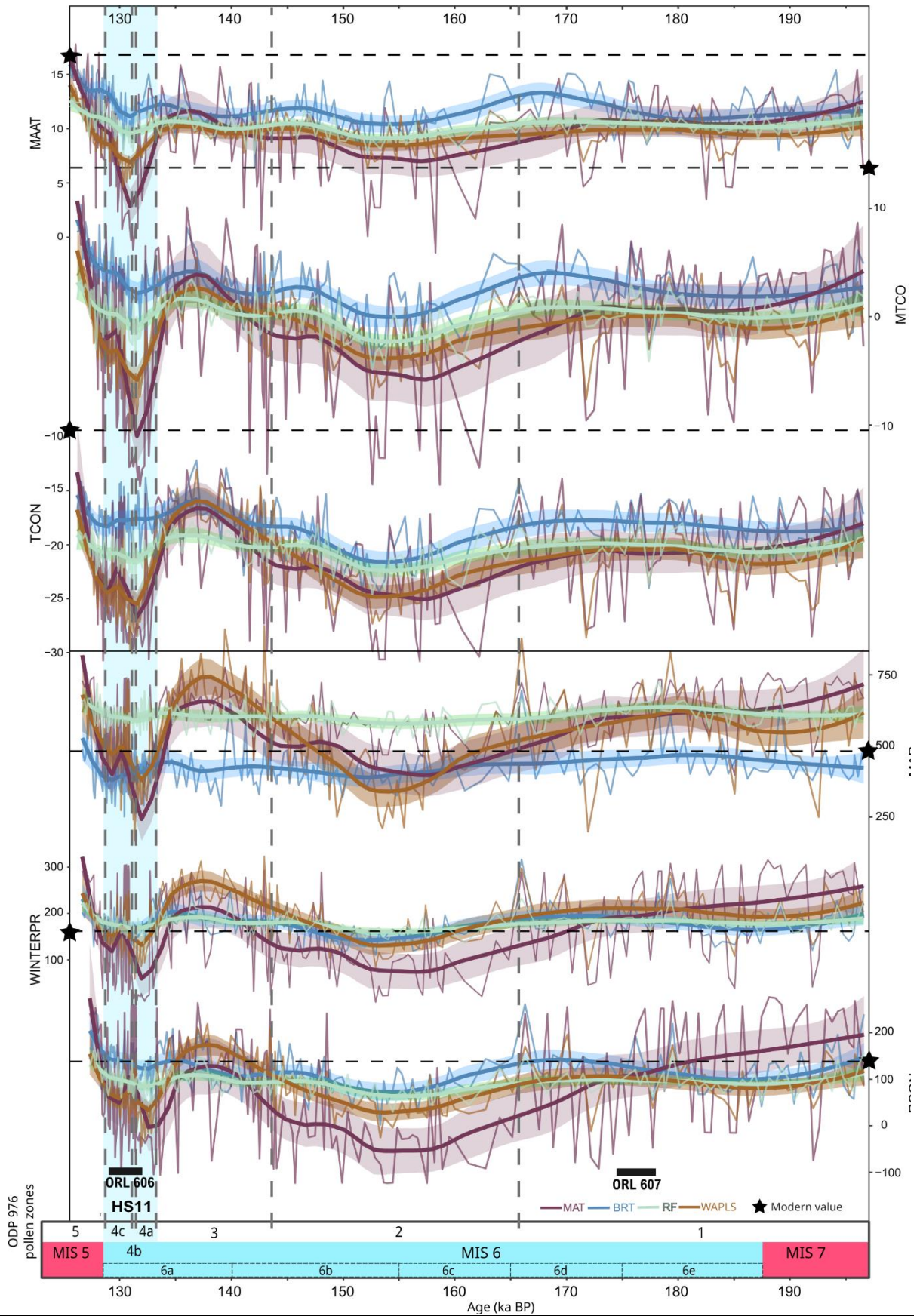
325

326 4.2. Pollen-inferred climate reconstructions

327 Results show significant temperatures and precipitation variations in connection with the
328 glacial / interglacial cyclicality and shorter-term variability (Fig. 5, Table 2). The most reliable methods
329 according to the two R^2 and RMSE indicators are MAT and BRT, and the most accurately reconstructed
330 parameters are MAAT and MTCO (Table 3). The four methods are in agreement for the general trends,
331 although MAT shows the widest amplitude of variations, and RF has the smoothest curve.

332 Temperatures are lower than the present during the complete MIS 6 interval, except at the
333 onset of MIS 5. A cooling trend is reconstructed during the final stage of MIS 7 (pollen zone 1, MIS 6e
334 and 6d), while MTCO and the seasonal temperature contrast (TCON) are stable. The methods do not
335 agree on the precipitation patterns during this phase, with MAT showing a trend toward aridity,
336 decreasing WINTERPR and seasonal precipitation contrast (PCON), while the three other methods
337 display a slight precipitation increase and stable PCON. From 166 ka BP onward (pollen zone 2, MIS 6c
338 and 6b), both temperatures and precipitation decrease, and the seasonal contrast between winter and
339 summer climate conditions reduced progressively. The MIS 6 minimum temperatures and precipitation
340 are reconstructed in pollen zone 2 between around 150 and 160 ka BP, corresponding to the transition
341 between MIS 6c and 6b. Subsequently, both temperatures and precipitation increase progressively in
342 the late pollen zone 2 and early pollen zone 3 (MIS 6b to 6a). Between 140-135 ka BP (early MIS 6a),
343 the four methods reconstruct temperatures similar to late MIS 7, a seasonal contrast close to the
344 present, and precipitation higher than the present (except for BRT). This climate optimum is abruptly
345 interrupted by the HS11 extreme arid event between ~134 and ~129 ka BP (pollen zone 4, late MIS 6a),
346 during which temperatures, precipitation and seasonal contrasts are significantly reduced, reaching
347 climate conditions similar to the MIS 6 glacial maxima ~155 ka BP. A short climate amelioration is
348 evidenced at ~132 ka BP (pollen zone 4b), where precipitation and seasonal contrasts increase
349 abruptly. Finally, after 130 ka BP the climate amelioration toward the MIS 5 interglacial conditions
350 happens very fast (pollen zone 5).

351



352 **Fig. 5. Pollen-based climate reconstructions for MIS 6 interval from the ODP 976 record.** MAAT (Mean
 353 Annual Temperature), MTCO (Mean Temperature of the Coldest Month), TCON (Temperature
 354 Contrast, see methods), MAP (Mean Annual Precipitation), WINTERPR (Winter Precipitation) and

355 PCON (Precipitation contrast, see methods) for the four different methods applied: MAT (Modern
 356 Analogue Technique), WA-PLS (Weighted Averaging Partial Least Square), BRT (Boosted Regression
 357 Trees) and RF (Random Forest). The light-coloured interval represents the 95% confidence window,
 358 and the bold curves the loess smoothed values (alpha = 0.25). Modern values (see methods) are
 359 indicated by the horizontal dashed line and the black star. Grey vertical dashed lines separate the
 360 pollen zones defined by CONISS cluster analysis.

361

	BRT		MAT		WA-PLS		RF	
	R ²	RMSE	R ²	RMSE	R ²	RMSE	R ²	RMSE
MTCO	0.87	2.96	0.88	3.19	0.71	4.44	0.77	3.88
MAAT	0.83	2.31	0.83	2.48	0.66	3.22	0.69	3.00
SUMMERPR	0.77	44.86	0.82	46.61	0.52	66.87	0.65	56.48
MAP	0.77	148.52	0.79	163.70	0.50	225.68	0.66	182.32
MTWA	0.76	2.25	0.79	2.33	0.53	3.16	0.61	2.81
WINTERPR	0.69	60.69	0.72	65.81	0.43	82.58	0.59	69.34

362

363 **Table 3. R² (coefficient of determination) and RMSE (Root Mean Square Error) values for the different**
 364 **climate parameters reconstructed with the four methods applied.** The lower the RMSE and the higher
 365 the R² (in bold), the more reliable the reconstruction.

366

367 5. Discussion

368 5.1. Paleoenvironment of MIS 6 and Termination II in the western Mediterranean

369 Important changes are recorded during MIS 6, that are consistent with orbital-scale variability
 370 during the different glacial substages.

371 Three phases can be discerned. The early phase (pollen zone 1) spans late MIS 7, MIS 6e and
 372 6d (~196-166 ka) and is characterized by high percentages of deciduous *Quercus*, *Cedrus* and
 373 Cichorioideae, with marked variability and several abrupt semi-desert and steppe increases under cool
 374 and humid climate conditions, with seasonal contrast similar to present-day. The middle phase (pollen
 375 zone 2) extends from MIS 6c to late 6b (~165-143 ka), and displays the maximum expansion of steppe
 376 and semi-desert taxa together with very low temperatures and precipitation between ~160 and ~150
 377 ka, a chronology compatible with the maximum Drenthe ice advance (Ehlers et al., 2011). Finally, the
 378 late phase (pollen zone 3), spanning late MIS 6b and 6a (~143-133 ka), is marked by a major expansion
 379 of Ericaceae vegetation associated with higher reconstructed precipitation and winter temperatures,
 380 as well as enhanced seasonal contrast during this phase.

381 Previous studies are consistent with a subdivision of MIS 6 into three phases characterized by
 382 different general trends and amplitude of millennial-scale oscillations (Margari et al., 2014; Nehme et

383 al., 2020). Margari et al. (2014) described an early phase between 185 and 160 ka BP, with warmer and
384 wetter conditions and important rapid climate variability, a middle transitional phase between 160
385 and 150 ka BP, and a late phase with stable glacial conditions between 150 and 135 ka BP. This three-
386 phasing for MIS 6 glaciation matches our interpretation of ODP 976 pollen zones 1, 2 and 3.

387 The final phase of MIS 6 is characterized by important changes in vegetation and climate,
388 indicating a rapid modification of vegetation communities and atmospheric configuration at the
389 transition between MIS 6 and MIS 5. Termination II (TII), defined as the period of fast reorganization
390 of the climate system from full glacial (MIS 6) to full interglacial (MIS 5) conditions, is indeed
391 characterized by extreme and fast internal dynamics including a major Heinrich Stadial, HS11 (Broecker
392 & Henderson, 1998; Gouzy et al., 2004; Martrat et al., 2014; Moseley et al., 2015; Ovsepyan &
393 Murdmaa, 2017). The timing for TII has been estimated based on the initialisation and termination of
394 Weak Asian Monsoon evidenced in the Dongge cave speleothems, lasting from ~136 to 129 ka BP (Bajo
395 et al., 2020; Kelly et al., 2006; Menviel et al., 2019). These boundaries for TII give a total duration of
396 about 7 ka. The timing of TII in the ODP 976 marine record is directly dependent on the Dongge Cave
397 chronology (see methods, section 3.1). Approximately the same duration is observed in the vegetation
398 response to TII, but with ~1 ka delay: the imprint of HS11 on the vegetation in the Western
399 Mediterranean region is indeed recorded here between 133.3 – 128.8 ka BP (pollen zone 4). This delay
400 in marine and terrestrial proxies may reflect the vegetation response to the first cold pulse of HS11.
401 ODP 976 provides for the first time a very detailed record of vegetation successions during this arid
402 event (pollen zones 4a, 4b and 4c), in agreement with other SSTs and speleothem records that depict
403 a three-phases or “W” pattern for the event (see section 5.4). After the first rapid increase of steppe
404 and semi-desert taxa (pollen zone 4a), the middle phase shows an abrupt decrease of steppe and semi-
405 desert vegetation, and a fast increase of montane trees (mainly *Cedrus*) percentages (pollen zone 4b).
406 Climate reconstructions reflect this event through a fast increase of both precipitation and
407 temperatures. This pattern is fully compatible with the ODP 976 SSTs trend (Jiménez-Amat and Zahn,
408 2015; Martrat et al., 2014), although a delay of about 1 kyr is observed between the abrupt drop in
409 alkenone-based SSTs at the onset of HS11 and the expansion of steppe and semi-desert vegetation. In
410 the same way, the abrupt sea surface warming in the middle of HS11 (~133 ka BP) is shifted in the
411 pollen record, to around 131.5 ka BP (pollen zone 4b).

412 5.2. Hydroclimate connection with ORLs deposition during MIS 6

413 Pollen analyses help us to characterize the processes behind Organic Rich Layers (ORLs) deposition
414 in this western Mediterranean region. Like sapropels, ORLs reveal important changes in the water
415 stratification and circulation, with reduced bottom water ventilation and enhanced organic

416 productivity in direct connection with (i) increase in the freshwaters Atlantic inflow at times of
417 deglaciation and (ii) enhanced rivers runoff regionally linked with increased precipitation (Murat, 1999;
418 Pérez-Asensio et al., 2020; Rogerson et al., 2008). Although they are often considered as “ghost
419 sapropels”, their timing and the mechanism behind them may differ from those of Eastern
420 Mediterranean sapropels (Rogerson et al., 2008).

421 ORL bed 607 coincides with a period of enhanced precipitation around 176 ka reconstructed
422 through our pollen-based approach (Fig. 7). Its basis appears almost synchronous with the onset of
423 Sapropel S6 layer deposition in the Eastern Mediterranean (Emeis et al., 2003; Rohling et al., 2015;
424 Savannah et al., 2024). Its duration also appears shorter than Sapropel S6, possibly indicating an
425 interruption of favourable climate conditions in the Western Mediterranean region by a stadial event
426 occurring around 172 ka BP and marked by an abrupt decrease in precipitation (Fig. 7).

427 ORL bed 606 was deposited during the second half of Termination II, at a time of deglaciation and
428 directly following the first aridity pulse of HS11. Pollen-based reconstructions show enhanced
429 precipitation and seasonal contrast during this time, suggesting intense precipitation together with
430 deglacial freshwater input as combined causes for ORL deposition in the Western Mediterranean,
431 which finds no counterpart in the Eastern Mediterranean. The implications of such organic layer
432 deposition occurring at times of enhanced precipitation or deglaciation will be further discussed in
433 section 6.2.6.4.

434 5.3. Mediterranean vegetation changes during the penultimate glaciation: a 435 synthesis

436 The ODP 976 pollen record documents MIS 6 vegetation changes in the Western
437 Mediterranean with a temporal resolution comparable to the most detailed terrestrial palynological
438 sequences from the Eastern Mediterranean (Tenaghi Philippon and Ioannina). A W-E transect of
439 Mediterranean palynological records offers valuable insights on the spatial pattern of vegetation
440 changes during the penultimate glaciation (Fig. 6).

441 At the MIS 7-6 transition, no abrupt decline of temperate forest is recorded in the ODP 976 and
442 Padul records, in contrast with central and Eastern pollen records such as Tenaghi Philippon, Ioannina,
443 Ohrid and Castiglione where the transition is very abrupt (Follieri et al., 1988; Koutsodendris et al.,
444 2023; Roucoux et al., 2011; Sadori et al., 2016). At these sites, a higher contrast has been described
445 between interglacial periods with very high percentages of temperate deciduous forest taxa and glacial
446 periods with very reduced tree cover (Tzedakis, 1993; Tzedakis et al., 2006). The western
447 Mediterranean region, at the contrary, was generally characterized by a high proportion of herbaceous

448 taxa, even during interglacial periods, attenuating the vegetation contrasts during transitions to glacial
449 periods.

450 The first half of MIS 6 (~185-165 ka BP) is marked by relatively high percentages of arboreal
451 pollen across all records, especially deciduous forest (Roucoux et al., 2011; Margari et al., 2010, 2014).
452 The abundance of montane taxa (mainly *Cedrus*) is characteristic of ODP 976 record, and reflects the
453 development of altitudinal trees on the Moroccan mountains. Montane elements also increase during
454 early MIS 6 at Valle di Castiglione, mainly represented by *Fagus* and *Abies* (Follieri et al., 1988), and at
455 Ioannina, mainly represented by *Pinus* (Roucoux et al., 2011). No equivalent pattern is recorded in
456 Padul where herbaceous vegetation is largely dominant. The scarcity of palynological data from the
457 western Mediterranean, especially from North Africa, limits our understanding of the spatio-temporal
458 significance of *Cedrus* expansions during MIS 6, and past glaciations in general.

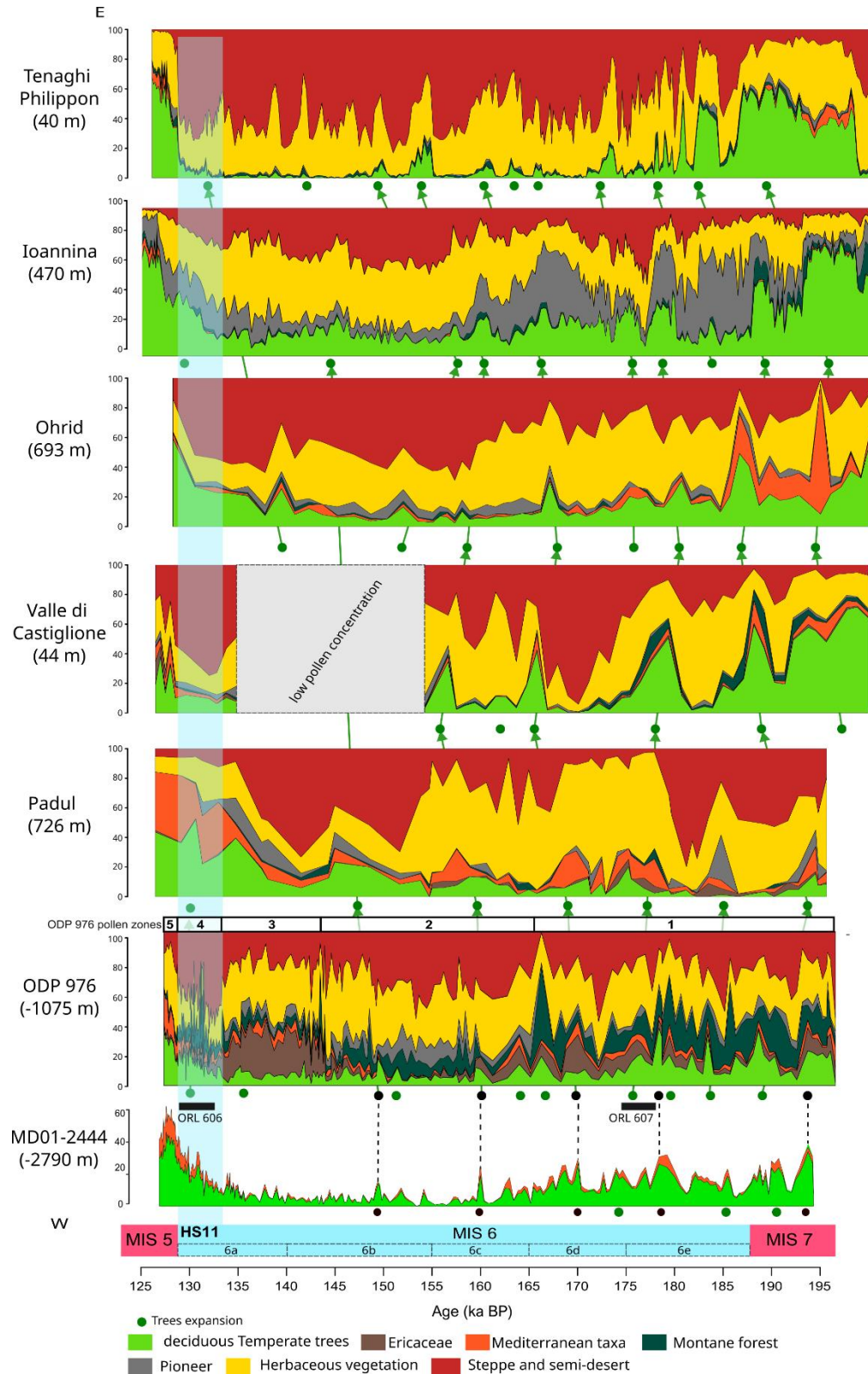


Fig. 6. Synthesis of vegetation changes in the Mediterranean during MIS 6 based on available palynological sequences, from west (bottom) to east (top): MD01-2444 (Margari et al., 2010; Tzedakis et al., 2018), ODP 976 (this study), Padul (Camuera et al., 2019), Valle di Castiglione (Follieri et al., 1988), Ohrid (Sadori et al., 2016), Ioannina (Roucoux et al., 2011), Tenaghi Philippon (Koutsodendris et al., 2023). Each synthetic pollen diagram is plotted according to its own age model. ODP 976 and Ioannina's chronologies are based on alignment with MD01-2444 temperate pollen curve on AICC2012 timescale. The ecological groups are the same as for ODP 976, except

Pinus was included in pioneer vegetation at Ioannina, as it is the only record where *Pinus* is not over-represented. Green dots indicate temperate vegetation increases, with tentative correlations between records. The two Organic Rich Layers (ORLs) identified in the ODP 976 core (Murat, 1999), were placed at the bottom.

459 The main phase of steppe and semi-arid vegetation is recorded between ~165-145 ka BP in the
460 Alboran Sea record, consistent with Ohrid and Ioannina pollen sequences (Fig. 6). In Padul, however,
461 the maximum expansion of steppe and semi-desert taxa occurs later, between ~155 and ~137 ka BP.
462 This time window corresponds to the glacial maximum recorded at Azzano X (northern Italy) between
463 148 and 135 ka BP (Pini et al., 2009), and to a period of low pollen concentration at Valle di Castiglione,
464 likely reflecting full glacial conditions. The ~10 ka lag in the vegetation glacial maxima between ODP
465 976 and Padul is probably the result of the low temporal resolution of the latter, in addition to
466 differences in the age models used. However, the presence of pioneer vegetation and to a lesser extent
467 of montane elements in Padul during the maximum glacial phase matches the ODP 976 pattern in
468 pollen zone 2, where Cupressaceae and *Cedrus* display high abundance.

469 A distinctive feature of the Western Mediterranean vegetation recorded during the final stage
470 of MIS 6 (pollen zone 3) is the marked increase in Ericaceae observed in the ODP 976 record, whereas
471 Ericaceae are almost absent in the rest of the Mediterranean region. A similar expansion is observed
472 in the Atlantic margin, where core MD01-2444 recorded patterns of Ericaceae expansion matching the
473 three insolation minima during MIS 6 (Margari et al., 2014). Ericaceae development during minimal
474 summer insolation is particularly favoured by reduced summer evaporation at times of low seasonal
475 contrast in precipitation, as already noted in the Alboran Sea during the last glacial (Fletcher and
476 Sánchez Goñi, 2008). Following the same interpretation, the expansion of heathland vegetation in the
477 Iberian Peninsula as recorded in ODP 976 during the final stage of MIS 6 may therefore mark the
478 renewed influence of westerlies and Atlantic moisture preceding the onset of the transition to MIS 5
479 interglacial (Margari et al., 2014). Supporting this state, an increase in temperate deciduous forest at
480 the end of MIS 6 is also seen in Padul, Ohrid and Ioannina records before the transition to MIS 5.

481 Despite some discrepancies due to the differences in age models and temporal resolutions, all
482 records display comparable variations in temperate pollen percentages during the penultimate glacial.
483 These variations support the persistent sensitivity of Mediterranean plant ecosystems to global-scale
484 millennial climate variability during the penultimate glaciation, with modulation of the vegetation
485 response depending on the local geography. Strong similarities can be observed between ODP 976 and
486 Padul, despite the lower temporal resolution of Padul record. In both sequences, temperate pollen
487 percentages reached ~30 % of total pollen as a maximum during the rapid forest expansion events in
488 the first half of MIS 6. This similarity supports the validity of the ODP 976 marine record to reconstruct

489 the SW Iberian Peninsula temperate forest history. However, ODP 976 sequence provides a more
490 regional image of the vegetation, including higher percentages of Ericaceae pollen coming from the
491 Atlantic coast, and *Cedrus* pollen from the Moroccan mountains (Jiménez-Moreno et al., 2020),
492 compared to Padul where percentages of Mediterranean taxa and hygrophYTE herbaceous are higher
493 due to the local nature of the signal (Camuera et al., 2019). Looking further east, Valle di Castiglione
494 recorded various temperate trees expansions and contractions during the lower MIS 6, before the full
495 glacial conditions. In the Italian Peninsula, various interstadials have also been identified further north
496 at Azzano X (Pini et al., 2009). In the Balkans, Tenaghi Philippon shows the highest percentages of semi-
497 desert and herbaceous vegetation throughout MIS 6, with more abrupt changes than all the other
498 Mediterranean records, and more amplitude of the trees' contractions. This pattern was already
499 described during the last climatic cycle and reflects the exacerbated vegetation dynamics locally, with
500 episodes of rapid and enhanced colonization by tree vegetation (Koutsodendris et al., 2023; Tzedakis,
501 2005; Tzedakis et al., 2004). This has been mainly explained by the location of the site in a low
502 altitudinal plain characterized by a more continental climate with lower winter precipitation: tree
503 populations at lower altitudinal location are closer to their ecological threshold in term of precipitation,
504 and are likely to be very affected even by minimal changes in the amount of rainfall. On the contrary,
505 the Ioannina record shows the highest deciduous forest percentages of all the records presented here,
506 supporting its character as a local trees refugium (Roucoux et al., 2011).

507 Termination II displays a particular pattern in vegetation records from the Mediterranean
508 region: while the expansion of trees and temperate vegetation is fast and continuous, HS11 represents
509 at the same time a remarkable episode of abrupt steppe and semi-desert expansion. Although this
510 event is visible in almost all the records, it is particularly prominent in the ODP 976 record (pollen zone
511 4), and appears less pronounced in the eastern Mediterranean sequences. This observation is
512 compatible with previous observations that Heinrich stadials during the last glacial had a minor impact
513 on the eastern Mediterranean vegetation compared to the western Mediterranean, likely due to the
514 already limited presence of tree vegetation in the eastern records during glacials (Tzedakis, 2005). A
515 similar interpretation can be proposed for the differential response of eastern and western
516 Mediterranean vegetation to HS11, supporting the major sensitivity of the southwestern
517 Mediterranean vegetation to North Atlantic cold events. In Padul, no major expansion of xerophyte
518 vegetation is detected, but a small decrease of temperate deciduous taxa was interpreted as the HS11
519 imprint (Camuera et al., 2019), and the signal might be hindered by the low resolution of the record.
520 A pattern of fast arid vegetation increase contemporaneous to the temperate forest expansion is also
521 found in central Italy at Lago Grande di Monticchio, which was not presented in Fig. 6 as its record
522 does not extend beyond 132 ka BP (Allen and Huntley, 2009; Brauer et al., 2007).

523 Finally, all palynological sequences reveal high-frequency oscillations of temperate and semi-
524 desert pollen, compatible at first look with DO-like variability based on their duration and intensity.
525 They represent a particularly distinctive feature of the lower part of MIS 6.

526 5.4. Rapid climate variability during MIS 6: a regional multiproxy comparison

527 In order to investigate the character of rapid climate variability during MIS 6, a comparison
528 with regional and global climatic archives is essential. The events of arboreal pollen increase observed
529 in the ODP 976 record show percentages and timing comparable to those from the Portuguese margin
530 core MD01-2444 (Margari et al., 2010, 2014; Tzedakis et al., 2018) (Fig. 7, m). However, the ODP 976
531 record generally presents lower values of temperate deciduous pollen percentages compared to the
532 Atlantic record, due to its more semiarid Mediterranean influence as previously evidenced for the last
533 glacial period (Charton et al., 2025; Fletcher et al., 2010b). To better capture temperate vegetation
534 dynamics, we added Ericaceae, a clear marker of Atlantic influence in the ODP 976 record, to the
535 deciduous temperate forest, to obtain a “total temperate pollen sum” which enhances the main
536 warming peaks and strengthens the correlation between the two marine cores on both sides of
537 Gibraltar Strait (Fig. 7, m and l). The ODP 976 pollen-inferred climate reconstructions show generally
538 consistent patterns with the SSTs trends based on alkenones (Martrat et al., 2004, 2007), and the
539 southern Iberian humidity recorded in the speleothem from Cueva Gitana (Hodge et al., 2008) (Fig. 7,
540 e and g). The ODP 976 pollen and climate record therefore appears to reflect well regional variations
541 in both temperature and humidity across MIS 6.

542 Warm events in the northern hemisphere are generally well-correlated to peaks in the ODP
543 976 temperate pollen curve (Fig. 7, c and l). An active bipolar seesaw dynamics was described during
544 the penultimate glacial Davtian & Bard, 2023; EPICA Community Members, 2006; Stocker, 1998), and
545 the Antarctic record was used to elaborate the Greenland GL_T-syn (Greenland temperature synthetic)
546 curve showing predicted $\delta^{18}\text{O}$ millennial-scale events for the past glacial eight climatic cycles, which
547 are not directly recorded in Greenland ice (Barker et al., 2011; Bazin et al., 2013; Jouzel et al., 2007).
548 Six Antarctic Isotopic maxima (AIM) events were recognized on the Deuterium curve during MIS 6 (6i
549 to 6vi), correlated with increases in CO₂ concentrations and benthic isotope minima in the North
550 Atlantic (Barker et al., 2011; Hodell et al., 2023; Margari et al., 2010, 2014; Shin et al., 2020) (Fig. 7, a-
551 c). These AIM and benthic minima in the Atlantic are not easily correlated with steppe expansions in
552 the ODP 976 record, indicating a limited response of vegetation in the Western Mediterranean to the
553 Antarctic warm events.

554 Barker et al. (2011) predicted the occurrence of eleven millennial-scale warming events during
555 MIS 6 (Fig. 7, c), while nine interstadials were recognized in the Alboran Sea from the alkenone record

556 (Fig. 7, e), (Martrat et al., 2004, 2007). In the loess record of Harletz in central Europe, ten interstadials
557 were described (Rousseau et al., 2020), strongly matching the Chinese speleothems records of stadial
558 and interstadial events related to the Asian Monsoon dynamics (Cheng et al., 2006; Li et al., 2014;
559 Wang et al., 2018; Wang et al., 2001; Xue et al., 2019). The global nature of fast climate oscillations in
560 the northern hemisphere thus appears controlled by the coupled influence of Atlantic cold events, and
561 tropical monsoon variations as evidenced by the eastern Mediterranean speleothems records from
562 Sofular, Soreq and Kanaan caves (Ayalon et al., 2002; Held et al., 2024; Matthews et al., 2021; Nehme
563 et al., 2018).

564

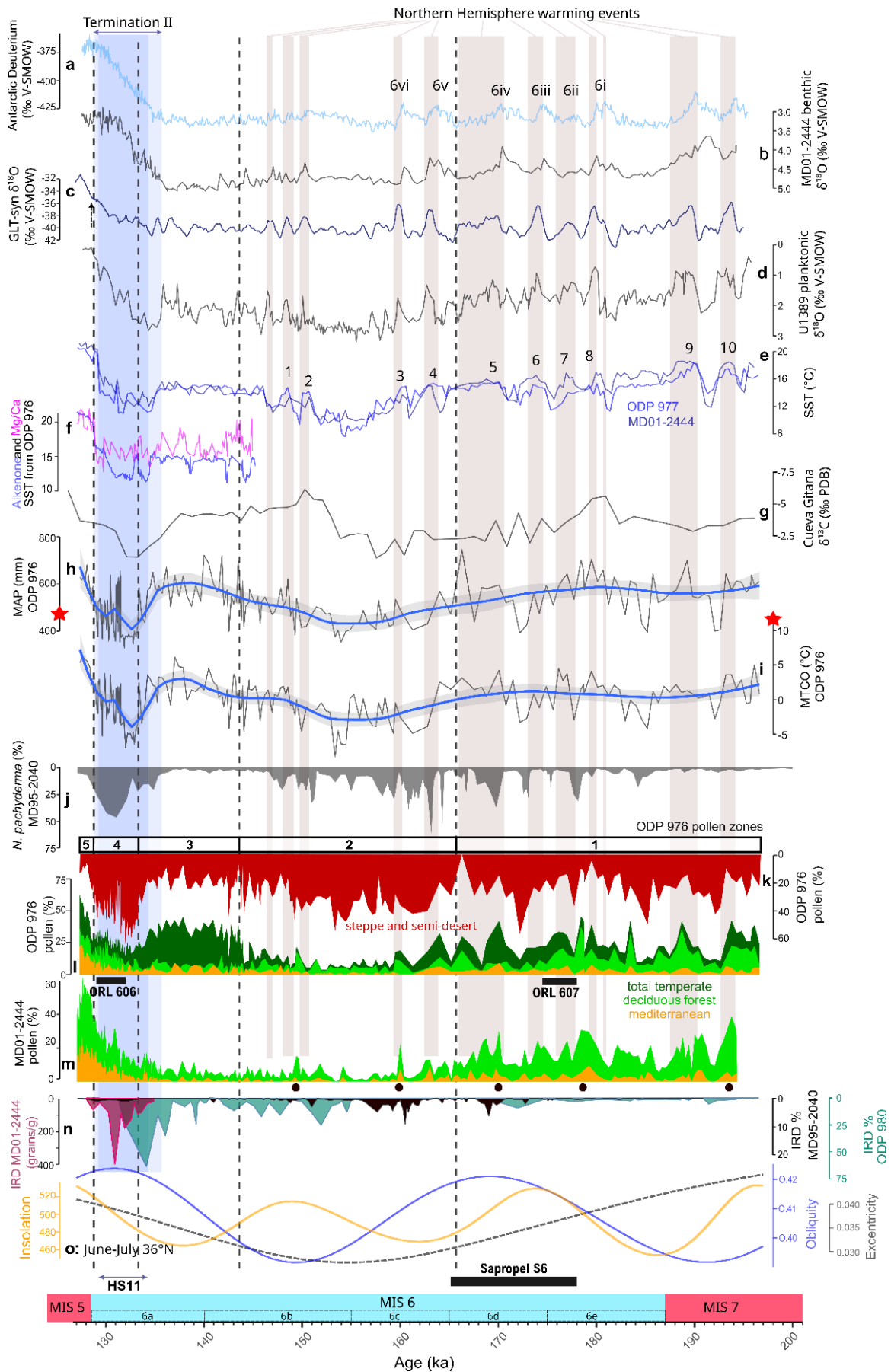


Fig. 7. Millennial-scale climate changes during MIS 6. a) Antarctic Dome C δD (Bazin et al., 2013; Jouzel et al., 2007); **b)** Benthic $\delta^{18}O$ from MD01-2444 (Margari et al., 2010); **c)** Greenland synthetic

$\delta^{18}\text{O}$ (Barker et al., 2011); **d**) Planktonic $\delta^{18}\text{O}$ from U1389 (Sierro & Andersen, 2022); **e**) alkenone-based SST from ODP 977 (darker blue) and MD01-2444 (lighter blue) (Martrat et al., 2004, 2007); **f**) Alkenone-based SST (Martrat et al., 2014) and Mg/Ca-based SST (Jiménez-Amat and Zahn, 2015) from ODP 976; **g**) $\delta^{13}\text{C}$ from Cueva Gitana (Hodge et al., 2008); **h**) Mean Annual Precipitation (MAP) reconstructed from ODP 976 pollen assemblage, mean of the four methods used in this study (MAT, WA-PLS, RF, BRT), with the red star showing the modern value ; **i**) Mean Temperature of the Coldest Month (MTCO) reconstructed from ODP 976 pollen assemblage, mean of the four methods used in this study (MAT, WA-PLS, RF, BRT), with the red star showing the modern value; **j**) *N. pachyderma* percentages from MD95-2040 (de Abreu et al., 2003; Voelker & de Abreu, 2011); **k**) ODP 976 pollen percentages of semi-desert and steppe taxa, with ODP 976 pollen zones (this study); **l**) ODP 976 pollen percentages of total temperate taxa including temperate deciduous forest + Ericaceae + Mediterranean (dark green), deciduous forest (light green), Mediterranean (orange) (this study); **m**) MD01-2444 pollen percentages of temperate tree (light green) and Mediterranean (orange) taxa (Margari et al., 2010; Tzedakis et al., 2018); **n**) Ice-Rafted Debris (IRD) percentages from MD01-2444, 37° N (pink) (Skinner & Shackleton, 2006) redrawn from Tzedakis et al. (2018), MD95-2040 (black), 40°N (de Abreu et al., 2003) and ODP 980 (blue), 55°N (McManus et al., 1999; Oppo et al., 2001, 2006); **o**) orbital parameters (Laskar et al., 2004) calculated for June-July at 36°N: Eccentricity (black), Obliquity (blue) and Insolation (yellow). The black rectangle indicates the interval of deposition of Sapropel layer S6 in the eastern Mediterranean (Ziegler et al., 2010). The marine substages MIS 6a-e follow (Railsback et al., 2015). All data are plotted on AICC2012 chronology (Bazin et al., 2013) following Sierro et al. (2020, 2022), except for the IRD records and Gitana Cave which is plotted on its own age model based on U-series absolute dating. The vertical grey bars indicate the Northern Atlantic interstadial events based on the planktonic isotope record and the predicted millennial-scale warming events from Greenland synthetic record, with the numbers of the Alboran interstadials (AI-1 to AI-10) from Martrat et al. (2004, 2007). Numbers 6i-6vi correspond to the Antarctic Isotope Maxima (AIM) from Margari et al. (2010). The vertical blue bar represents Heinrich Stadial 11 (HS11). Black dots and dotted lines show the five temperate pollen peaks in MD01-2444 used as control points for ODP 976 chronology.

565

566 The three phases identified during MIS 6 based on the ODP 976 vegetation and climate record
567 can be compared with regional and global records to be interpreted in a broader context, based on
568 general climatic trends and the expression of climatic instability:

569 Early MIS 6 (187-166 ka BP): warm/wet conditions and instability. The first phase encompasses
570 the two substages MIS 6e and 6d, and is characterized by humid and rather warm climate conditions
571 in the Mediterranean at the transition from MIS 7 to MIS 6. This phase aligns well with the deposition
572 of ORL bed 607 in the Alboran Sea, and the sapropel layer S6 in the Eastern Mediterranean, associated
573 with the maximum summer insolation and increased intensification of the summer monsoonal system
574 in the eastern Mediterranean between 178.5 to 165.5 ka (Emeis et al., 2003; Rohling et al., 2015;
575 Ziegler et al., 2010). At the same time of S6 deposition, Cheddadi and Rossignol-Strick (1995) described
576 an increase in temperate pollen in the Nile region, and Soreq cave speleothem records climatic
577 conditions typical of an interglacial (Ayalon et al., 2002). Sapropel depositions usually occur during
578 interglacial periods as MIS 1 (Holocene), which makes sapropel S6 an exceptional feature of early MIS
579 6. It reflects particularly warm and humid conditions, and intense freshwater input in the

580 Mediterranean which can result from various sources, including increased rainfall and monsoon
581 activity, Atlantic freshwater entrance, and enhanced river discharges (Sierro & Andersen, 2022). The
582 long speleothem records in China report a period of northern shift of the Intertropical Convergence
583 Zone associated with enhanced Asian Monsoon activity during this phase (Wang et al., 2018). Higher
584 pluviometry is also supported by foraminifera isotopic and SSTs signal throughout the Mediterranean
585 Sea, which were used to reconstruct past salinity and freshwater budget regionally (Kallel et al., 2000).
586 Enhanced rainfall in the Balkans is evidenced by the Ioannina lake deepening (Wilson et al., 2021), and
587 a more humid period is documented in speleothem records from Argentarola cave in Italy (Bard et al.,
588 2002) and Gitana cave in southern Spain (Hodge et al., 2008) (Fig. 7, g). Therefore, humid conditions
589 during this phase were not restricted to the eastern Mediterranean where the sapropel deposition
590 occurred. ODP 976 organic layer 607 together with the pollen-based climate reconstructions support
591 this view, with enhanced seasonal precipitation contrast during this interval driven by enhanced winter
592 precipitation (Fig. 5). Comparison with Padul pollen-based hydroclimate reconstructions (Camuera et
593 al., 2022) further strengthens this scenario: despite the chronological delay between the two
594 sequences, this early MIS 6 humid phase and ORL deposition likely matches the Western
595 Mediterranean Humid Period (WMHP 6) dated between 180-155 ka BP (Fig. 8). The same study made
596 the case for a co-occurrence of humid periods in the Western Mediterranean and in West Africa
597 (African Humid Periods) during periods of high precipitation seasonality and enhanced West African
598 Monsoon. Pollen-inferred climate reconstructions from lake Ohrid have also shown the phase
599 relationship between African Monsoons and periods of high winter precipitation in the Mediterranean
600 region (Wagner et al., 2019; Sinopoli et al., 2019).

601 Another characteristic of this early MIS 6 phase is the strong variations in pollen and isotopic
602 curves in the Atlantic and Western Mediterranean (Fig. 7, a-d and l-m). Variations in temperate
603 deciduous and Ericaceae percentages are observed in the ODP 976 record, in close correspondence
604 with the Atlantic record from MD01-2444. The largest interstadial peak in ODP 976 around 179 ka BP
605 is also identified in all the different records and marked by warmer conditions in the sea, and more
606 effective precipitation in SE Iberia (Hodge et al., 2008). It is well correlated with the stadial following
607 Antarctic event 6i (Margari et al., 2010), the associated predicted millennial-scale warming event in
608 Greenland synthetic curve, and the Alboran Sea SST interstadial event 8 (Martrat et al., 2004). In Padul
609 record, the temperate deciduous, Mediterranean and *Abies* percentages increase correlates well with
610 this event (Camuera et al., 2019). It could also match the WMHP 6.1 interstadial (Camuera et al., 2022)
611 (Fig. 8). This large interstadial was suggested to be at the origin of the initialisation of the sapropel S6
612 deposition (Sierro & Andersen, 2022), and could also have participated in the initialization of ORL 607
613 deposition in the Alboran Sea (Murat, 1999). On the other hand, the most important tree population

614 decline and semi-desert expansion in ODP 976 is recorded at ~ 172 ka BP, which could match Antarctic
 615 event 6iv, and is associated to a moderate increase of IRD deposition at the latitude of ODP 980 (Fig.
 616 7, n). A similar stadial can be observed in the Ioannina and Tenaghi Philippon records with a close
 617 chronology (Roucoux et al., 2011) (Fig. 6). Dry conditions at this time are also recorded in the eastern
 618 Mediterranean as shown in the Pentadactylos and Soreq speleothems (Ayalon et al., 2002; Nehme et
 619 al., 2018).

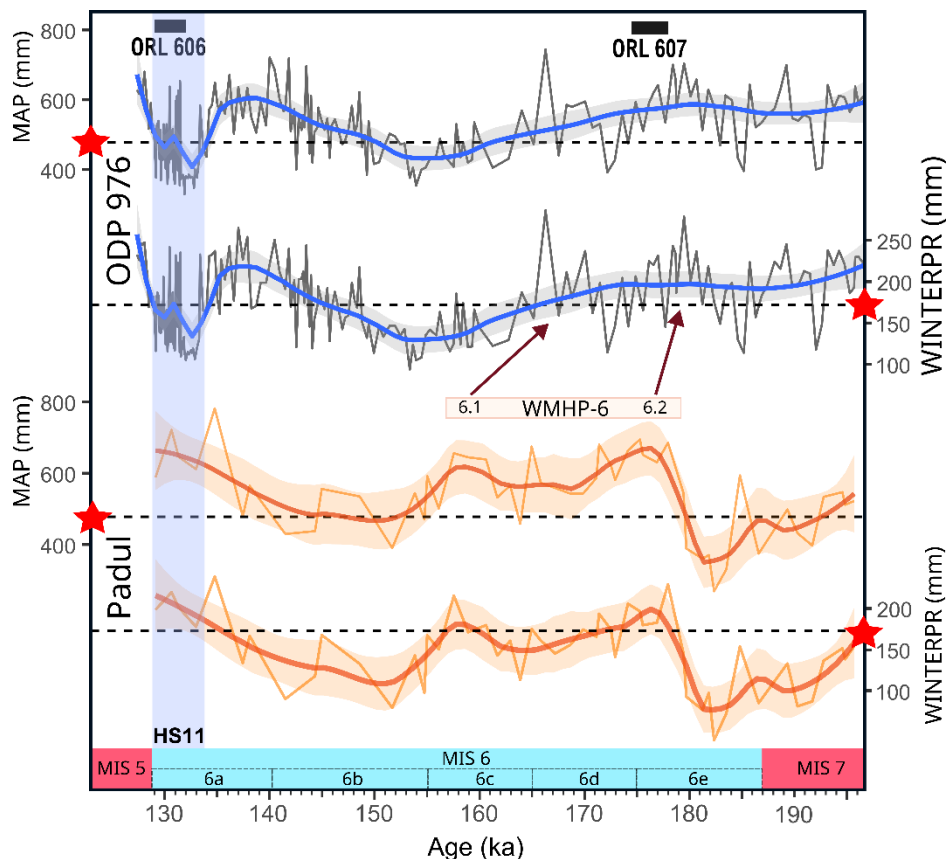


Fig. 8. Comparison between the precipitation pattern reconstructed from ODP 976 with our multi-method approach (mean) (this study) and from Padul with only the WA-PLS method (Camuera et al., 2022). Mean Annual Precipitation (MAP) and Winter Precipitation (WINTERPR) are represented, together with the two Organic Rich Layers (ORLs) identified in ODP 976 (Murat, 1999) and the Western Mediterranean Humid Period (WMHP) 6 defined by Camuera et al. (2022). Red arrows indicate tentative correlation between the two phases of WMHP 6, and the precipitation reconstructions from ODP 976. Red stars and dashed lines indicate the modern climate value (see methods).

620 Middle MIS 6 (165-144 ka BP): maximum glacial conditions and stability. This phase is marked
 621 by the maximum expansion of semi-desert vegetation and the almost complete collapse of forest
 622 vegetation between ~ 163 and 150 ka BP, according to the ODP 976 pollen and MD01-2444 records,
 623 synchronous with the minimum in orbital eccentricity. This is in agreement with the lowest SSTs values
 624 reconstructed in the Alboran Sea from the alkenone record occurring around 155 ka BP, and low SSTs
 625 in the Gulf of Lions too (Cortina et al., 2015). At the same time, high percentages of the cold species *N.*

626 *pachyderma*, together with important ice-detritus pulses, are recorded on the Portuguese margin (de
627 Abreu et al., 2003; Voelker & de Abreu, 2011) (Fig. 7, j and n). The occurrence of the cold Atlantic
628 species *Limacina retroversa* shells in the ODP 976 sediments at ~155 ka BP is consistent with the
629 enhanced entrance of cold subpolar water masses in the Alboran sea at the time of full glacial
630 conditions. In parallel, there is an intensification of “Fleuve Manche” paleo river discharges evidenced
631 in various sedimentary cores from the Bay of Biscay (Boswell et al., 2019; Eynaud et al., 2007; Penaud
632 et al., 2009, 2016; Toucanne et al., 2009), and a fluvial aggradation linked with reduced vegetation
633 cover in Spanish river basins (Macklin et al., 2002). A long-term aridification is recorded in SE Spain in
634 Gitana cave close to the ODP 976 location (Hodge et al., 2008). The glacial maximum in Soreq cave
635 speleothem is also recorded around 154 ka BP (Bard et al., 2002), and might be responsible for the
636 hiatus in the Pentadactylos speleothem in Cyprus (Nehme et al., 2020). In Italy, the Tana che Urla cave
637 also recorded cooling and aridification between 159-132 ka BP, indicated by both the carbon and
638 oxygen isotopic ratio (Regattieri et al., 2014). The coolest phase in Abaliget Cave speleothem in central
639 Europe is also recorded at that time (Koltai et al., 2017). Climate conditions reconstructed at ODP 976
640 site during this phase show the maximum aridity and cold temperatures, which are consistent and fall
641 within the range of reconstructed temperatures and precipitation at the same time at Ohrid (Sinopoli
642 et al., 2019). This main phase of glaciation in Europe took place after 163 ka BP, corresponding to the
643 Drenthe glacial advance (Ehlers et al., 2018; Margari et al., 2014). The maximum ice expansion
644 probably led to the almost complete collapse of temperate vegetation across the Mediterranean
645 region, except in specific climate refugia like Ioannina or Padul (Fig. 6). The Mediterranean vegetation
646 taxa were particularly affected and almost disappeared at this time in the ODP 976 record.

647 Few interstadial events are observed during this cold and dry phase, probably due to the
648 extended ice volume reaching a critical threshold (McManus et al., 1999) and leading to higher climate
649 stability at time of glacial maximum expansion (Sierro and Andersen, 2022). One moderate interstadial
650 event around 150 ka BP is expressed in the ODP 976 and MD01-2444 records through an increase in
651 temperate deciduous tree taxa (Fig. 7, l and m). It may correspond to the interstadial recognized in
652 Gitana Cave speleothem approximately at the same time, and is compatible with the Alboran
653 Interstadial events 1 or 2 (Martrat et al., 2004), while a larger trees increase in Padul record is also
654 observed (Camuera et al., 2019) (Fig. 6). It is also compatible with interstadials recognized in other
655 speleothem records in eastern and central Mediterranean (Ayalon et al., 2002; Bard et al., 2002;
656 Regattieri et al., 2014). Sierro et al. (2022) described a major event of low Mediterranean overturning
657 and high freshwater entrance through the Gibraltar Strait at that time and contemporaneous to the
658 insolation maximum (Fig. 7, o). This configuration was similar to the one contemporaneous to sapropel
659 S6 and ORL 607 deposition during early MIS 6, but did not lead to any new sapropel deposition at 150

660 ka BP, probably because the climate conditions were more favourable but not enough for a sapropel
661 deposition.

662 Late MIS 6 (144-129 ka BP): increased precipitation during the last glacial, and arid conditions
663 during HS11. Between 150 and 140 ka BP, warmer and wetter conditions are indicated by ODP 976
664 pollen percentages of Ericaceae (pollen zone 3). Ericaceae expansions in the Iberian margin sediments
665 were found to be associated to insolation minima in core MD01-2444 (Margari et al., 2014). This
666 pattern is consistent with the ODP 976 Ericaceae curve (Fig. 7, l). The climate reconstructions
667 evidenced high precipitation and especially high WINTERPR values. These higher humidity and
668 temperature values are supported by the carbon isotope record from Gitana Cave (Hodge et al., 2008)
669 and the Alboran Sea SSTs (Martrat et al., 2007) (Fig. 7, e-g). In central Europe, Abaliget Cave
670 speleothem also shows more favourable climate conditions during this phase (Koltai et al., 2017).
671 Climatic oscillations appear subdued in the Western Mediterranean pollen records during this last
672 phase. The high resolution ODP 976 record shows some SST variations (Jiménez-Amat and Zahn, 2015;
673 Martrat et al., 2014) : Ericaceae pollen contractions and semi-desert elements expansions could be
674 correlated to three abrupt drops in alkenone-based SSTs at 144, 142, and 139 ka BP (Fig. 7, f, k and l).
675 Fifteen Chinese Interstadials (CIS) were identified at Hulu Cave during late MIS 6, linked with Asian
676 Monsoon dynamics (Wang et al., 2018), and the ultra-high-resolution record of planktonic isotope ratio
677 at U1389 by Sierro and Andersen (2022) also expresses some variability. However, the vegetation
678 response in the SW Mediterranean was apparently limited.

679 Following the Ericaceae expansion, the most prominent feature of the late MIS 6 phase is the
680 large and fast expansion of steppe and semi-desert vegetation during HS11, between 133 and 129 ka
681 BP (pollen zone 4). It is characterized by a first large IRD peak at high latitude (ODP 980) around 134 ka
682 BP, and later at the MD01-2444 latitude, around 131 ka BP (Skinner & Shackleton, 2006; Tzedakis et
683 al., 2018). This event also corresponds to an increase in the oxygen isotopic ratio at the Portuguese
684 margin (especially planktonic, starting around 136 ka BP), also broadly synchronous to an important
685 decrease in SSTs of the Atlantic and the Mediterranean Sea (Jiménez-Amat and Zahn, 2015; Martrat et
686 al., 2004, 2007, 2014). A pronounced increase in *N. pachyderma* (sinistral) abundance is also recorded
687 on the Portuguese margin (Voelker & de Abreu, 2011). Climate reconstructions show particularly harsh
688 conditions in the Western Mediterranean region during this event, compatible with the
689 reconstructions from Lake Ohrid (Sinopoli et al., 2019) and from three French sites (Les Echets, la
690 Grande Pile and Le Bouchet) for the latest phase of MIS 6 (Guiot et al., 1989, 1993). An arid phase is
691 also evidenced at Gitana Cave (Hodge et al., 2008), which closely matches the trend of the ODP 976
692 precipitation curve (Fig. 8). Aridity is evidenced in other speleothem records in Europe like Villars
693 (Wainer et al., 2011), Sieben in the Alps (Moseley et al., 2015), and Abaliget cave in central Europe

694 (Koltai et al., 2017). Dryness over western Europe is also supported by an episode of intense loess
695 deposition in Rodderberg crater in northern Germany between 136-129 ka BP (Zhang et al., 2024). If
696 HS11 is also recorded in China speleothems (Wang et al., 2018), it appears subdued in the eastern
697 palynological Mediterranean records (Fig. 6), indicating that the Western Mediterranean region was
698 more severely impacted by the dry and cold pulse of HS11. The “W” shape of HS11 described in section
699 5.1 for the ODP 976 record matches well the Hulu cave record, where the particular event in the middle
700 of HS11 was linked with a strong Asian Monsoon episode that could represent an analogue to the
701 Bølling-Allerød during Termination I (Wang et al., 2018). The fast and multiphase vegetation and
702 climate dynamics evidenced in the ODP 976 record is in agreement with the description of a “HS11
703 complex” with multiple phases (Tzedakis et al., 2018), and will require more focused attention in the
704 future.

705 HS11 has been described as a “pause” in the glacial termination II (Gouzy et al., 2004; Hodge
706 et al., 2008). However, in the ODP 976 and MD01-2444 records, temperate vegetation keeps increasing
707 all along the event, despite the supposed cessation of the warming and moistening trend for almost
708 2000 years. Therefore, the trend toward increased temperate vegetation during Termination II did not
709 seem to be strongly affected by the abrupt arid event, following the continuous climate amelioration
710 described in various speleothem records from Italy covering Termination II, at Corchia cave, Tana che
711 Urla and Argentarola (Bard et al., 2002; Drysdale et al., 2005; Regattieri et al., 2014). On the contrary,
712 the Gitana Cave speleothem records a strong moisture deficit (Fig. 7, g), supporting a stronger impact
713 of HS11 in the SW Mediterranean compared to the Italian Peninsula.

714 Finally, it is to be pointed out that HS12, occurring around 140 ka BP (Lisiecki & Stern, 2016),
715 apparently did not have any imprint on the vegetation record of ODP 976, implying a subdued impact
716 of this event on Mediterranean vegetation compared to HS11.

717 5.5. Comparison of MIS 6 with the last glacial period (MIS 4-2)

718 Various studies have pointed out strong similarities between the millennial-scale oscillations
719 of the last glacial period and the penultimate glacial period, with the division between MIS 3 and MIS
720 2 being analogous to the early and mid-late phase of MIS 6 respectively (Held et al., 2024; Margari et
721 al., 2010, 2014; Roucoux et al., 2011; Rousseau et al., 2020; Shin et al., 2020; Sierro et al., 2020). The
722 same studies argued in favour of pervasive impact of stadial events on the continental climate and
723 vegetation in the Mediterranean region, even in absence of typical Heinrich layers (Roucoux et al.,
724 2011). The ODP 976 record shows a cooling and aridification trend during the first half of MIS 6 (Fig.
725 9), with decreasing intensity of interstadial events, that recalls the pattern of MIS 3 D-O cycles (Bond
726 et al., 1993).

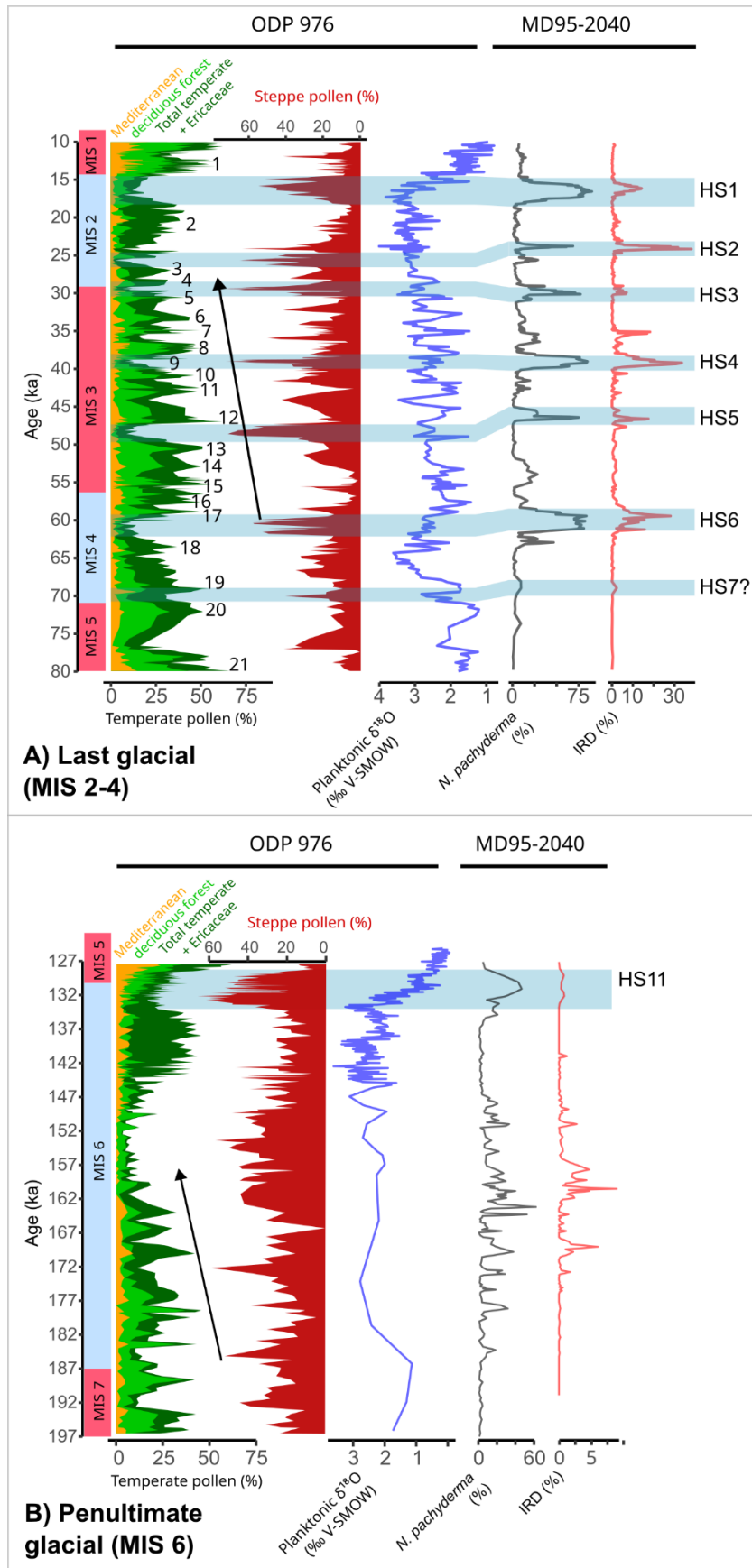


Fig. 9. Comparison of millennial-scale changes during A) the last glacial (MIS 2-4) and B) the penultimate glacial (MIS 6), including the main pollen data from ODP 976 (Charton et al., 2025; Combourieu-Nebout et al., 2002, 2009, and unpublished data for the last climatic cycle, and this

study for MIS 6), the ODP 976 planktonic isotopic ratio from *G. bulloides* (Combourieu-Nebout et al., 2002; Jiménez-Amat & Zahn, 2015; von Grafenstein et al., 1999, and unpublished data), and the *N. pachyderma* and IRD record from core MD95-2040 (de Abreu et al., 2003; Voelker and de Abreu, 2011). Marine Isotope Stages follow the boundaries from Lisiecki & Raymo (2005). Numbers on the Last Glacial correspond to the Greenland D-O events chronology (Fletcher et al., 2010a; Rasmussen et al., 2014). Black arrows mark the aridification trend and decreasing interstadials intensity during MIS 3 and early MIS 6.

727

728 However, the absence of clear successions of stadial events and especially Heinrich stadials,
729 together with the more subdued expression of interstadials in the vegetation record, limits the
730 resemblance between the two glacial periods. The pacing of interstadial peaks also seems to be
731 reduced compared to the last glacial period high-frequency oscillations, as previously highlighted from
732 the high-resolution speleothem record from Sofular cave in Turkey (Held et al., 2024).

733 A comparison of millennial-scale changes during the past two glacial periods based on the ODP
734 976 and MD95-2040 records, on either side of the Gibraltar Strait, supports our view (Fig. 9). The last
735 glacial period (encompassing MIS 4 to MIS 2) was characterized in the Alboran Sea by high-intensity
736 oscillations in both temperate and semi-desert vegetation correlated with D-O cycles and intense ice-
737 rafting events HE1 to HE7 in MD95-2040. During interstadial events, temperate and Mediterranean
738 vegetation (deciduous forest + Mediterranean + Ericaceae) could reach values above 60 % of total
739 pollen; during stadial events, the semi-desert pollen values reached values as high as 70% of total
740 pollen (during HS3, HS4 and HS5). In comparison, the penultimate glacial (MIS 6) displays much lower
741 intensity events, with interstadials characterized by 45% as a maximum value for temperate
742 vegetation, and stadials with 65% for the steppe and semi-desert vegetation (during HS11). High-
743 intensity cold episodes during MIS 6 are limited to the HS11, and the ~172 ka BP event. This is
744 consistent with the multiproxy record of core MD95-2040 on the Portuguese margin, which evidenced
745 reduced variability in the *N. pachyderma* abundance and IRD deposition during the penultimate glacial
746 compared to the last glacial (de Abreu et al., 2003; Voelker & de Abreu, 2011). The ice rafting episodes
747 appear to be of different nature during MIS 6 (Hodell et al., 2008; Liu et al., 2018; McCarron et al.,
748 2021), with the main iceberg discharges originating from the European ice sheet, contrary to the typical
749 Hudson Strait origin of the last glacial Heinrich layers. SST reconstructions in the western
750 Mediterranean also show less intense cooling during MIS 6 than during MIS 3 (Martrat et al., 2004,
751 2007), supporting limited incursions of polar waters in the Mediterranean during MIS 6 compared to
752 MIS 3 coldest stadials, and especially Heinrich stadials (Cacho et al., 1999).

753 Like ODP 976, Ioannina records lower intensity arboreal pollen oscillations during early MIS 6
754 compared to the last glacial (Roucoux et al., 2011). In comparison, the Atlantic pollen record from
755 MD01-2444 core displays similar amplitude of tree percentages during the last and the penultimate

756 glacial (Margari et al., 2010). This difference can be explained by the different climate conditions, and
757 the higher sensitivity to cold and aridity of sclerophyllous and deciduous forest vegetation on the
758 Mediterranean side, as recorded in the ODP 976 and Ioannina palynological sequence. It appears that
759 temperate vegetation in SW Mediterranean responded to millennial-scale climatic oscillations with
760 higher intensity during the last glacial compared to the penultimate, probably because the climate in
761 Europe was colder during MIS 6 compared to MIS 2. This is supported by larger European ice-sheet
762 extension during the penultimate glacial (Ehlers et al., 2011; Ehlers & Gibbard, 2007; Shackleton, 1987),
763 favouring the long-term establishment of open landscapes mainly composed by steppe and semi-
764 desert plants. The differences in humidity might not be as easily interpretable, with an early MIS 6
765 more humid, and a MIS 6 glacial maximum more arid, compared to MIS 3 and MIS 2 as also suggested
766 by the Ioannina record (Roucoux et al., 2011). Future climate reconstructions applied to the complete
767 last glacial cycle in ODP 976 and other Mediterranean long pollen sequences will help understanding
768 the different climate configurations between the last two glacial periods.

769 5.6. Human occupation during MIS 6 in SW Europe

770 Only a limited number of sites in South-Western Europe has yielded archaeological layers
771 attributed to MIS 6, and even fewer of them have been radiometrically dated allowing for a robust
772 comparison with the environmental changes (Fig. 10 and Supplements table S2). The environmental
773 proxies available in the archaeological layers (pollen, charcoal, macro and microfauna) can help the
774 chronological attribution, but are often insufficient to establish a precise correlation with the high-
775 resolution chrono-environmental framework of marine and glacial archives. Even when absolute dates
776 are available, their large uncertainty range and the poor resolution of the archaeological record
777 represent a major limitation and make it difficult to correlate the human occupation phases with a
778 specific substage of MIS 6.

779 It is generally accepted that the northern part of Europe was almost completely depopulated
780 during MIS 6, with very few sites identified compared to the southern European fringes, indicating
781 discontinuous occupation during more favourable climatic episodes (Hérisson et al., 2016) or total
782 abandonment like in the British lands (Scott, 2011; Shaw et al., 2016; White and Pettitt, 2011).
783 Southern France, Italy and the Iberian Peninsula could have represented climate refugia during the
784 most extreme ice-cap advances (Bicho and Carvalho, 2022). Notably, Italy is particularly deprived of
785 sites well-dated to MIS 6 (Fig. 10) including the isolated Neanderthal of Altamura, the short episode of
786 elephant scavenging at Poggetti Vecchi, and the long sequence of San Bernardino cave which
787 chronological range extends up to ~154 ka BP, a period marked by the most extensive glacial conditions
788 of MIS 6. Some other few archaeological layers have been attributed to MIS 6, but they lack a robust

789 chronological attribution (Aureli & Ronchitelli, 2018; Fontana et al., 2010, Fig. 10). One can hypothesise
 790 that regional climate conditions in the peninsula were particularly harsh after 150 ka, and that
 791 potential refugia sites remain to be identified in Italy. Palaeoecological reconstructions at the Poggetti
 792 Vecchi site indicated cold and dry open environment (Aranguren et al., 2019; Benvenuti et al., 2017).
 793 Interestingly, the chronological range for the site could coincide with a major stadial event at 171 ka
 794 BP identified in the ODP 976 core, and particularly well expressed in the Valle di Castiglione record (Fig.
 795 6).

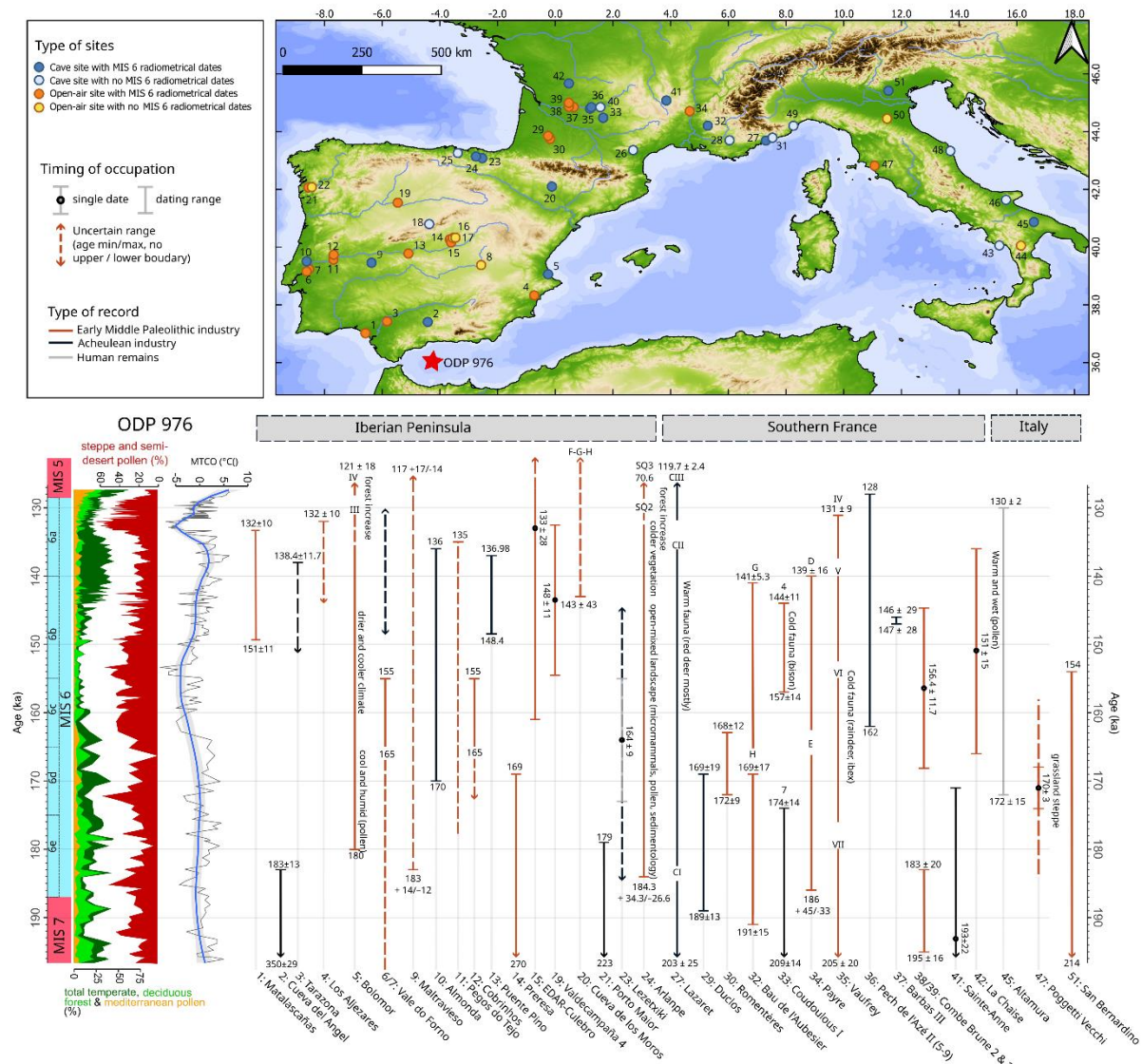


Fig. 10. Distribution of archaeological sites and radiometrically dated human occupation in western Mediterranean attributed to MIS 6, with some relevant palaeoecological information when available. The dates used and references can be found in Supplementary table S2. Sites on the map are numbered from south to north in each country: 1: Matalascañas ; 2: Cueva del Angel ; 3: Tarazona ; 4: Los Aljezares ; 5: Cueva del Bolomor ; 6: Vale do Forno ; 7: VF3 (Milharos) ; 8: El Provencio ; 9: Cueva de Maltravieso ; 10: Almonda ; 11: Pegos do Tejo ; 12: Cobrinhos ; 13: Puente Pino ; 14: Preresa ; 15: EDAR-Culebro 2 ; 16: Arriaga II/III ; 17: Arganda II (Valdocarros) ; 18: Villacastin ; 19: Valdecampana ; 20: Cueva de los Moros de Gabasa ; 21: Porto Maior ; 22 : Arbo ; 23: Lezetxiki ; 24: Arlanpe ; 27: Lazaret ; 29: Ducios ; 30: Romeneres ; 32: Bau de l'Audésier ; 33: Coudalouis I ; 34: Payre ; 35: Vaufrey ; 36: Feich de l'Avé II (5-9) ; 37: Barbas III ; 38: Combe Brunne 2 & ; 41: Poggetti Vecchi ; 42: La Chaise ; 45: Altamura ; 47: Poggetti Vecchi ; 51: San Bernardino

24 : Arlanpe ; **25**: Ventalaperra ; **26**: Aldènes ; **27** : Grotte du Lazaret ; **28** : Baume Bonne ; **29** : Duclos ; **30**: Romenteres ; **31**: Grotte du Prince ; **32**: Bau de l'Aubesier; **33**: Coudoulous I ; **34**: Payre ; **35**: Grotte Vaufrey ; **36** : Pech de l'Aze II ; **37**: Barbas III ; **38**: Combe Brune 3 ; **39**: Combe Brune 2 ; **40**: Grotte Sirogne; **41**: Sainte -Anne ; **42**: La Chaise ; **43**: Riparo del Poggio; **44**: Rosaneto; **45**: Altamura; **46**: Riparo Paglicci; **47**: Poggetti Vecchi ; **48**: Monte Conero; **49**: Grotta del Colombo; **50**: Due Pozzi/Scornetta; **51**: Grotta di San Bernardino.

796 In Southern France and the Iberian Peninsula, according to available radiometric dates, human
797 occupation appears to have been continuous across MIS 6, even during the glacial maximum, with both
798 cave and open-air sites. France provides a comparable number of cave and open-air sites mainly
799 concentrated in the southwestern region. The Portuguese record is mainly constituted by open-air
800 sites in fluvial terrace systems of the lower Tagus, offering important insights into short-term
801 occupations during the full-glacial stage, but with complex chronological attribution (Cunha et al.,
802 2012, 2017; Pereira et al., 2019). The Spanish record includes various open-air settlements in the upper
803 Tagus valley (Panera et al., 2011, 2014; Yravedra et al., 2019), as well as the Duero (Diez-Martín, 2010)
804 and the Guadalquivir (Caro Gómez et al., 2011) valleys. Cave sites are fewer and are mainly located
805 closer to the coast (Cueva del Bolomor, Cueva del Angel, Lezetxiki, Arlanpe, Ventalaperra), with the
806 two exceptions of Cueva de Maltravieso and Villacastín. Key sites like Lazaret Cave (Late Acheulean,
807 France) and Cueva del Bolomor (Middle Palaeolithic, Spain) evidence the persistence of human groups
808 in possible climate refugia (Ochando et al., 2019; Valensi et al., 2005).

809 MIS 6 in Europe saw the final stage of the cultural transition from the Lower to the Middle
810 Palaeolithic industries (MIS 8-5), mainly characterized by the emergence of more complex core
811 technologies such as Levallois debitage and changes in subsistence strategies. No rupture is observed
812 between the technocomplexes, as cultural diversity and the permanence of Acheulean bifacial tools
813 associated to technological innovation mark these Early Middle Palaeolithic industries in Southern
814 Europe (Santonja et al., 2016; Terradillos-Bernal et al., 2023). The distribution of archaeological sites
815 and timing of human occupation in South-Western Mediterranean at that time reflect this pattern (Fig.
816 10). A mosaic of traditional and innovative behavioural traits can be observed, with late Acheulean and
817 Early Middle Palaeolithic coexisting continuously (Cueto et al., 2016; de Lumley, 2018; Mathias et al.,
818 2020; Moncel et al., 2025; Santonja et al., 2022; Torres et al., 2024; Valensi et al., 2013). Acheulean
819 technocomplexes are progressively abandoned during MIS 6 in Europe (Álvarez-Alonso, 2014; Key et
820 al., 2021), with the latest chronologies found possibly in the Manzanares basin in central Iberia at
821 Arriaga sites (Panera et al., 2014; Rubio-Jara et al., 2016; Rubio-Jara and Panera, 2019; Silva et al.,
822 2013), or at Lazaret cave (Michel et al., 2022), and dated to the beginning of MIS 5. No clear explanation
823 is accepted for the emergence and generalization of the Levallois debitage, and while cognition might
824 not be the only factor, some authors suggested that MIS 6 glaciation could have played a role in the
825 final abandonment of Acheulean industries (Moncel et al., 2020; Valensi et al., 2005). It is hard to claim

826 that specific environmental pressures favoured Levallois technology over bifacial production, as these
827 lithic technologies seem to have co-existed in Western Europe since MIS 12-11 over several
828 glacial/interglacial cycles (Baena et al., 2017; Moncel et al., 2020), including extremely cold stages (like
829 MIS 12 and 10). This “mosaic” pattern for the Lower to Middle Palaeolithic transition, although at least
830 partly imputable to the large dating uncertainties, points toward more complex processes leading to
831 the generalization of Middle Palaeolithic industries from MIS 5. Interestingly, the end of the Lower to
832 Middle Palaeolithic transition is also associated with a shift in the morphology of human remains, from
833 “Early Neanderthals” (MIS 7-5) to “Classical Neanderthals” (MIS 5-3) (Di Vincenzo and Manzi, 2023).
834 Sites like La Chaise (Abri Suard), Lazaret and Altamura provide fossil evidence for these “Early
835 Neanderthals” which share characteristics with earlier Middle Pleistocene populations, and with later
836 Neanderthals (Buzi et al., 2025; Couture-Veschambre et al., 2021; de Lumley, 2018). Genetic data also
837 support an important population shift in western Europe sometimes around the transition from MIS 6
838 to MIS 5 (Peyrégne et al., 2019). Therefore, an important population reorganization seems to have
839 occurred at the time of the final Acheulean industries, leading to the onset of the so-called “Classical
840 neanderthal world” in western Eurasia, with generalized Middle Palaeolithic industries and established
841 Neanderthal morphological features. The role of environmental changes occurring during MIS 6 in this
842 population reorganization remains poorly understood.

843 Changes in land use and mobility pattern have been evidenced in north-central Iberia, and can
844 be viewed as adaptations to the severe climatic conditions of MIS 6 evidenced in the ODP 976 sequence
845 during pollen zone/phase 2: increasing mobility, more short-term occupations and reliance on more
846 local resources for subsistence strategies (Diez-Martín, 2010; Diez-Martín et al., 2008; Rios-Garaizar,
847 2016; Sánchez-Yustos, 2009). However, identifying cultural phases in the archaeological sequences
848 linked with specific climatic episodes is generally hindered by the poor resolution of the archaeological
849 record and chronological data. Among the sites identified in this synthesis, Lazaret and Bolomor caves
850 probably present the most informative and well-dated sequences with several archaeological layers
851 dated to MIS 6.

852 Cueva del Bolomor stands out in the Iberian Peninsula record as it provided an exceptionally
853 long and continuous record of human presence, and the oldest evidence of fire use in Spain during the
854 Middle Palaeolithic (Vidal-Matutano et al., 2019). Climate changes during MIS 6 documented in
855 Bolomor’s sediments through multiple proxies are consistent with the different phases identified in
856 the ODP 976 record, with a more humid and cool phase at the beginning of MIS 6, and the most arid
857 phase taking place at the middle of Phase III (layers X-VIII) (Arsuaga et al., 2012; Fernández Peris et al.,
858 2008). The site is described as a climatic refugium where Mediterranean vegetation persisted during
859 the colder phase of MIS 6 thanks to the coastal reservoir character of the site (Ochando et al., 2019).

860 No clear change in lithic production has been identified in the MIS 6 layers of Bolomor: according to
861 Fernández Peris et al. (2008), archaeological layers XII to VII (Phase III, MIS 6) are all dominated by
862 limestone flakes with few retouches, few recycling, and the presence non-Acheulean macro-lithic
863 elements. These layers are characterized by expeditive flaking (including Levallois *débitage*) relying on
864 local raw-material, pointing toward a high degree of mobility and search for immediate effectiveness.
865 It is thus hard to distinguish different techno-cultural tendencies during this phase. The most visible
866 change in the archaeological sequence occurs in layer VI (MIS 5) which shows an intensification of lithic
867 production dominated by flint, the production of more specialized tools including microlithic elements
868 and associated to more intense and stable occupation in the cave (Fernández Peris et al., 2008).
869 Therefore, a clear behavioural change in the technological and economical exploitation of raw
870 materials is identified at the beginning of MIS 5. Faunal remains show a large and constant diversity,
871 including abundant micro supporting both short-term and long-term not-specialized occupation, with
872 no clear change in the site's function across the sequence (Blasco et al., 2013).

873 Lazaret Cave, in south-eastern France, shows a very distinct scheme: the Lower to Middle
874 Palaeolithic transition is well documented in the archaeological sequence (Unit CII and CIII), with the
875 progressive replacement of large bifacial tools production by more standardized and smaller flakes
876 (Cauche, 2012). Levallois *débitage* is already present and well-mastered in the lower MIS 6 levels,
877 although rare, and becomes dominant in the upper levels (early MIS 5). Therefore, a subdivision of unit
878 CII can be made with a lower interval rich in handaxes, and an upper layer characterized as “final
879 Acheulean” with rare handaxes and more abundant flakes. Faunal assemblages are very constant
880 throughout MIS 6, with the large dominance of red deers and rare presence of cold species (*Rangifer*
881 *tarandus*, *Coelodonta antiquitatis*). Thus, the climatic oscillations of MIS 6 do not seem to have
882 influenced different hunting strategies or prey selection by human populations at Lazaret Cave, as large
883 game hunting of red deer prevailed (Valensi et al., 2013).

884 Therefore, Lazaret and Bolomor caves are examples of different strategies of site exploitation
885 and technological evolution during MIS 6: Lazaret Cave represents a specialized red-deer hunting camp
886 evidencing a progressive change from Lower to Middle Palaeolithic tools, while Cueva del Bolomor can
887 be characterized as a short-term camp with more generalized hunting and stable expeditive Middle
888 Palaeolithic industry. Despite these differences both sites provide evidence for a change in lithic
889 assemblages occurring at the end of MIS 6/ beginning of MIS 5: the disappearance of handaxes and
890 generalization of Levallois flakes in Lazaret, and the intensification and standardization of flint flakes
891 in Bolomor.

892 The fast climate dynamics during Termination II as evidenced in the ODP 976
893 paleoenvironmental record could have represented a critical period for human population. At the end
894 of MIS 6, more sites have been identified in the Iberian Peninsula than Southern France, showing the
895 latter could have represented a climate refugium at the time of maximum glacial expansion, with more
896 intense human occupation regionally. Many of these late MIS 6 sites present a chronological boundary
897 at the top of the sequence compatible with the onset of Termination II around 136 ka BP, and with
898 HS11, within the dating uncertainty: Matalascañas, Tarrazona, Los Aljezares, Bolomor Unit III,
899 Almonda, Pegos do Tejo, Puente Pino, Arlanpe Unit SQ2, Lazaret Unit CII, Payre layer D, Vauffrey unit
900 IV, and Pech de l'Azé II layer 5. The extreme character of this event in the South-Western
901 Mediterranean as expressed in the ODP 976 sequence could have put further environmental pressure
902 on hominin groups already diminished. A niche modelling approach based on 41 sites of Western
903 Eurasia since 145 ka BP has shown that the projected potential niche space for Neanderthals at the
904 end of MIS 6 (~145ka BP) was very reduced and concentrated in Western Europe (Yaworsky et al.,
905 2024). This coincides with the end of pollen zone/phase 2 in the ODP 976 record, the most cold and
906 arid phase of the penultimate Glacial before HS11. Then, the authors reconstruct a progressive
907 expansion of Neanderthal potential niche space between 145 and 130 ka, compatible with the climatic
908 warming and moistening during pollen zone/phase 3 in the ODP 976 record (Yaworsky et al., 2024).
909 The temporal resolution of the model (1000 years) does not allow to detect the impact of HS11 on the
910 niche projection, and only a small slowdown and decline of the projected niche is visible at ~130 ka BP,
911 before the MIS 5e optimum (Yaworsky et al., 2024, Fig. 5). A regional study focused on North-Western
912 Spain argued in favour of a demographic vacuum at the end of MIS 6, compatible with HS11 and leading
913 to a population reorganization implying contraction or micro-extinction, before the generalization of
914 Middle Palaeolithic industries during MIS 5 (Sánchez-Yustos and Díez-Martín, 2015). According to the
915 same authors, following this crisis, Neanderthal population entered a "reorganisation phase" leading
916 to demographical stability and more technological standardization, visible in the explosion of the
917 number of sites in Europe in general, especially after the MIS 5e climatic optimum (Bringmans, 2007;
918 Lewis et al., 2011; Wenzel, 2007). This statement is supported by niche modelling which shows a peak
919 in projected potential niche space of Neanderthal during MIS 5e (Yaworsky et al., 2024), and by recent
920 genetic data which provided evidence for at least two radiation events linked with the environmental
921 conditions of the last interglacial (Vernot et al., 2021), and Neanderthal population continuity since
922 ~120 ka BP (Peyrégne et al., 2019). Thus, HS11 did not lead to complete extinction of hominin groups
923 but might have induced deep demographical and technological reorganization, representing the first
924 and one of the most intense abrupt changes that Neanderthal population had to face in South-Western
925 Europe before the Last Glacial largest oscillations (HS6-4). According to this view, the emergence of
926 the "classical Neanderthal" world in Europe after the MIS 6/5 transition corresponds to the

927 initialization of dynamics of repeated population contraction and expansion in response to the Upper
928 Pleistocene instability, especially during MIS 4-2 (Sánchez-Yustos, 2009). This view is increasingly
929 supported by genetic data (Fotiadou et al., 2026). In that sense, the subdued environmental instability
930 during MIS 6 evidenced in the ODP site 976 record compared to the last glacial period (Section 5.5 and
931 Fig. 9) could also have implications for human populations, with less fragmented (although harsh)
932 habitats and more stable (although reduced) population during MIS 6. This hypothesis remains
933 however hard to test based on the very different nature and quality of preservation of the
934 archaeological record during MIS 6 compared to MIS 4-2 (e.g. Charton et al., 2025).

935 6. Conclusion

936 The ODP site 976 record sheds light on the environmental and climate changes during MIS 6 in
937 the SW Mediterranean. The sequence is characterized by the high representation of *Cedrus* and
938 Ericaceae pollen, resulting from the combined influence of African and Atlantic input respectively. ODP
939 976 position, at the confluence of Mediterranean versus Atlantic, and Eurasian versus African climatic
940 areas, is ideal to decipher the processes behind orbital and sub-orbital climate dynamics during past
941 glaciations. Three main phases have been distinguished during MIS 6 with different trends in
942 vegetation and climate changes. Millennial-scale oscillations are recorded especially during the early
943 part of MIS 6 (~187-166 ka BP) through the rapid increases of temperate and Mediterranean pollen,
944 some of which are similar to millennial-scale warming events identified in the ice-core and marine
945 temperature records, as well as other palynological sequences in the Mediterranean region. This Early
946 MIS 6 phase is characterized by overall warmer and wetter climate conditions, in agreement with other
947 paleoclimate archives in the Mediterranean showing enhanced moisture availability at the beginning
948 of MIS 6. This phase of enhanced moisture availability was likely connected with enhanced Asian and
949 African monsoon activity and was probably at the origin of the deposition of the Organic Rich Layer
950 607 in the Alboran Sea and sapropel S6 in the eastern Mediterranean. The second phase (165-144 ka
951 BP) shows the establishment of full glacial conditions in the Mediterranean, with the maximum spread
952 of steppe and semi-desert vegetation associated to cold and arid climate conditions and limited rapid
953 oscillations. Finally, the final stages of MIS 6 are marked by increased humidity and the development
954 of Ericaceae, with moderate millennial-scale oscillations seen in the vegetation record. Termination II
955 is very particular in the ODP 976 record, with the continuous increase of temperate and Mediterranean
956 vegetation being contemporaneous to a major episode of steppe expansion and aridity increase
957 identified as HS11. This event shows a particular three phases or “W” shape, in agreement with other
958 records, and had a major impact on the SW Mediterranean environments. A comparison with the
959 changes occurring during the last glacial period (MIS 4-2) inferred from the same core highlighted the
960 limited duration, frequency and intensity of MIS 6 millennial-scale climatic events compared to the last

961 Glacial D-O cycles and Heinrich Stadials (MIS 4-2). These results support a subdued impact of the
962 millennial-scale climatic oscillations on the continental vegetation in the Mediterranean region during
963 the Penultimate glaciation compared to the Last Glacial. The only exception is HS11, which stands out
964 by its notable intensity and duration and is of particular interest to understand the mechanisms behind
965 Termination II.

966 Human populations continuously inhabited the SW Mediterranean territory during MIS 6.
967 While few sites are available and robustly dated to MIS 6 in Italy, Southern France and the Iberian
968 Peninsula appear to have been intensely populated, supporting their nature of Pleistocene Climate
969 refugia. More ecological data from well-dated archaeological sites during MIS 6 would be needed to
970 increase the quality of human-environmental dynamics comparison. However, the synthesis drawn in
971 the present study highlights the extreme nature of events characterizing Termination II, and
972 particularly HS11, which could have represented an important environmental crisis for human
973 population at that time, catalysing the end of the Lower to Middle Palaeolithic Transition and the onset
974 of the “classical” Neanderthal world through a drastic population bottleneck.

975 7. Data availability

976 Pollen counts and climate reconstruction results from ODP 976 will be soon submitted to PANGAEA
977 data repository (<https://www.pangaea.de/>).

978 8. Supplements

979

980 The supplementary figures and tables related to this study can be downloaded at the following
981 link:

982 9. Author contribution

983

984 LC, NC, AB and VL designed the project. LC and NC carried out the palynological analyses. LC, OP
985 and MR applied the four methods of pollen-based climate reconstruction to the ODP 976 record. LC
986 and MHM led the archaeological synthesis. LC made the figures and wrote the text. All authors
987 contributed to improve the manuscript by their expertise.

988 10. Acknowledgments

989

990 We want to thank the three anonymous reviewers and the editor for their very helpful
991 comments on this manuscript. We acknowledge the International Ocean Drilling Project and the
992 MARUM Bremen Core Repository for making available the ODP 976 samples. The sample processing
993 was funded by the CNRS and the MNHN. We thank the European Research Council (ERC) under the

994 European Union's HORIZON1.1 research program (LATEUROPE project, grant agreement ID
995 101052653) for funding this publication. L. Charton doctoral contract was funded by the French
996 Ministère de l'Enseignement Supérieur et de la Recherche at the doctoral school ED 227 of the
997 Muséum National d'Histoire Naturelle, Paris. The international cotutorship with the University of
998 Florence is supported by the Ecole Franco-Italienne Vinci grant (project C2-166). We thank Lionel
999 Dubost for assistance in laboratory treatment of samples to HF. We are grateful to Francisco Sierro for
1000 sharing the isotopic data on AICC2012 timescale, to Jon Camuera for the pollen data from Padul and
1001 to Katherine Roucoux for the pollen data from Ioannina. This is an ISEM contribution.

1002

1003 11. References

1004

1005 de Abreu, L., Shackleton, N. J., Schönfeld, J., Hall, M., and Chapman, M.: Millennial-scale oceanic
1006 climate variability off the Western Iberian margin during the last two glacial periods, *Marine Geology*,
1007 196, 1–20, [https://doi.org/10.1016/S0025-3227\(03\)00046-X](https://doi.org/10.1016/S0025-3227(03)00046-X), 2003.

1008 Allen, J. R. M. and Huntley, B.: Last Interglacial palaeovegetation, palaeoenvironments and chronology:
1009 a new record from Lago Grande di Monticchio, southern Italy, *Quaternary Science Reviews*, 28, 1521–
1010 1538, <https://doi.org/10.1016/j.quascirev.2009.02.013>, 2009.

1011 Álvarez-Alonso, D.: First Neanderthal settlements in northern Iberia: The Acheulean and the
1012 emergence of Mousterian technology in the Cantabrian region, *Quaternary International*, 326–327,
1013 288–306, <https://doi.org/10.1016/j.quaint.2012.12.023>, 2014.

1014 Aranguren, B., Grimaldi, S., Benvenuti, M., Capalbo, C., Cavanna, F., Cavulli, F., Ciani, F., Comencini, G.,
1015 Giuliani, C., Grandinetti, G., Mariotti Lippi, M., Masini, F., Mazza, P. P. A., Pallecchi, P., Santaniello, F.,
1016 Savorelli, A., and Revedin, A.: Poggetti Vecchi (Tuscany, Italy): A late Middle Pleistocene case of
1017 human–elephant interaction, *Journal of Human Evolution*, 133, 32–60,
1018 <https://doi.org/10.1016/j.jhevol.2019.05.013>, 2019.

1019 Arsuaga, J. L., Fernández Peris, J., Gracia-Téllez, A., Quam, R., Carretero, J. M., Barciela González, V.,
1020 Blasco, R., Cuartero, F., and Sañudo, P.: Fossil human remains from Bolomor Cave (Valencia, Spain),
1021 *Journal of Human Evolution*, 62, 629–639, <https://doi.org/10.1016/j.jhevol.2012.02.002>, 2012.

1022 Auffret, G.-A., Pastouret, L., Chamley, H., and Lanoix, F.: Influence of the prevailing current regime on
1023 sedimentation in the Alboran Sea, *Deep Sea Research and Oceanographic Abstracts*, 21, 839–849,
1024 [https://doi.org/10.1016/0011-7471\(74\)90003-5](https://doi.org/10.1016/0011-7471(74)90003-5), 1974.

1025 Aureli, D. and Ronchitelli, A.: The Lower Tyrrhenian Versant: was it a techno-cultural area during the
1026 Middle Palaeolithic? Evolution of the lithic industries of the Riparo del Molare sequence in the frame
1027 of Neanderthal peopling dynamics in Italy, 59–94, 2018.

1028 Ayalon, A., Bar-Matthews, M., and Kaufman, A.: Climatic conditions during marine oxygen isotope
1029 stage 6 in the eastern Mediterranean region from the isotopic composition of speleothems of Soreq
1030 Cave, Israel, *Geology*, 30, [https://doi.org/10.1130/0091-7613\(2002\)030<0303:CCDMOI>2.0.CO;2](https://doi.org/10.1130/0091-7613(2002)030<0303:CCDMOI>2.0.CO;2),
1031 2002a.

- 1032 Ayalon, A., Bar-Matthews, M., and Kaufman, A.: Climatic conditions during marine oxygen isotope
1033 stage 6 in the eastern Mediterranean region from the isotopic composition of speleothems of Soreq
1034 Cave, Israel, *Geol*, 30, 303, [https://doi.org/10.1130/0091-7613\(2002\)030<0303:CCDMOI>2.0.CO;2](https://doi.org/10.1130/0091-7613(2002)030<0303:CCDMOI>2.0.CO;2),
1035 2002b.
- 1036 Baena, J., Moncel, M.-H., Cuartero, F., Chacón Navarro, M. G., and Rubio, D.: Late Middle Pleistocene
1037 genesis of Neanderthal technology in Western Europe: The case of Payre site (south-east France),
1038 *Quaternary International*, 436, 212–238, <https://doi.org/10.1016/j.quaint.2014.08.031>, 2017.
- 1039 Bailey, G., Carrión, J., Fa, D., Finlayson, C., Finlayson, G., and Vidal, J.: The coastal shelf of the
1040 Mediterranean and beyond: Corridor and refugium for human populations in the Pleistocene
1041 Introduction, *Quaternary Science Reviews*, 27, 2095–2099,
1042 <https://doi.org/10.1016/j.quascirev.2008.08.005>, 2008.
- 1043 Bajo, P., Drysdale, R. N., Woodhead, J. D., Hellstrom, J. C., Hodell, D., Ferretti, P., Voelker, A. H. L.,
1044 Zanchetta, G., Rodrigues, T., Wolff, E., Tyler, J., Frisia, S., Spötl, C., and Fallick, A. E.: Persistent influence
1045 of obliquity on ice age terminations since the Middle Pleistocene transition, *Science*, 367, 1235–1239,
1046 <https://doi.org/10.1126/science.aaw1114>, 2020.
- 1047 Barbante, C., Barnola, J.-M., Becagli, S., Beer, J., Bigler, M., Boutron, C., Blunier, T., Castellano, E.,
1048 Cattani, O., Chappellaz, J., Dahl-Jensen, D., Debret, M., Delmonte, B., Dick, D., Falourd, S., Faria, S.,
1049 Federer, U., Fischer, H., Freitag, J., Frenzel, A., Fritzsche, D., Fundel, F., Gabrielli, P., Gaspari, V.,
1050 Gersonde, R., Graf, W., Grigoriev, D., Hamann, I., Hansson, M., Hoffmann, G., Hutterli, M. A.,
1051 Huybrechts, P., Isaksson, E., Johnsen, S., Jouzel, J., Kaczmarzka, M., Karlin, T., Kaufmann, P., Kipfstuhl,
1052 S., Kohno, M., Lambert, F., Lambrecht, A., Lambrecht, A., Landais, A., Lawer, G., Leuenberger, M., Littot,
1053 G., Loulergue, L., Lüthi, D., Maggi, V., Marino, F., Masson-Delmotte, V., Meyer, H., Miller, H., Mulvaney,
1054 R., Narcisi, B., Oerlemans, J., Oerter, H., Parrenin, F., Petit, J.-R., Raisbeck, G., Raynaud, D.,
1055 Röthlisberger, R., Ruth, U., Rybak, O., Severi, M., Schmitt, J., Schwander, J., Siegenthaler, U., Siggaard-
1056 Andersen, M.-L., Spahni, R., Steffensen, J. P., Stenni, B., Stocker, T. F., Tison, J.-L., Traversi, R., Udisti,
1057 R., Valero-Delgado, F., van den Broeke, M. R., van de Wal, R. S. W., Wagenbach, D., Wegner, A., Weiler,
1058 K., Wilhelms, F., Winther, J.-G., Wolff, E., and EPICA Community Members: One-to-one coupling of
1059 glacial climate variability in Greenland and Antarctica, *Nature*, 444, 195–198,
1060 <https://doi.org/10.1038/nature05301>, 2006.
- 1061 Bard, E., Delaygue, G., Rostek, F., Antonioli, F., Silenzi, S., and Schrag, D. P.: Hydrological conditions
1062 over the western Mediterranean basin during the deposition of the cold Sapropel 6 (ca. 175 kyr BP),
1063 *Earth and Planetary Science Letters*, 202, 481–494, [https://doi.org/10.1016/S0012-821X\(02\)00788-4](https://doi.org/10.1016/S0012-821X(02)00788-4),
1064 2002a.
- 1065 Bard, E., Antonioli, F., and Silenzi, S.: Sea-level during the penultimate interglacial period based on a
1066 submerged stalagmite from Argentarola Cave (Italy), *Earth and Planetary Science Letters*, 196, 135–
1067 146, [https://doi.org/10.1016/S0012-821X\(01\)00600-8](https://doi.org/10.1016/S0012-821X(01)00600-8), 2002b.
- 1068 Barker, S. and Knorr, G.: Millennial scale feedbacks determine the shape and rapidity of glacial
1069 termination, *Nat Commun*, 12, 2273, <https://doi.org/10.1038/s41467-021-22388-6>, 2021.
- 1070 Barker, S., Knorr, G., Edwards, R. L., Parrenin, F., Putnam, A. E., Skinner, L. C., Wolff, E., and Ziegler, M.:
1071 800,000 Years of Abrupt Climate Variability, *Science*, 334, 347–351,
1072 <https://doi.org/10.1126/science.1203580>, 2011.
- 1073 Bayr, D., Plaza, M. P., Gilles, S., Kolek, F., Leier-Wirtz, V., Traidl-Hoffmann, C., and Damialis, A.: Pollen
1074 long-distance transport associated with symptoms in pollen allergics on the German Alps: An old story

- 1075 with a new ending?, *Sci Total Environ*, 881, 163310, <https://doi.org/10.1016/j.scitotenv.2023.163310>,
1076 2023.
- 1077 Bazin, L., Landais, A., Lemieux-Dudon, B., Toyé Mahamadou Kele, H., Veres, D., Parrenin, F., Martinerie,
1078 P., Ritz, C., Capron, E., Lipenkov, V., Loutre, M.-F., Raynaud, D., Vinther, B., Svensson, A., Rasmussen,
1079 S. O., Severi, M., Blunier, T., Leuenberger, M., Fischer, H., Masson-Delmotte, V., Chappellaz, J., and
1080 Wolff, E.: An optimized multi-proxy, multi-site Antarctic ice and gas orbital chronology (AICC2012):
1081 120–800 ka, *Climate of the Past*, 9, 1715–1731, <https://doi.org/10.5194/cp-9-1715-2013>, 2013.
- 1082 Benvenuti, M., Bahain, J.-J., Capalbo, C., Capretti, C., Ciani, F., D’Amico, C., Esu, D., Giachi, Gi., Giuliani,
1083 C., Gliozzi, E., Lazzeri, S., Macchioni, N., Lippi, M. M., Masini, F., Mazza, P. P. A., Pallecchi, P., Revedin,
1084 A., Savorelli, A., Spadi, M., Sozzi, L., Vietti, A., Voltaggio, M., and Aranguren, B.: Paleoenvironmental
1085 context of the early Neanderthals of Poggetti Vecchi for the late middle Pleistocene of Central Italy,
1086 *Quat. res.*, 88, 327–344, <https://doi.org/10.1017/qua.2017.51>, 2017.
- 1087 Bermúdez de Castro, J. M. and Martínón-Torres, M.: A new model for the evolution of the human
1088 Pleistocene populations of Europe, *Quaternary International*, 295, 102–112,
1089 <https://doi.org/10.1016/j.quaint.2012.02.036>, 2013.
- 1090 Bicho, N. and Carvalho, M.: Peninsular southern Europe refugia during the Middle Palaeolithic: an
1091 introduction, *J Quaternary Science*, 37, 133–135, <https://doi.org/10.1002/jqs.3410>, 2022.
- 1092 Bisschop, K., Mortier, F., Etienne, R. S., and Bonte, D.: Transient local adaptation and source–sink
1093 dynamics in experimental populations experiencing spatially heterogeneous environments,
1094 *Proceedings of the Royal Society B: Biological Sciences*, 286, 20190738,
1095 <https://doi.org/10.1098/rspb.2019.0738>, 2019.
- 1096 Blasco, R., Rosell, J., Fernández Peris, J., Arsuaga, J. L., Bermúdez de Castro, J. M., and Carbonell, E.:
1097 Environmental availability, behavioural diversity and diet: a zooarchaeological approach from the
1098 TD10-1 sublevel of Gran Dolina (Sierra de Atapuerca, Burgos, Spain) and Bolomor Cave (Valencia,
1099 Spain), *Quaternary Science Reviews*, 70, 124–144, <https://doi.org/10.1016/j.quascirev.2013.03.008>,
1100 2013.
- 1101 Bond, G., Heinrich, H., Broecker, W., Labeyrie, L., McManus, J., Andrews, J., Huon, S., Jantschik, R.,
1102 Clasen, S., Simet, C., Tedesco, K., Klas, M., Bonani, G., and Ivy, S.: Evidence for massive discharges of
1103 icebergs into the North Atlantic ocean during the last glacial period, *Nature*, 360, 245–249,
1104 <https://doi.org/10.1038/360245a0>, 1992.
- 1105 Bond, G., Broecker, W., Johnsen, S., McManus, J., Labeyrie, L., Jouzel, J., and Bonani, G.: Correlations
1106 between climate records from North Atlantic sediments and Greenland ice, *Nature*, 365, 143–147,
1107 <https://doi.org/10.1038/365143a0>, 1993.
- 1108 Bond, G., Showers, W., Cheseby, M., Lotti, R., Almasi, P., Demenocal, P., Priore, P., Cullen, H., Hajdas,
1109 I., and Bonani, G.: A pervasive millennial-scale cycle in the North Atlantic Holocene and glacial climates,
1110 *sci*, 278, 1257, <https://doi.org/10.1126/science.278.5341.1257>, 1997.
- 1111 Bond, G. C., Showers, W., Elliot, M., Evans, M., Lotti, R., Hajdas, I., Bonani, G., and Johnson, S.: The
1112 North Atlantic’s 1-2 kyr climate rhythm: Relation to Heinrich events, Dansgaard/Oeschger cycles and
1113 the Little Ice Age, *Washington DC American Geophysical Union Geophysical Monograph Series*, 112,
1114 35–58, <https://doi.org/10.1029/GM112p0035>, 1999.

- 1115 Boswell, S. M., Toucanne, S., Pitel-Roudaut, M., Creyts, T. T., Eynaud, F., and Bayon, G.: Enhanced
 1116 surface melting of the Fennoscandian Ice Sheet during periods of North Atlantic cooling, *Geology*, 47,
 1117 664–668, <https://doi.org/10.1130/G46370.1>, 2019.
- 1118 Bout-Roumazielles, V., Combourieu Nebout, N., Peyron, O., Cortijo, E., Landais, A., and Masson-
 1119 Delmotte, V.: Connection between South Mediterranean climate and North African atmospheric
 1120 circulation during the last 50,000yrBP North Atlantic cold events, *Quaternary Science Reviews*, 26,
 1121 3197–3215, <https://doi.org/10.1016/j.quascirev.2007.07.015>, 2007.
- 1122 ter Braak, C. and Juggins, S.: Weighted Averaging Partial Least Squares Regression (WA-PLS): An
 1123 Improved Method for Reconstructing Environmental Variables from Species Assemblages,
 1124 *Hydrobiologia*, 269–270, 485–502, <https://doi.org/10.1007/BF00028046>, 1993.
- 1125 Bradtmöller, M., Pastoors, A., Weninger, B., and Weniger, G.-C.: The repeated replacement model –
 1126 Rapid climate change and population dynamics in Late Pleistocene Europe, *Quaternary International*,
 1127 247, 38–49, <https://doi.org/10.1016/j.quaint.2010.10.015>, 2012.
- 1128 Brauer, A., Allen, J. R. M., Mingram, J., Dulski, P., Wulf, S., and Huntley, B.: Evidence for last interglacial
 1129 chronology and environmental change from Southern Europe, *Proceedings of the National Academy
 1130 of Sciences*, 104, 450–455, <https://doi.org/10.1073/pnas.0603321104>, 2007.
- 1131 Bringmans, P.: First Evidence of Neanderthal Presence in Northwest Europe during the Late Saalian
 1132 “Zeifen Interstadial” (MIS 6.01) found at the VLL and VLB Sites at Veldwezelt-Hezerwater, Belgium,
 1133 *Journal of Archaeology of Northwest Europe*, 1, 2007.
- 1134 Broecker, W. S. and Henderson, G. M.: The sequence of events surrounding Termination II and their
 1135 implications for the cause of glacial-interglacial CO₂ changes, *Paleoceanography*, 13, 352–364, 1998.
- 1136 Burns, S. J., Welsh, L. K., Scroxton, N., Cheng, H., and Edwards, R. L.: Millennial and orbital scale
 1137 variability of the South American Monsoon during the penultimate glacial period, *Sci Rep*, 9, 1234,
 1138 <https://doi.org/10.1038/s41598-018-37854-3>, 2019.
- 1139 Buzi, C., Profico, A., Lorenzo, C., and Manzi, G.: The first preserved nasal cavity in the human fossil
 1140 record: The Neanderthal from Altamura, *Proceedings of the National Academy of Sciences*, 122,
 1141 e2426309122, <https://doi.org/10.1073/pnas.2426309122>, 2025.
- 1142 Cacho, I., Grimalt, J. O., Pelejero, C., Canals, M., Sierro, F. J., Flores, J. A., and Shackleton, N.: Dansgaard-
 1143 Oeschger and Heinrich event imprints in Alboran Sea paleotemperatures, *Paleoceanography*, 14, 698–
 1144 705, <https://doi.org/10.1029/1999PA900044>, 1999.
- 1145 Cacho, I., Shackleton, N., Elderfield, H., Sierro, F. J., and Grimalt, J. O.: Glacial rapid variability in deep-
 1146 water temperature and $\delta^{18}O$ from the Western Mediterranean Sea, *Quaternary Science Reviews*, 25,
 1147 3294–3311, <https://doi.org/10.1016/j.quascirev.2006.10.004>, 2006.
- 1148 Camuera, J., Jiménez-Moreno, G., Ramos-Román, M. J., García-Alix, A., Toney, J. L., Anderson, R. S.,
 1149 Jiménez-Espejo, F., Bright, J., Webster, C., Yanes, Y., and Carrión, J. S.: Vegetation and climate changes
 1150 during the last two glacial-interglacial cycles in the western Mediterranean: A new long pollen record
 1151 from Padul (southern Iberian Peninsula), *Quaternary Science Reviews*, 205, 86–105,
 1152 <https://doi.org/10.1016/j.quascirev.2018.12.013>, 2019.
- 1153 Camuera, J., Ramos-Román, M. J., Jiménez-Moreno, G., García-Alix, A., Ilvonen, L., Ruha, L., Gil-Romera,
 1154 G., González-Sampériz, P., and Seppä, H.: Past 200 kyr hydroclimate variability in the western

- 1155 Mediterranean and its connection to the African Humid Periods, *Sci Rep*, 12, 9050,
1156 <https://doi.org/10.1038/s41598-022-12047-1>, 2022.
- 1157 Caro Gómez, J. A., Díaz Del Olmo, F., Artigas, R. C., Recio Espejo, J. M., and Barrera, C. B.:
1158 Geoarchaeological alluvial terrace system in Tarazona: Chronostratigraphical transition of Mode 2 to
1159 Mode 3 during the middle-upper pleistocene in the Guadalquivir River valley (Seville, Spain),
1160 *Quaternary International*, 243, 143–160, <https://doi.org/10.1016/j.quaint.2011.04.022>, 2011.
- 1161 Chapman, M. R. and Shackleton, N. J.: Global ice-volume fluctuations, North Atlantic ice-rafting events,
1162 and deep-ocean circulation changes between 130 and 70 ka, *Geology*, 27, 795,
1163 [https://doi.org/10.1130/0091-7613\(1999\)027<0795:GIVFNA>2.3.CO;2](https://doi.org/10.1130/0091-7613(1999)027<0795:GIVFNA>2.3.CO;2), 1999.
- 1164 Chappellaz, J., Brook, E., Blunier, T., and Malaizé, B.: CH₄ and δ¹⁸O of O₂ records from Antarctic and
1165 Greenland ice: A clue for stratigraphic disturbance in the bottom part of the Greenland Ice Core Project
1166 and the Greenland Ice Sheet Project 2 ice cores, *J. Geophys. Res.*, 102, 26547–26557,
1167 <https://doi.org/10.1029/97JC00164>, 1997.
- 1168 Charton, L., Combourieu-Nebout, N., Bertini, A., Lebreton, V., Peyron, O., Robles, M., Sassoon, D., and
1169 Moncel, M.-H.: Vegetation and climate changes during the Middle to Upper Palaeolithic transition in
1170 the southwestern Mediterranean: What happened to the last Neanderthals during Heinrich stadial 4?,
1171 *Quaternary Science Reviews*, 359, 109345, <https://doi.org/10.1016/j.quascirev.2025.109345>, 2025.
- 1172 Cheddadi, R. and Rossignol-Strick, M.: Eastern Mediterranean Quaternary paleoclimates from pollen
1173 and isotope records of marine cores in the Nile Cone Area, *Paleoceanography*, 10, 291–300,
1174 <https://doi.org/10.1029/94PA02672>, 1995.
- 1175 Cheng, H., Edwards, R. L., Wang, Y., Kong, X., Ming, Y., Kelly, M. J., Wang, X., Gallup, C. D., and Liu, W.:
1176 A penultimate glacial monsoon record from Hulu Cave and two-phase glacial terminations, *Geology*,
1177 34, 217–220, <https://doi.org/10.1130/G22289.1>, 2006.
- 1178 Chevalier, M., Davis, B. A. S., Heiri, O., Seppä, H., Chase, B. M., Gajewski, K., Lacourse, T., Telford, R. J.,
1179 Finsinger, W., Guiot, J., Kühl, N., Maezumi, S. Y., Tipton, J. R., Carter, V. A., Brussel, T., Phelps, L. N.,
1180 Dawson, A., Zanon, M., Vallé, F., Nolan, C., Mauri, A., de Vernal, A., Izumi, K., Holmström, L., Marsicek,
1181 J., Goring, S., Sommer, P. S., Chaput, M., and Kupriyanov, D.: Pollen-based climate reconstruction
1182 techniques for late Quaternary studies, *Earth-Science Reviews*, 210,
1183 <https://doi.org/10.1016/j.earscirev.2020.103384>, 2020.
- 1184 Colleoni, F., Wekerle, C., Näslund, J.-O., Brandefelt, J., and Masina, S.: Constraint on the penultimate
1185 glacial maximum Northern Hemisphere ice topography (≈140 kyrs BP), *Quaternary Science Reviews*,
1186 137, 97–112, <https://doi.org/10.1016/j.quascirev.2016.01.024>, 2016.
- 1187 Combourieu-Nebout, N., Turon, J. L., Zahn, R., Capotondi, L., Londeix, L., and Pahnke, K.: Enhanced
1188 aridity and atmospheric high-pressure stability over the western Mediterranean during the North
1189 Atlantic cold events of the past 50 k.y., *Geol*, 30, 863, [https://doi.org/10.1130/0091-7613\(2002\)030<0863:EAAAHP>2.0.CO;2](https://doi.org/10.1130/0091-7613(2002)030<0863:EAAAHP>2.0.CO;2), 2002.
- 1191 Combourieu-Nebout, N., Peyron, O., Dormoy, I., Desprat, S., Célia, B., Kotthoff, U., and Marret, F.:
1192 Rapid climatic variability in the west Mediterranean during the last 25 000 years from high resolution
1193 pollen data, *Climate of the Past*, 5, <https://doi.org/10.5194/cpd-5-671-2009>, 2009.
- 1194 Cortina, A., Sierro, F. J., Flores, J. A., Martrat, B., and Grimalt, J. O.: The response of SST to insolation
1195 and ice sheet variability from MIS 3 to MIS 11 in the northwestern Mediterranean Sea (Gulf of Lions),
1196 *Geophysical Research Letters*, 42, 10,366-10,374, <https://doi.org/10.1002/2015GL065539>, 2015.

- 1197 Couture-Veschambre, C., López-Onaindia, D., Sala, N., Arlegi, M., Balzeau, A., Crevecoeur, I., Maureille,
1198 B., Tournepiche, J.-F., and Gómez-Olivencia, A.: Reassessment of the Neandertal fossil collection from
1199 Abri Suard (La Chaise de Vouthon, Charente, France), *Bulletins et mémoires de la Société*
1200 *d'Anthropologie de Paris. BMSAP*, 33, <https://doi.org/10.4000/bmsap.6982>, 2021.
- 1201 Cueto, S., Preysler, J., Pérez-González, A., Torres, C., Pérez, I., and Miguel, J.: Acheulian flint quarries in
1202 the Madrid Tertiary basin, central Iberian Peninsula: First data obtained from geoarchaeological
1203 studies, *Quaternary International*, 411, <https://doi.org/10.1016/j.quaint.2016.01.041>, 2016.
- 1204 Cunha, P. P., Almeida, N. A. C., Aubry, T., Martins, A. A., Murray, A. S., Buylaert, J.-P., Sohbaty, R.,
1205 Raposo, L., and Rocha, L.: Records of human occupation from Pleistocene river terrace and aeolian
1206 sediments in the Arneiro depression (Lower Tejo River, central eastern Portugal), *Geomorphology*,
1207 165–166, 78–90, <https://doi.org/10.1016/j.geomorph.2012.02.017>, 2012.
- 1208 Cunha, P. P., Martins, A. A., Buylaert, J.-P., Murray, A. S., Raposo, L., Mozzi, P., and Stokes, M.: New
1209 data on the chronology of the Vale do Forno sedimentary sequence (Lower Tejo River terrace staircase)
1210 and its relevance as a fluvial archive of the Middle Pleistocene in western Iberia, *Quaternary Science*
1211 *Reviews*, 166, 204–226, <https://doi.org/10.1016/j.quascirev.2016.11.001>, 2017.
- 1212 Damialis, A., Kaimakamis, E., Konoglou, M., Akritidis, I., Traidl-Hoffmann, C., and Gioulekas, D.:
1213 Estimating the abundance of airborne pollen and fungal spores at variable elevations using an aircraft:
1214 how high can they fly?, *Sci Rep*, 7, 44535, <https://doi.org/10.1038/srep44535>, 2017.
- 1215 Dansgaard, W., Johnsen, S. J., Clausen, H. B., Dahl-Jensen, D., Gundestrup, N. S., Hammer, C. U.,
1216 Hvidberg, C. S., Steffensen, J. P., Sveinbjörnsdóttir, A. E., and Jouzel, J.: Evidence for general instability
1217 of past climate from a 250-kyr ice-core record, *Nature*, 364, 218–220, 1993.
- 1218 Davtian, N. and Bard, E.: A new view on abrupt climate changes and the bipolar seesaw based on
1219 paleotemperatures from Iberian Margin sediments, *Proceedings of the National Academy of Sciences*,
1220 120, e2209558120, <https://doi.org/10.1073/pnas.2209558120>, 2023.
- 1221 Dennell, R. W., Martín-Torres, M., and Bermúdez de Castro, J. M.: Hominin variability, climatic
1222 instability and population demography in Middle Pleistocene Europe, *Quaternary Science Reviews*, 30,
1223 1511–1524, <https://doi.org/10.1016/j.quascirev.2009.11.027>, 2011.
- 1224 D'Errico, F. and Sánchez Goñi, M. F. S.: Neandertal extinction and the millennial scale climatic variability
1225 of OIS 3, *Quaternary Science Reviews*, 22, 769–788, [https://doi.org/10.1016/S0277-3791\(03\)00009-X](https://doi.org/10.1016/S0277-3791(03)00009-X),
1226 2003.
- 1227 Di Vincenzo, F. and Manzi, G.: *Homo heidelbergensis* as the Middle Pleistocene common ancestor of
1228 Denisovans, Neanderthals and modern humans, *Journal of Mediterranean Earth Sciences*, Vol. 15
1229 (2023): In progress, <https://doi.org/10.13133/2280-6148/18074>, 2023.
- 1230 Díez-Martín, F.: Evaluating the effect of plowing on the archaeological record: The early middle
1231 palaeolithic in the river Duero basin plateaus (north-central Spain), *Quaternary International*, 214, 30–
1232 43, <https://doi.org/10.1016/j.quaint.2009.10.024>, 2010.
- 1233 Díez-Martín, F., Sánchez-Yustos, P., Gómez-González, J. Á., and Gómez De La Rúa, D.: Earlier
1234 Palaeolithic Settlement Patterns: Landscape Archaeology on the River Duero Basin Plateaus (Castilla y
1235 León, Spain), *J World Prehist*, 21, 103–137, <https://doi.org/10.1007/s10963-008-9012-0>, 2008.
- 1236 D'Oliveira, L., Dugerdil, L., Ménot, G., Evin, A., Muller, S., Ansanay-Alex, S., Azuara, J., Bonnet, C.,
1237 Bremond, L., Shah, M., and Peyron, O.: Reconstructing 15 000 years of southern France temperatures

- 1238 from coupled pollen and molecular (branched glycerol dialkyl glycerol tetraether) markers (Canroute,
1239 Massif Central), *Climate of the Past*, 19, 2127–2156, <https://doi.org/10.5194/cp-19-2127-2023>, 2023.
- 1240 Drysdale, R. N., Zanchetta, G., Hellstrom, J. C., Fallick, A. E., and Zhao, J.: Stalagmite evidence for the
1241 onset of the Last Interglacial in southern Europe at 129 ± 1 ka, *Geophysical Research Letters*, 32,
1242 <https://doi.org/10.1029/2005GL024658>, 2005.
- 1243 Ehlers, J. and Gibbard, P. L.: The extent and chronology of Cenozoic Global Glaciation, *Quaternary*
1244 *International*, 164–165, 6–20, <https://doi.org/10.1016/j.quaint.2006.10.008>, 2007.
- 1245 Ehlers, J., Grube, A., Stephan, H.-J., and Wansa, S.: Pleistocene Glaciations of North Germany—New
1246 Results, in: *Developments in Quaternary Sciences*, vol. 15, Elsevier, 149–162,
1247 <https://doi.org/10.1016/B978-0-444-53447-7.00013-1>, 2011.
- 1248 Ehlers, J., Gibbard, P. L., and Hughes, P. D.: Chapter 4 - Quaternary Glaciations and Chronology, in: *Past*
1249 *Glacial Environments (Second Edition)*, edited by: Menzies, J. and van der Meer, J. J. M., Elsevier, 77–
1250 101, <https://doi.org/10.1016/B978-0-08-100524-8.00003-8>, 2018.
- 1251 Emeis, K., Schulz, H., Struck, U., Rossignol-Strick, M., Erlenkeuser, H., Howell, M., Kroon, D.,
1252 Mackensen, A., Ishizuka, S., Oba, T., Sakamoto, T., and Koizumi, I.: Eastern Mediterranean surface
1253 water temperatures and $\delta^{18}O$ composition during deposition of sapropels in the late Quaternary,
1254 *Paleoceanography*, 18, 1005, <https://doi.org/10.1029/2000PA000617>, 2003a.
- 1255 Eynaud, F., Zaragosi, S., Scourse, J. D., Mojtahid, M., Bourillet, J. F., Hall, I. R., Penaud, A., Locascio, M.,
1256 and Reijonen, A.: Deglacial laminated facies on the NW European continental margin: The
1257 hydrographic significance of British-Irish Ice Sheet deglaciation and Fleuve Manche paleoriver
1258 discharges, *Geochemistry, Geophysics, Geosystems*, 8, <https://doi.org/10.1029/2006GC001496>, 2007.
- 1259 Faegri, K. and Iversen, J.: *Textbook of Pollen Analysis*, 4th Edition., John Wiley and Sons, Chichester,
1260 UK, 338 pp., 1964.
- 1261 Fernández Peris, J., Barciela, V., Blasco, R., Cuartero, F., and Sañudo, P.: El Paleolítico Medio en el
1262 territorio valenciano y la variabilidad tecno-económica de la Cova del Bolomor, *Treballs d'Arqueologia*,
1263 141–169, 2008.
- 1264 Fernández-Rodríguez, S., Skjøth, C. A., Tormo-Molina, R., Brandao, R., Caeiro, E., Silva-Palacios, I.,
1265 Gonzalo-Garijo, A., and Smith, M.: Identification of potential sources of airborne *Olea* pollen in the
1266 Southwest Iberian Peninsula, *Int J Biometeorol*, 58, 337–348, <https://doi.org/10.1007/s00484-012-0629-4>, 2014.
- 1268 Finlayson, C. and Carrión, J. S.: Rapid ecological turnover and its impact on Neanderthal and other
1269 human populations, *Trends in Ecology & Evolution*, 22, 213–222,
1270 <https://doi.org/10.1016/j.tree.2007.02.001>, 2007.
- 1271 Fletcher, W. J. and Sánchez Goñi, M. F.: Orbital- and sub-orbital-scale climate impacts on vegetation of
1272 the western Mediterranean basin over the last 48,000 yr, *Quaternary Research*, 70, 451–464,
1273 <https://doi.org/10.1016/j.yqres.2008.07.002>, 2008.
- 1274 Fletcher, W. J., Sánchez Goñi, M. F., Allen, J. R. M., Cheddadi, R., Combourieu-Nebout, N., Huntley, B.,
1275 Lawson, I., Londeix, L., Magri, D., Margari, V., Müller, U. C., Naughton, F., Novenko, E., Roucoux, K., and
1276 Tzedakis, P. C.: Millennial-scale variability during the last glacial in vegetation records from Europe,
1277 *Quaternary Science Reviews*, 29, 2839–2864, <https://doi.org/10.1016/j.quascirev.2009.11.015>, 2010.

- 1278 Foerster, V., Asrat, A., Bronk Ramsey, C., Brown, E. T., Chapot, M. S., Deino, A., Duesing, W., Grove, M.,
 1279 Hahn, A., Junginger, A., Kaboth-Bahr, S., Lane, C. S., Opitz, S., Noren, A., Roberts, H. M., Stockhecke,
 1280 M., Tiedemann, R., Vidal, C. M., Vogelsang, R., Cohen, A. S., Lamb, H. F., Schaebitz, F., and Trauth, M.
 1281 H.: Pleistocene climate variability in eastern Africa influenced hominin evolution, *Nat Geosci*, 15, 805–
 1282 811, <https://doi.org/10.1038/s41561-022-01032-y>, 2022.
- 1283 Follieri, M., Magri, D., and Sadori, L.: A 250 000-years pollen record from Valle di Castiglione (Roma),
 1284 *Pollen et Spores*, 30, 329–356, 1988.
- 1285 Fontana, F., Nenzioni, G., and Peretto, C.: The southern Po plain area (Italy) in the mid-late Pleistocene:
 1286 Human occupation and technical behaviours, *Quaternary International*, 223, 465–471,
 1287 <https://doi.org/10.1016/j.quaint.2010.02.013>, 2010.
- 1288 Fotiadou, C. M., Pedersen, J. B., Rougier, H., Roksandic, M., Spyrou, M. A., Nägele, K., Reiter, E.,
 1289 Bocherens, H., Kandel, A. W., Haidle, M. N., Streicher, T. P., Conard, N. J., Schilt, F., Godinho, R. M.,
 1290 Uthmeier, T., Doyon, L., Semal, P., Krause, J., Barbieri, A., Mihailović, D., Crevecoeur, I., and Posth, C.:
 1291 Archaeogenetic insights into the demographic history of Late Neanderthals, *Proceedings of the*
 1292 *National Academy of Sciences*, 123, e2520565123, <https://doi.org/10.1073/pnas.2520565123>, 2026.
- 1293 Gouzy, A., Malaizé, B., Pujol, C., and Charlier, K.: Climatic “pause” during Termination II identified in
 1294 shallow and intermediate waters off the Iberian margin, *Quaternary Science Reviews*, 23, 1523–1528,
 1295 <https://doi.org/10.1016/j.quascirev.2004.03.002>, 2004.
- 1296 von Grafenstein, R., Zahn, R., and Tiedemann, R.: Planktonic d18O records at Sites 976 and 977,
 1297 Alboran Sea: stratigraphy, forcing, and paleoceanographic implications. In Curry, W.B., Shackleton,
 1298 N.J., and Richter, C, *Proceedings Ocean Drilling Program Scientific Results*, 154, 299–318, 1999.
- 1299 Guiot, J.: Methodology of the last climatic cycle reconstruction in France from pollen data,
 1300 *Palaeogeography, Palaeoclimatology, Palaeoecology*, 80, 49–69, [https://doi.org/10.1016/0031-](https://doi.org/10.1016/0031-0182(90)90033-4)
 1301 [0182\(90\)90033-4](https://doi.org/10.1016/0031-0182(90)90033-4), 1990.
- 1302 Guiot, J., Pons, A., De Beaulieu, J. L., and Reille, M.: A 140,000-year continental climate reconstruction
 1303 from two European pollen records, *Nature*, 338, 309–313, <https://doi.org/10.1038/338309a0>, 1989.
- 1304 Guiot, J., De Beaulieu, J. L., Cheddadi, R., David, F., Ponel, P., and Reille, M.: The climate in Western
 1305 Europe during the last Glacial/Interglacial cycle derived from pollen and insect remains,
 1306 *Palaeogeography, Palaeoclimatology, Palaeoecology*, 103, 73–93, [https://doi.org/10.1016/0031-](https://doi.org/10.1016/0031-0182(93)90053-L)
 1307 [0182\(93\)90053-L](https://doi.org/10.1016/0031-0182(93)90053-L), 1993.
- 1308 Heinrich, H.: Origin and Consequences of Cyclic Ice Rafting in the Northeast Atlantic Ocean During the
 1309 Past 130,000 Years, *Quaternary Research*, 29, 142–152, [https://doi.org/10.1016/0033-](https://doi.org/10.1016/0033-5894(88)90057-9)
 1310 [5894\(88\)90057-9](https://doi.org/10.1016/0033-5894(88)90057-9), 1988.
- 1311 Held, F., Cheng, H., Edwards, R. L., Tüysüz, O., Koç, K., and Fleitmann, D.: Dansgaard-Oeschger cycles
 1312 of the penultimate and last glacial period recorded in stalagmites from Türkiye, *Nat Commun*, 15, 1183,
 1313 <https://doi.org/10.1038/s41467-024-45507-5>, 2024.
- 1314 Hemming, S. R.: Heinrich events: Massive late Pleistocene detritus layers of the North Atlantic and
 1315 their global climate imprint, *Reviews of Geophysics*, 42, <https://doi.org/10.1029/2003RG000128>,
 1316 2004.
- 1317 Hérisson, D., Brenet, M., Cliquet, D., Moncel, M.-H., Richter, J., Scott, B., Van Baelen, A., Di Modica, K.,
 1318 Loecker, D., Ashton, N., Bourguignon, L., Delagnes, A., Faivre, J.-P., Folgado-Lopez, M., Loch, J.-L.,

- 1319 Pope, M., Raynal, J.-P., Roebroeks, W., Santagata, C., and Peer, P.: The emergence of the Middle
1320 Palaeolithic in north-western Europe and its southern fringes, *Quaternary International*, 411,
1321 <https://doi.org/10.1016/j.quaint.2016.02.049>, 2016.
- 1322 Hersbach, H., Bell, B., Berrisford, P., Hirahara, S., Horányi, A., Muñoz-Sabater, J., Nicolas, J., Peubey, C.,
1323 Radu, R., Schepers, D., Simmons, A., Soci, C., Abdalla, S., Abellan, X., Balsamo, G., Bechtold, P., Biavati,
1324 G., Bidlot, J., Bonavita, M., De Chiara, G., Dahlgren, P., Dee, D., Diamantakis, M., Dragani, R., Flemming,
1325 J., Forbes, R., Fuentes, M., Geer, A., Haimberger, L., Healy, S., Hogan, R. J., Hólm, E., Janisková, M.,
1326 Keeley, S., Laloyaux, P., Lopez, P., Lupu, C., Radnoti, G., de Rosnay, P., Rozum, I., Vamborg, F., Villaume,
1327 S., and Thépaut, J.-N.: The ERA5 global reanalysis, *Quarterly Journal of the Royal Meteorological*
1328 *Society*, 146, 1999–2049, <https://doi.org/10.1002/qj.3803>, 2020.
- 1329 Hodell, D. A., Channell, J. E. T., Curtis, J. H., Romero, O. E., and Röhl, U.: Onset of “Hudson Strait”
1330 Heinrich events in the eastern North Atlantic at the end of the middle Pleistocene transition (~640
1331 ka)?, *Paleoceanography*, 23, 2008PA001591, <https://doi.org/10.1029/2008PA001591>, 2008.
- 1332 Hodell, D. A., Crowhurst, S. J., Lourens, L., Margari, V., Nicolson, J., Rolfe, J. E., Skinner, L. C., Thomas,
1333 N. C., Tzedakis, P. C., Mleneck-Vautravets, M. J., and Wolff, E. W.: A 1.5-million-year record of orbital
1334 and millennial climate variability in the North Atlantic, *Clim. Past*, 19, 607–636,
1335 <https://doi.org/10.5194/cp-19-607-2023>, 2023.
- 1336 Hodge, E., Richards, D., Smart, P., Andreo, B., Hoffmann, D., Matthey, D., and González-Ramón, A.:
1337 Effective precipitation in southern Spain (~ 266 to 46 ka) based on a speleothem stable carbon isotope
1338 record, *Quaternary Research*, 69, 447–457, <https://doi.org/10.1016/j.yqres.2008.02.013>, 2008.
- 1339 Hublin, J. J.: The origin of Neandertals, *Proceedings of the National Academy of Sciences*, 106, 16022–
1340 16027, <https://doi.org/10.1073/pnas.0904119106>, 2009.
- 1341 Jiménez-Amat, P. and Zahn, R.: Offset timing of climate oscillations during the last two glacial-
1342 interglacial transitions connected with large-scale freshwater perturbation, *Paleoceanography*, 30,
1343 768–788, <https://doi.org/10.1002/2014PA002710>, 2015.
- 1344 Jiménez-Moreno, G., Anderson, R. S., Ramos-Román, M. J., Camuera, J., Mesa-Fernández, J. M., García-
1345 Alix, A., Jiménez-Espejo, F. J., Carrión, J. S., and López-Avilés, A.: The Holocene *Cedrus* pollen record
1346 from Sierra Nevada (S Spain), a proxy for climate change in N Africa, *Quaternary Science Reviews*, 242,
1347 106468, <https://doi.org/10.1016/j.quascirev.2020.106468>, 2020.
- 1348 Johnsen, S. J., Clausen, H. B., Dansgaard, W., Fuhrer, K., Gundestrup, N., Hammer, C. U., Iversen, P.,
1349 Jouzel, J., Stauffer, B., and Steffensen, J. P.: Irregular glacial interstadials recorded in a new Greenland
1350 record, *Nature*, 359, 311–313, 1992.
- 1351 Jouzel, J., Masson-Delmotte, V., Cattani, O., Dreyfus, G., Falourd, S., Hoffmann, G., Minster, B., Nouet,
1352 J., Barnola, J. M., Chappellaz, J., Fischer, H., Gallet, J. C., Johnsen, S., Leuenberger, M., Loulergue, L.,
1353 Luethi, D., Oerter, H., Parrenin, F., Raisbeck, G., Raynaud, D., Schilt, A., Schwander, J., Selmo, E.,
1354 Souchez, R., Spahni, R., Stauffer, B., Steffensen, J. P., Stenni, B., Stocker, T. F., Tison, J. L., Werner, M.,
1355 and Wolff, E. W.: Orbital and millennial Antarctic climate variability over the past 800,000 years,
1356 *Science*, 317, 793–796, <https://doi.org/10.1126/science.1141038>, 2007.
- 1357 Kallel, N., Duplessy, J.-C., Labeyrie, L., Fontugne, M., Paterne, M., and Montacer, M.: Mediterranean
1358 pluvial periods and sapropel formation over the last 200 000 years, *Palaeogeography*,
1359 *Palaeoclimatology*, *Palaeoecology*, 157, 45–58, [https://doi.org/10.1016/S0031-0182\(99\)00149-2](https://doi.org/10.1016/S0031-0182(99)00149-2),
1360 2000.

- 1361 Kelly, M., Edwards, R., Cheng, H., Yuan, D., Cai, Y., Zhang, M., Lin, Y., and An, Z.: High resolution
 1362 characterization of the Asian Monsoon between 146,000 and 99,000 years B.P. from Dongge Cave,
 1363 China and global correlation of events surrounding Termination II, *Palaeogeography,*
 1364 *Palaeoclimatology, Palaeoecology*, 236, 20–38, <https://doi.org/10.1016/j.palaeo.2005.11.042>, 2006.
- 1365 Key, A. J. M., Jarić, I., and Roberts, D. L.: Modelling the end of the Acheulean at global and continental
 1366 levels suggests widespread persistence into the Middle Palaeolithic, *Humanit Soc Sci Commun*, 8, 55,
 1367 <https://doi.org/10.1057/s41599-021-00735-8>, 2021.
- 1368 Koltai, G., Spötl, C., Shen, C.-C., Wu, C.-C., Rao, Z., Palcsu, L., Kele, S., Surányi, G., and Bárányi-Kevei, I.:
 1369 A penultimate glacial climate record from southern Hungary, *Journal of Quaternary Science*, 32, 946–
 1370 956, <https://doi.org/10.1002/jqs.2968>, 2017.
- 1371 Koutsodendris, A., Dakos, V., Fletcher, W. J., Knipping, M., Kotthoff, U., Milner, A. M., Müller, U. C.,
 1372 Kaboth-Bahr, S., Kern, O. A., Kolb, L., Vakhrameeva, P., Wulf, S., Christanis, K., Schmiedl, G., and Pross,
 1373 J.: Atmospheric CO₂ forcing on Mediterranean biomes during the past 500 kyrs, *Nat Commun*, 14,
 1374 1664, <https://doi.org/10.1038/s41467-023-37388-x>, 2023.
- 1375 Laskar, J., Robutel, P., Joutel, F., Gastineau, M., Correia, A. C. M., and Levrard, B.: A long-term numerical
 1376 solution for the insolation quantities of the Earth, *A&A*, 428, 261–285, <https://doi.org/10.1051/0004-6361:20041335>, 2004.
- 1378 Lewis, S., Ashton, N., and Jacobi, R.: 9 - Testing Human Presence During the Last Interglacial (MIS 5e):
 1379 A Review of the British Evidence, in: *Developments in Quaternary Sciences*, vol. 14, edited by: Ashton,
 1380 N., Lewis, S. G., and Stringer, C., Elsevier, 125–164, <https://doi.org/10.1016/B978-0-444-53597-9.00009-1>, 2011.
- 1382 Li, T.-Y., Shen, C.-C., Huang, L.-J., Jiang, X.-Y., Yang, X.-L., Mii, H.-S., Lee, S.-Y., and Lo, L.: Stalagmite-
 1383 inferred variability of the Asian summer monsoon during the penultimate glacial–interglacial period,
 1384 *Climate of the Past*, 10, 1211–1219, <https://doi.org/10.5194/cp-10-1211-2014>, 2014.
- 1385 Lionello, P., Malanotte-Rizzoli, P., Boscolo, R., Alpert, P., Artale, V., Li, L., Luterbacher, J., May, W., Trigo,
 1386 R., Tsimplis, M., Ulbrich, U., and Xoplaki, E.: The Mediterranean climate: An overview of the main
 1387 characteristics and issues, in: *Developments in Earth and Environmental Sciences*, vol. 4, edited by:
 1388 Lionello, P., Malanotte-Rizzoli, P., and Boscolo, R., Elsevier, 1–26, [https://doi.org/10.1016/S1571-9197\(06\)80003-0](https://doi.org/10.1016/S1571-9197(06)80003-0), 2006.
- 1390 Lisiecki, L. and Raymo, M.: Pliocene-Pleistocene stack of 57 globally distributed benthic 18O records.,
 1391 *Paleoceanography*, 20, <https://doi.org/10.1029/2004PA001071>, 2005.
- 1392 Lisiecki, L. E. and Stern, J. V.: Regional and global benthic $\delta^{18}\text{O}$ stacks for the last glacial cycle,
 1393 *Paleoceanography*, 31, 1368–1394, <https://doi.org/10.1002/2016PA003002>, 2016.
- 1394 Liu, J., Fang, N., Wang, F., Yang, F., and Ding, X.: Features of ice-rafted debris (IRD) at IODP site U1312
 1395 and their palaeoenvironmental implications during the last 2.6 Myr, *Palaeogeography,*
 1396 *Palaeoclimatology, Palaeoecology*, 511, 364–378, <https://doi.org/10.1016/j.palaeo.2018.09.002>,
 1397 2018.
- 1398 de Lumley, M. A.: Les restes humains fossiles de la grotte du Lazaret. Généralités, approche
 1399 démographique., in: *Les restes humains fossiles de la grotte du Lazaret, Nice, Alpes-Maritimes. Des*
 1400 *Homo erectus européens évolués en voie de néandertalisation*, CNRS Editions, 217–220, 2018.

- 1401 Macklin, M. G., Fuller, I. C., Lewin, J., Maas, G. S., Passmore, D. G., Rose, J., Woodward, J. C., Black, S.,
 1402 Hamlin, R. H. B., and Rowan, J. S.: Correlation of fluvial sequences in the Mediterranean basin over the
 1403 last 200 ka and their relationship to climate change, *Quaternary Science Reviews*, 21, 1633–1641,
 1404 [https://doi.org/10.1016/S0277-3791\(01\)00147-0](https://doi.org/10.1016/S0277-3791(01)00147-0), 2002.
- 1405 Magri, D. and Parra, I.: Late Quaternary western Mediterranean pollen records and African winds,
 1406 *Earth and Planetary Science Letters*, 200, 401–408, [https://doi.org/10.1016/S0012-821X\(02\)00619-2](https://doi.org/10.1016/S0012-821X(02)00619-2),
 1407 2002.
- 1408 Margari, V., Skinner, L. C., Tzedakis, P. C., Ganopolski, A., Vautravers, M., and Shackleton, N. J.: The
 1409 nature of millennial-scale climate variability during the past two glacial periods, *Nature Geosci*, 3, 127–
 1410 131, <https://doi.org/10.1038/ngeo740>, 2010.
- 1411 Margari, V., Skinner, L., Hodell, D., Martrat, B., Toucanne, S., Gibbard, P., Lunkka, J., and Tzedakis, C.:
 1412 Land-ocean changes on orbital and millennial time scales and the penultimate glaciation, *Geology*,
 1413 <https://doi.org/10.1130/G35070.1>, 2014.
- 1414 Martrat, B., Grimalt, J. O., Lopez-Martinez, C., Cacho, I., Sierro, F. J., Flores, J. A., Zahn, R., Canals, M.,
 1415 Curtis, J. H., and Hodell, D. A.: Abrupt Temperature Changes in the Western Mediterranean over the
 1416 Past 250,000 Years, *Science*, 306, 1762–1765, <https://doi.org/10.1126/science.1101706>, 2004.
- 1417 Martrat, B., Grimalt, J. O., Shackleton, N. J., de Abreu, L., Hutterli, M. A., and Stocker, T. F.: Four Climate
 1418 Cycles of Recurring Deep and Surface Water Destabilizations on the Iberian Margin, *Science*, 317, 502–
 1419 507, <https://doi.org/10.1126/science.1139994>, 2007.
- 1420 Martrat, B., Jimenez-Amat, P., Zahn, R., and Grimalt, J. O.: Similarities and dissimilarities between the
 1421 last two deglaciations and interglaciations in the North Atlantic region, *Quaternary Science Reviews*,
 1422 99, 122–134, <https://doi.org/10.1016/j.quascirev.2014.06.016>, 2014.
- 1423 Masson-Delmotte, V., Stenni, B., Pol, K., Braconnot, P., Cattani, O., Falourd, S., Kageyama, M., Jouzel,
 1424 J., Landais, A., Minster, B., Barnola, J. M., Chappellaz, J., Krinner, G., Johnsen, S., Röthlisberger, R.,
 1425 Hansen, J., Mikolajewicz, U., and Otto-Bliesner, B.: EPICA Dome C record of glacial and interglacial
 1426 intensities, *Quaternary Science Reviews*, 29, 113–128,
 1427 <https://doi.org/10.1016/j.quascirev.2009.09.030>, 2010.
- 1428 Mathias, C., Bourguignon, L., Brenet, M., Grégoire, S., and Moncel, M.-H.: Between new and inherited
 1429 technical behaviours: a case study from the Early Middle Palaeolithic of Southern France, *Archaeol*
 1430 *Anthropol Sci*, 12, 146, <https://doi.org/10.1007/s12520-020-01114-1>, 2020.
- 1431 Matthews, A., Affek, H. P., Ayalon, A., Vonhof, H. B., and Bar-Matthews, M.: Eastern Mediterranean
 1432 climate change deduced from the Soreq Cave fluid inclusion stable isotopes and carbonate clumped
 1433 isotopes record of the last 160 ka, *Quaternary Science Reviews*, 272, 107223,
 1434 <https://doi.org/10.1016/j.quascirev.2021.107223>, 2021.
- 1435 McCarron, A. P., Bigg, G. R., Brooks, H., Leng, M. J., Marshall, J. D., Ponomareva, V., Portnyagin, M.,
 1436 Reimer, P. J., and Rogerson, M.: Northwest Pacific ice-rafted debris at 38°N reveals episodic ice-sheet
 1437 change in late Quaternary Northeast Siberia, *Earth and Planetary Science Letters*, 553, 116650,
 1438 <https://doi.org/10.1016/j.epsl.2020.116650>, 2021.
- 1439 McManus, J. F., Oppo, D. W., and Cullen, J. L.: A 0.5-Million-Year Record of Millennial-Scale Climate
 1440 Variability in the North Atlantic, *Science*, 283, 971–975,
 1441 <https://doi.org/10.1126/science.283.5404.971>, 1999.

- 1442 Melchionna, M., Di Febbraro, M., Carotenuto, F., Rook, L., Mondanaro, A., Castiglione, S., Serio, C.,
 1443 Vero, V. A., Tesone, G., Piccolo, M., Diniz-Filho, J. A. F., and Raia, P.: Fragmentation of Neanderthals'
 1444 pre-extinction distribution by climate change, *Palaeogeography, Palaeoclimatology, Palaeoecology*,
 1445 496, 146–154, <https://doi.org/10.1016/j.palaeo.2018.01.031>, 2018.
- 1446 Menviel, L., Capron, E., Govin, A., Dutton, A., Tarasov, L., Abe-Ouchi, A., Drysdale, R. N., Gibbard, P. L.,
 1447 Gregoire, L., He, F., Ivanovic, R. F., Kageyama, M., Kawamura, K., Landais, A., Otto-Bliesner, B. L., Oyabu,
 1448 I., Tzedakis, P. C., Wolff, E., and Zhang, X.: The penultimate deglaciation: protocol for Paleoclimate
 1449 Modelling Intercomparison Project (PMIP) phase 4 transient numerical simulations between 140 and
 1450 127 ka, version 1.0, *Geoscientific Model Development*, 12, 3649–3685,
 1451 <https://doi.org/10.5194/gmd-12-3649-2019>, 2019.
- 1452 Michel, V., Shen, G., Shen, C.-C., Duval, M., Woodhead, J., Chou, Y.-M., Hu, H.-M., Wu, C.-C., Kan, Y.-C.,
 1453 Yang, H., Yu, T.-L., Gallet, S., and Valensi, P.: Datations radioisotopiques (U-Th, U-Pb) et
 1454 paléodosimétriques (ESR) des plus anciens sites préhistoriques des Alpes-Maritimes: la grotte du
 1455 Vallonnet, le site de plein air de Terra Amata et la grotte du Lazaret, in: *Bulletin du Musée*
 1456 *d'Anthropologie préhistorique de Monaco*, vol. 61, 65–80, 2022.
- 1457 Moncel, M., Vaissié, E., Marin, J., Fernandes, P., Abrunhosa, A., Hardy, B., Richard, M., Torres, C., and
 1458 Baena, J.: Early Middle Palaeolithic Occupations Dated to MIS 7 at the Abri du Maras (Ardèche,
 1459 Southeast France), *Journal of Paleolithic Archaeology*, 2025.
- 1460 Moncel, M.-H., Ashton, N., Arzarello, M., Fontana, F., Lamotte, A., Scott, B., Muttillio, B., Berruti, G.,
 1461 Nenzioni, G., Tuffreau, A., and Peretto, C.: Early Levallois core technology between Marine Isotope
 1462 Stage 12 and 9 in Western Europe, *Journal of Human Evolution*, 139, 102735,
 1463 <https://doi.org/10.1016/j.jhevol.2019.102735>, 2020.
- 1464 Moseley, G. E., Spötl, C., Cheng, H., Boch, R., Min, A., and Edwards, R. L.: Termination-II
 1465 interstadial/stadial climate change recorded in two stalagmites from the north European Alps,
 1466 *Quaternary Science Reviews*, 127, 229–239, <https://doi.org/10.1016/j.quascirev.2015.07.012>, 2015.
- 1467 Mudie, P.: Pollen distribution in recent marine sediments, eastern Canada, *Canadian Journal of Earth*
 1468 *Sciences*, 19, 729–747, <https://doi.org/10.1139/e82-062>, 2011.
- 1469 Murat, A. (Ed.): Chapitre 41: Pliocene–pleistocene occurrence of sapropels in the western
 1470 mediterranean sea and their relation to eastern mediterranean sapropels, in: *Proceedings of the*
 1471 *Ocean Drilling Program, 161 Scientific Results*, vol. 161, Ocean Drilling Program,
 1472 <https://doi.org/10.2973/odp.proc.sr.161.1999>, 1999.
- 1473 Nehme, C., Verheyden, S., Breitenbach, S. F. M., Gillikin, D. P., Verheyden, A., Cheng, H., Edwards, R.
 1474 L., Hellstrom, J., Noble, S. R., Farrant, A. R., Sahy, D., Goovaerts, T., Salem, G., and Claeys, P.: Climate
 1475 dynamics during the penultimate glacial period recorded in a speleothem from Kanaan Cave, Lebanon
 1476 (central Levant), *Quaternary Research*, 90, 10–25, <https://doi.org/10.1017/qua.2018.18>, 2018.
- 1477 Nehme, C., Kluge, T., Verheyden, S., Nader, F., Charalambidou, I., Weissbach, T., Gucel, S., Cheng, H.,
 1478 Edwards, R. L., Satterfield, L., Eiche, E., and Claeys, P.: Speleothem record from Pentadactylos cave
 1479 (Cyprus): new insights into climatic variations during MIS 6 and MIS 5 in the Eastern Mediterranean,
 1480 *Quaternary Science Reviews*, 250, 106663, <https://doi.org/10.1016/j.quascirev.2020.106663>, 2020.
- 1481 Obrochta, S. P., Crowley, T. J., Channell, J. E. T., Hodell, D. A., Baker, P. A., Seki, A., and Yokoyama, Y.:
 1482 Climate variability and ice-sheet dynamics during the last three glaciations, *Earth and Planetary Science*
 1483 *Letters*, 406, 198–212, <https://doi.org/10.1016/j.epsl.2014.09.004>, 2014.

- 1484 Ochando, J., Carrión, J. S., Blasco, R., Fernández, S., Amorós, G., Munuera, M., Sañudo, P., and
 1485 Fernández Peris, J.: Silvicolous Neanderthals in the far West: the mid-Pleistocene palaeoecological
 1486 sequence of Bolomor Cave (Valencia, Spain), *Quaternary Science Reviews*, 217, 247–267,
 1487 <https://doi.org/10.1016/j.quascirev.2019.03.015>, 2019.
- 1488 Okuda, M., Yasuda, Y., and Setoguchi, T.: Middle to Late Pleistocene vegetation history and climatic
 1489 changes at Lake Kopais, Southeast Greece, *Boreas*, 30, 73–82, <https://doi.org/10.1111/j.1502-3885.2001.tb00990.x>, 2001.
- 1491 Oppo, D. W., Keigwin, L. D., McManus, J. F., and Cullen, J. L.: Persistent suborbital climate variability in
 1492 marine isotope stage 5 and termination II, *Paleoceanography*, 16, 280–292,
 1493 <https://doi.org/10.1029/2000PA000527>, 2001.
- 1494 Oppo, D. W., McManus, J. F., and Cullen, J. L.: Evolution and demise of the Last Interglacial warmth in
 1495 the subpolar North Atlantic, *Quaternary Science Reviews*, 25, 3268–3277,
 1496 <https://doi.org/10.1016/j.quascirev.2006.07.006>, 2006.
- 1497 Ovsepyan, E. A. and Murdmaa, I. O.: Response of the bering sea to Heinrich Event 11, *Lithol Miner
 1498 Resour*, 52, 442–446, <https://doi.org/10.1134/S0024490217060062>, 2017.
- 1499 Panera, J., Torres, T., Pérez-González, A., Ortiz, J. E., Rubio-Jara, S., and Val, D. U. del: Geocronología
 1500 de la Terraza Compleja de Arganda en el valle del río Jarama (Madrid, España), *Estudios Geológicos*,
 1501 67, 495–504, <https://doi.org/10.3989/egeol.40550.204>, 2011.
- 1502 Panera, J., Rubio-Jara, S., Yravedra, J., Blain, H.-A., Sesé, C., and Pérez-González, A.: Manzanares Valley
 1503 (Madrid, Spain): A good country for Proboscideans and Neanderthals, *Quaternary International*, 326–
 1504 327, 329–343, <https://doi.org/10.1016/j.quaint.2013.09.009>, 2014.
- 1505 Penaud, A., Eynaud, F., Turon, J. L., Zaragosi, S., Malaizé, B., Toucanne, S., and Bourillet, J. F.: What
 1506 forced the collapse of European ice sheets during the last two glacial periods (150 ka B.P. and 18 ka
 1507 cal B.P.)? Palynological evidence, *Palaeogeography, Palaeoclimatology, Palaeoecology*, 281, 66–78,
 1508 <https://doi.org/10.1016/j.palaeo.2009.07.012>, 2009.
- 1509 Penaud, A., Eynaud, F., Voelker, A. H. L., and Turon, J.-L.: Palaeohydrological changes over the last 50
 1510 ky in the central Gulf of Cadiz: complex forcing mechanisms mixing multi-scale processes,
 1511 *Biogeosciences*, 13, 5357–5377, <https://doi.org/10.5194/bg-13-5357-2016>, 2016.
- 1512 Pereira, T., Cunha, P. P., Martins, A. A., Nora, D., Paixão, E., Figueiredo, O., Raposo, L., Henriques, F.,
 1513 Caninas, J., Moura, D., and Bridgland, D. R.: Geoarchaeology of the Cobrinhos site (Vila Velha de Ródão,
 1514 Portugal) - a record of the earliest Mousterian in western Iberia, *Journal of Archaeological Science:
 1515 Reports*, 24, 640–654, <https://doi.org/10.1016/j.jasrep.2018.11.026>, 2019.
- 1516 Pérez-Asensio, J. N., Frigola, J., Pena, L. D., Sierro, F. J., Reguera, M. I., Rodríguez-Tovar, F. J., Dorador,
 1517 J., Asioli, A., Kuhlmann, J., Huhn, K., and Cacho, I.: Changes in western Mediterranean thermohaline
 1518 circulation in association with a deglacial Organic Rich Layer formation in the Alboran Sea, *Quaternary
 1519 Science Reviews*, 228, 106075, <https://doi.org/10.1016/j.quascirev.2019.106075>, 2020.
- 1520 Peyrégne, S., Slon, V., Mafessoni, F., de Filippo, C., Hajdinjak, M., Nagel, S., Nickel, B., Essel, E., Le Cabec,
 1521 A., Wehrberger, K., Conard, N. J., Kind, C. J., Posth, C., Krause, J., Abrams, G., Bonjean, D., Di Modica,
 1522 K., Toussaint, M., Kelso, J., Meyer, M., Pääbo, S., and Prüfer, K.: Nuclear DNA from two early
 1523 Neandertals reveals 80,000 years of genetic continuity in Europe, *Science Advances*, 5, eaaw5873,
 1524 <https://doi.org/10.1126/sciadv.aaw5873>, 2019.

- 1525 Pini, R., Ravazzi, C., and Donegana, M.: Pollen stratigraphy, vegetation and climate history of the last
1526 215 ka in the Azzano Decimo core (plain of Friuli, north-eastern Italy), *Quaternary Science Reviews*,
1527 28, 1268–1290, <https://doi.org/10.1016/j.quascirev.2008.12.017>, 2009.
- 1528 Prasad, A. M., Iverson, L. R., and Liaw, A.: Newer Classification and Regression Tree Techniques:
1529 Bagging and Random Forests for Ecological Prediction, *Ecosystems*, 9, 181–199,
1530 <https://doi.org/10.1007/s10021-005-0054-1>, 2006.
- 1531 Quézel, P.: *Réflexions sur l'évolution de la flore et de la végétation au Maghreb Méditerranéen*, Ibis
1532 Press., Paris, 117 pp., 2000.
- 1533 Raia, P., Mondanaro, A., Melchionna, M., Di Febbraro, M., Diniz-Filho, J. A., Rangel, T., Holden, P.,
1534 Carotenuto, F., Edwards, N., Lima-Ribeiro, M., Profico, A., Maiorano, L., Castiglione, S., Serio, C., and
1535 Rook, L.: Past Extinctions of Homo Species Coincided with Increased Vulnerability to Climatic Change,
1536 *One Earth*, 3, 480–490, <https://doi.org/10.1016/j.oneear.2020.09.007>, 2020.
- 1537 Railsback, L. B., Gibbard, P. L., Head, M. J., Voarintsoa, N. R. G., and Toucanne, S.: An optimized scheme
1538 of lettered marine isotope substages for the last 1.0 million years, and the climatostratigraphic nature
1539 of isotope stages and substages, *Quaternary Science Reviews*, 111, 94–106,
1540 <https://doi.org/10.1016/j.quascirev.2015.01.012>, 2015.
- 1541 Rasmussen, S. O., Bigler, M., Blockley, S. P., Blunier, T., Buchardt, S. L., Clausen, H. B., Cvijanovic, I.,
1542 Dahl-Jensen, D., Johnsen, S. J., Fischer, H., Gkinis, V., Guillevic, M., Hoek, W. Z., Lowe, J. J., Pedro, J. B.,
1543 Popp, T., Seierstad, I. K., Steffensen, J. P., Svensson, A. M., Vallenga, P., Vinther, B. M., Walker, M. J.
1544 C., Wheatley, J. J., and Winstrup, M.: A stratigraphic framework for abrupt climatic changes during the
1545 Last Glacial period based on three synchronized Greenland ice-core records: refining and extending
1546 the INTIMATE event stratigraphy, *Quaternary Science Reviews*, 106, 14–28,
1547 <https://doi.org/10.1016/j.quascirev.2014.09.007>, 2014.
- 1548 Rasmussen, T. L., Oppo, D. W., Thomsen, E., and Lehman, S. J.: Deep sea records from the southeast
1549 Labrador Sea: Ocean circulation changes and ice-rafting events during the last 160,000 years,
1550 *Paleoceanography*, 18, <https://doi.org/10.1029/2001PA000736>, 2003.
- 1551 Regattieri, E., Zanchetta, G., Drysdale, R. N., Isola, I., Hellstrom, J. C., and Roncioni, A.: A continuous
1552 stable isotope record from the penultimate glacial maximum to the Last Interglacial (159–121 ka) from
1553 Tana Che Urla Cave (Apuan Alps, central Italy), *Quaternary Research*, 82, 450, 2014.
- 1554 Renault, L., Oguz, T., Pascual, A., Vizoso, G., and Tintore, J.: Surface circulation in the Alborán Sea
1555 (western Mediterranean) inferred from remotely sensed data, *J. Geophys. Res.*, 117, 2011JC007659,
1556 <https://doi.org/10.1029/2011JC007659>, 2012.
- 1557 Rios-Garaizar, J.: Early Middle Palaeolithic occupations at Ventalaperra cave (Cantabrian Region,
1558 Northern Iberian Peninsula), *Journal of Lithic Studies*, 3, <https://doi.org/10.2218/jls.v3i1.1287>, 2016.
- 1559 Robles, M., Peyron, O., Ménot, G., Elisabetta, B., Wulf, S., Appelt, O., Blache, M., Vannièrè, B., Dugerdil,
1560 L., Paura, B., Ansanay-Alex, S., Cromartie, A., Charlet, L., Guedron, S., de Beaulieu, Jacques-L., and
1561 Joannin, S.: Climate changes during the Late Glacial in southern Europe: new insights based on pollen
1562 and brGDGTs of Lake Matese in Italy, 19, 493–515, <https://doi.org/10.5194/cp-19-493-2023>, 2023.
- 1563 Rogerson, M., Cacho, I., Jimenez-Espejo, F., Reguera, M. I., Sierro, F. J., Martinez-Ruiz, F., Frigola, J.,
1564 and Canals, M.: A dynamic explanation for the origin of the western Mediterranean organic-rich layers,
1565 *Geochemistry, Geophysics, Geosystems*, 9, <https://doi.org/10.1029/2007GC001936>, 2008.

- 1566 Rohling, E. J., Marino, G., and Grant, K. M.: Mediterranean climate and oceanography, and the periodic
1567 development of anoxic events (sapropels), *Earth-Science Reviews*, 143, 62–97,
1568 <https://doi.org/10.1016/j.earscirev.2015.01.008>, 2015.
- 1569 Rohling, E. J., Hibbert, F. D., Williams, F. H., Grant, K. M., Marino, G., Foster, G. L., Hennekam, R., de
1570 Lange, G. J., Roberts, A. P., Yu, J., Webster, J. M., and Yokoyama, Y.: Differences between the last two
1571 glacial maxima and implications for ice-sheet, $\delta^{18}\text{O}$, and sea-level reconstructions, *Quaternary Science*
1572 *Reviews*, 176, 1–28, <https://doi.org/10.1016/j.quascirev.2017.09.009>, 2017.
- 1573 Rojo, J., Orlandi, F., Pérez-Badia, R., Aguilera, F., Ben Dhiab, A., Bouziane, H., Díaz de la Guardia, C.,
1574 Galán, C., Gutiérrez-Bustillo, A. M., Moreno-Grau, S., Msallem, M., Trigo, M. M., and Fornaciari, M.:
1575 Modeling olive pollen intensity in the Mediterranean region through analysis of emission sources,
1576 *Science of The Total Environment*, 551–552, 73–82, <https://doi.org/10.1016/j.scitotenv.2016.01.193>,
1577 2016.
- 1578 Roucoux, K. H., de Abreu, L., Shackleton, N. J., and Tzedakis, P. C.: The response of NW Iberian
1579 vegetation to North Atlantic climate oscillations during the last 65kyr, *Quaternary Science Reviews*, 24,
1580 1637–1653, <https://doi.org/10.1016/j.quascirev.2004.08.022>, 2005.
- 1581 Roucoux, K. H., Tzedakis, P. C., Lawson, I. T., and Margari, V.: Vegetation history of the penultimate
1582 glacial period (Marine isotope stage 6) at Ioannina, north-west Greece, *Journal of Quaternary Science*,
1583 26, 616–626, <https://doi.org/10.1002/jqs.1483>, 2011.
- 1584 Rousseau, D.-D., Antoine, P., Boers, N., Lagroix, F., Ghil, M., Lomax, J., Fuchs, M., Debret, M., Christine,
1585 H., Moine, O., Gauthier, C., Jordanova, D., and Jordanova, N.: Dansgaard-Oeschger-like events of the
1586 penultimate climate cycle: the loess point of view, *Climate of the Past*, 16, 713–727,
1587 <https://doi.org/10.5194/cp-16-713-2020>, 2020.
- 1588 Rubio-Jara, S. and Panera, J.: Unravelling an essential archive for the European Pleistocene. The human
1589 occupation in the Manzanares valley (Madrid, Spain) throughout nearly 800,000 years, *Quaternary*
1590 *International*, 520, 5–22, <https://doi.org/10.1016/j.quaint.2018.08.007>, 2019.
- 1591 Rubio-Jara, S., Panera, J., Rodríguez-de-Tembleque, J., Santonja, M., and Pérez-González, A.: Large
1592 flake Acheulean in the middle of Tagus basin (Spain): Middle stretch of the river Tagus valley and lower
1593 stretches of the rivers Jarama and Manzanares valleys, *Quaternary International*, 411, 349–366,
1594 <https://doi.org/10.1016/j.quaint.2015.12.023>, 2016.
- 1595 Ruddiman, W. F.: Late Quaternary deposition of ice-rafted sand in the subpolar North Atlantic (lat 40°
1596 to 65°N), *Geol Soc America Bull*, 88, 1813, [https://doi.org/10.1130/0016-7606\(1977\)88<1813:LQDOIS>2.0.CO;2](https://doi.org/10.1130/0016-7606(1977)88<1813:LQDOIS>2.0.CO;2), 1977.
- 1598 Sadori, L., Koutsodendris, A., Panagiotopoulos, K., Masi, A., Bertini, A., Combourieu-Nebout, N.,
1599 Francke, A., Kouli, K., Joannin, S., Mercuri, A. M., Peyron, O., Torri, P., Wagner, B., Zanchetta, G.,
1600 Sinopoli, G., and Donders, T. H.: Pollen-based paleoenvironmental and paleoclimatic change at Lake
1601 Ohrid (south-eastern Europe) during the past 500 ka, *Biogeosciences*, 13, 1423–1437,
1602 <https://doi.org/10.5194/bg-13-1423-2016>, 2016.
- 1603 Salonen, J. S., Korpela, M., Williams, J. W., and Luoto, M.: Machine-learning based reconstructions of
1604 primary and secondary climate variables from North American and European fossil pollen data, *Sci*
1605 *Rep*, 9, 15805, <https://doi.org/10.1038/s41598-019-52293-4>, 2019.
- 1606 Sánchez Goñi, M.: The climatic and environmental context of the Late Pleistocene, in: *Updating*
1607 *Neanderthals. Understanding Behavioural Complexity in the Late Middle Palaeolithic.*

- 1608 Elsevier/Academic Press, London, 165–169, <https://doi.org/10.1016/B978-0-12-823498-3.00012-1>,
1609 2022.
- 1610 Sánchez Goñi, M. F.: Millennial-scale variability during the last glacial in vegetation records from
1611 Europe, *Quaternary Science Reviews*, 2010.
- 1612 Sánchez Goñi, M. S., I, C., J, T., J, G., F, S., J, P., J, G., and N, S.: Synchronicity between marine and
1613 terrestrial responses to millennial scale climatic variability during the last glacial period in the
1614 Mediterranean region, *Climate Dynamics*, 19, 95, 2002.
- 1615 Sánchez-Laulhé, J. M., Jansa, A., and Jiménez, C.: Alboran Sea Area Climate and Weather, in: *Alboran
1616 Sea - Ecosystems and Marine Resources*, edited by: Báez, J. C., Vázquez, J.-T., Camiñas, J. A., and
1617 Malouli Idrissi, M., Springer International Publishing, Cham, 31–83, [https://doi.org/10.1007/978-3-
1618 030-65516-7_3](https://doi.org/10.1007/978-3-030-65516-7_3), 2021.
- 1619 Sánchez-Yustos, P.: *El paleolítico antiguo en la cuenca del Duero. Instrumentos teóricos para la
1620 construcción de un modelo interpretativo de arqueología económica*, 2009.
- 1621 Sánchez-Yustos, P. and Díez-Martín, F.: Dancing to the rhythms of the Pleistocene? Early Middle
1622 Paleolithic population dynamics in NW Iberia (Duero Basin and Cantabrian Region), *Quaternary Science
1623 Reviews*, 121, <https://doi.org/10.1016/j.quascirev.2015.05.005>, 2015.
- 1624 Santonja, M., Pérez-González, A., Panera, J., Rubio-Jara, S., and Méndez-Quintas, E.: The coexistence
1625 of Acheulean and Ancient Middle Palaeolithic techno-complexes in the Middle Pleistocene of the
1626 Iberian Peninsula, *Quaternary International*, 411, 367–377,
1627 <https://doi.org/10.1016/j.quaint.2015.04.056>, 2016.
- 1628 Santonja, M., Pérez-González, A., Baena, J., Panera, J., Méndez-Quintas, E., Uribe-larrea, D., Demuro,
1629 M., Arnold, L., Abrunhosa, A., and Rubio-Jara, S.: The Acheulean of the Upper Guadiana River Basin
1630 (Central Spain). Morphostratigraphic Context and Chronology, *Front. Earth Sci.*, 10,
1631 <https://doi.org/10.3389/feart.2022.912007>, 2022.
- 1632 Sassoon, D., Lebreton, V., Combourieu-Nebout, N., Peyron, O., and Moncel, M.-H.:
1633 Palaeoenvironmental changes in the southwestern Mediterranean (ODP site 976, Alboran sea) during
1634 the MIS 12/11 transition and the MIS 11 interglacial and implications for hominin populations,
1635 *Quaternary Science Reviews*, 304, 108010, <https://doi.org/10.1016/j.quascirev.2023.108010>, 2023.
- 1636 Sassoon, D., Combourieu-Nebout, N., Peyron, O., Bertini, A., Toti, F., Lebreton, V., and Moncel, M.-H.:
1637 Pollen-based climatic reconstructions for the interglacial analogues of MIS 1 (MIS 19, 11, and 5) in the
1638 southwestern Mediterranean: insights from ODP Site 976, *Clim. Past*, 21, 489–515,
1639 <https://doi.org/10.5194/cp-21-489-2025>, 2025.
- 1640 Savannah, M., Eelco, R., Timme, D., Katharine, G., Jörg, K., Gianluca, M., Francesca, S., Francesca, C.,
1641 Caterina, M., Anna, S., and Alessandra, N.: The “glacial” sapropel S6 (172 ka; MIS 6): A multiproxy
1642 approach to solve a Mediterranean “cold case,” *Palaeogeography, Palaeoclimatology, Palaeoecology*,
1643 650, 112384, <https://doi.org/10.1016/j.palaeo.2024.112384>, 2024.
- 1644 Scott, B.: *Becoming Neanderthals: the earlier British middle palaeolithic*, Oxbow books, Oxford, 2011.
- 1645 Shackleton, N. J.: Oxygen isotopes, ice volume and sea level, *Quaternary Science Reviews*, 6, 183–190,
1646 [https://doi.org/10.1016/0277-3791\(87\)90003-5](https://doi.org/10.1016/0277-3791(87)90003-5), 1987.

- 1647 Shackleton, N. J., Hall, M. A., and Vincent, E.: Phase relationships between millennial-scale events
1648 64,000–24,000 years ago, *Paleoceanography*, 15, 565–569, <https://doi.org/10.1029/2000PA000513>,
1649 2000.
- 1650 Shackleton, N. J., Sánchez-Goñi, M. F., Pailler, D., and Lancelot, Y.: Marine Isotope Substage 5e and the
1651 Eemian Interglacial, *Global and Planetary Change*, 36, 151–155, [https://doi.org/10.1016/S0921-8181\(02\)00181-9](https://doi.org/10.1016/S0921-8181(02)00181-9), 2003.
- 1653 Shackleton, N. J., Fairbanks, R. G., Chiu, T., and Parrenin, F.: Absolute calibration of the Greenland time
1654 scale: implications for Antarctic time scales and for $\Delta 14C$, *Quaternary Science Reviews*, 23, 1513–1522,
1655 <https://doi.org/10.1016/j.quascirev.2004.03.006>, 2004.
- 1656 Shaw, A., Bates, M., Conneller, C., Gamble, C., Julien, M.-A., McNabb, J., Pope, M., and Scott, B.: The
1657 archaeology of persistent places: the Palaeolithic case of La Cotte de St Brelade, Jersey, *Antiquity*, 90,
1658 1437–1453, <https://doi.org/10.15184/aqy.2016.212>, 2016.
- 1659 Shin, J., Nehrbass-Ahles, C., Grilli, R., Chowdhry Beeman, J., Parrenin, F., Teste, G., Landais, A.,
1660 Schmidely, L., Silva, L., Schmitt, J., Bereiter, B., Stocker, T. F., Fischer, H., and Chappellaz, J.: Millennial-
1661 scale atmospheric CO₂ variations during the Marine Isotope Stage 6 period (190–135 ka),
1662 *Climate of the Past*, 16, 2203–2219, <https://doi.org/10.5194/cp-16-2203-2020>, 2020.
- 1663 Sierra, F. J. and Andersen, N.: An exceptional record of millennial-scale climate variability in the
1664 southern Iberian Margin during MIS 6: Impact on the formation of sapropel S6, *Quaternary Science*
1665 *Reviews*, 286, 107527, <https://doi.org/10.1016/j.quascirev.2022.107527>, 2022.
- 1666 Sierra, F. J., Hodell, D. A., Andersen, N., Azibeiro, L. A., Jimenez-Espejo, F. J., Bahr, A., Flores, J. A., Ausin,
1667 B., Rogerson, M., Lozano-Luz, R., Lebreiro, S. M., and Hernandez-Molina, F. J.: Mediterranean Overflow
1668 Over the Last 250 kyr: Freshwater Forcing From the Tropics to the Ice Sheets, *Paleoceanography and*
1669 *Paleoclimatology*, 35, e2020PA003931, <https://doi.org/10.1029/2020PA003931>, 2020.
- 1670 Silva, P. G., López-Recio, M., Tapias, F., Roquero, E., Morín, J., Rus, I., Carrasco-García, P., Giner-Robles,
1671 J. L., Rodríguez-Pascua, M. A., and Pérez-López, R.: Stratigraphy of the Arriaga Palaeolithic sites.
1672 Implications for the geomorphological evolution recorded by thickened fluvial sequences within the
1673 Manzanares River valley (Madrid Neogene Basin, Central Spain), *Geomorphology*, 196, 138–161,
1674 <https://doi.org/10.1016/j.geomorph.2012.10.019>, 2013.
- 1675 Sinopoli, G., Peyron, O., Masi, A., Holtvoeth, J., Francke, A., Wagner, B., and Sadori, L.: Pollen-based
1676 temperature and precipitation changes in the Ohrid Basin (western Balkans) between 160 and 70 ka,
1677 *Climate of the Past*, 15, 53–71, <https://doi.org/10.5194/cp-15-53-2019>, 2019.
- 1678 Skinner, L. C. and Shackleton, N. J.: Deconstructing Terminations I and II: revisiting the glacioeustatic
1679 paradigm based on deep-water temperature estimates, *Quaternary Science Reviews*, 25, 3312–3321,
1680 <https://doi.org/10.1016/j.quascirev.2006.07.005>, 2006.
- 1681 Stocker, T. F.: The Seesaw Effect, *Science*, 282, 61–62, <https://doi.org/10.1126/science.282.5386.61>,
1682 1998.
- 1683 Sumner, G., Homar, V., and Ramis, C.: Precipitation seasonality in eastern and southern coastal Spain,
1684 *Intl Journal of Climatology*, 21, 219–247, <https://doi.org/10.1002/joc.600>, 2001.
- 1685 Svendsen, J. I., Alexanderson, H., Astakhov, V. I., Demidov, I., Dowdeswell, J. A., Funder, S., Gataullin,
1686 V., Henriksen, M., Hjort, C., Houmark-Nielsen, M., Hubberten, H. W., Ingólfsson, Ó., Jakobsson, M.,
1687 Kjær, K. H., Larsen, E., Lokrantz, H., Lunkka, J. P., Lyså, A., Mangerud, J., Matiouchkov, A., Murray, A.,

- 1688 Möller, P., Niessen, F., Nikolskaya, O., Polyak, L., Saarnisto, M., Siegert, C., Siegert, M. J., Spielhagen, R.
1689 F., and Stein, R.: Late Quaternary ice sheet history of northern Eurasia, *Quaternary Science Reviews*,
1690 23, 1229–1271, <https://doi.org/10.1016/j.quascirev.2003.12.008>, 2004.
- 1691 Terradillos-Bernal, M., Demuro, M., Arnold, L. J., Jordá-Pardo, J. F., Clemente-Conte, I., Benito-Calvo,
1692 A., and Díez Fernández-Lomana, J. C.: San Quirce (Palencia, Spain): new chronologies for the Lower to
1693 Middle Palaeolithic transition of south-west Europe, *Journal of Quaternary Science*, 38, 21–37,
1694 <https://doi.org/10.1002/jqs.3460>, 2023.
- 1695 Thabet, A. A., Maas, A. E., Lawson, G. L., and Tarrant, A. M.: Life cycle and early development of the
1696 thecosomatous pteropod *Limacina retroversa* in the Gulf of Maine, including the effect of elevated
1697 CO₂ levels, *Mar Biol*, 162, 2235–2249, <https://doi.org/10.1007/s00227-015-2754-1>, 2015.
- 1698 Torres, C., Tapias, F., Demuro, M., Arnold, L., Arriolabengoa, M., Pérez, S., and Preysler, J.: The
1699 Acheulian site of Cantera Vieja (Madrid, Spain) and the Lower to Middle Palaeolithic transition in
1700 central Spain, <https://doi.org/10.21203/rs.3.rs-4195503/v1>, 2024.
- 1701 Toucanne, S., Zaragosi, S., Bourillet, J. F., Cremer, M., Eynaud, F., Van Vliet-Lanoë, B., Penaud, A.,
1702 Fontanier, C., Turon, J. L., Cortijo, E., and Gibbard, P. L.: Timing of massive ‘Fleuve Manche’ discharges
1703 over the last 350 kyr: insights into the European ice-sheet oscillations and the European drainage
1704 network from MIS 10 to 2, *Quaternary Science Reviews*, 28, 1238–1256,
1705 <https://doi.org/10.1016/j.quascirev.2009.01.006>, 2009.
- 1706 Tzedakis, P. C.: Long-term tree populations in northwest Greece through multiple Quaternary climatic
1707 cycles, *Nature*, 364, 437–440, <https://doi.org/10.1038/364437a0>, 1993.
- 1708 Tzedakis, P. C.: Towards an understanding of the response of southern European vegetation to orbital
1709 and suborbital climate variability, *Quaternary Science Reviews*, 24, 1585–1599,
1710 <https://doi.org/10.1016/j.quascirev.2004.11.012>, 2005.
- 1711 Tzedakis, P. C., Frogley, M. R., Lawson, I. T., Preece, R. C., Cacho, I., and de Abreu, L.: Ecological
1712 thresholds and patterns of millennial-scale climate variability: The response of vegetation in Greece
1713 during the last glacial period, *Geology*, 32, 109, <https://doi.org/10.1130/G20118.1>, 2004.
- 1714 Tzedakis, P. C., Hooghiemstra, H., and Pälike, H.: The last 1.35 million years at Tenaghi Philippon:
1715 revised chronostratigraphy and long-term vegetation trends, *Quaternary Science Reviews*, 25, 3416–
1716 3430, <https://doi.org/10.1016/j.quascirev.2006.09.002>, 2006.
- 1717 Tzedakis, P. C., Drysdale, R. N., Margari, V., Skinner, L. C., Menviel, L., Rhodes, R. H., Taschetto, A. S.,
1718 Hodell, D. A., Crowhurst, S. J., Hellstrom, J. C., Fallick, A. E., Grimalt, J. O., McManus, J. F., Martrat, B.,
1719 Mokeddem, Z., Parrenin, F., Regattieri, E., Roe, K., and Zanchetta, G.: Enhanced climate instability in
1720 the North Atlantic and southern Europe during the Last Interglacial, *Nat Commun*, 9, 4235,
1721 <https://doi.org/10.1038/s41467-018-06683-3>, 2018.
- 1722 Valensi, P., Aouraghe, H., Bailon, S., Cauche, D., Combier, J., Desclaux, E., Gagnepain, J., Gaillard, C.,
1723 Khatib, S., Lumley, H., Moigne, A.-M., Moncel, M.-H., and Notter, O.: Les peuplements préhistoriques
1724 dans le sud-est de la France à la fin du Pléistocène moyen : 400 - 120 000 ans. *Terra Amata*, Orgnac 3,
1725 Baume Bonne, Lazaret. Cadre géochronologique et biostratigraphique, paléoenvironnements et
1726 évolution culturelle des derniers anténéandertaliens., 2005.
- 1727 Valensi, P., Michel, V., El Guennouni, K., and Liouville, M.: New data on human behavior from a 160,000
1728 year old Acheulean occupation level at Lazaret cave, south-east France: An archaeozoological
1729 approach, *Quaternary International*, 316, <https://doi.org/10.1016/j.quaint.2013.10.034>, 2013.

- 1730 Vernot, B., Zavala, E., Gómez-Olivencia, A., Jacobs, Z., Slon, V., Mafessoni, F., Romagné, F., Pearson, A.,
 1731 Petr, M., Sala, N., Pablos, A., Aranburu, A., Bermúdez de Castro, J.-M., Carbonell, E., Li, B., Krajcarz, M.,
 1732 Krivosshapkin, A., Kolobova, K., Kozlikin, M., and Meyer, M.: Unearthing Neanderthal population history
 1733 using nuclear and mitochondrial DNA from cave sediments, *Science*, 372, eabf1667,
 1734 <https://doi.org/10.1126/science.abf1667>, 2021.
- 1735 Vidal-Matutano, P., Blasco, R., Sañudo, P., and Fernández Peris, J.: The Anthropogenic Use of Firewood
 1736 During the European Middle Pleistocene: Charcoal Evidence from Levels XIII and XI of Bolomor Cave,
 1737 Eastern Iberia (230–160 ka), *Environmental Archaeology*, 24, 269–284,
 1738 <https://doi.org/10.1080/14614103.2017.1406026>, 2019.
- 1739 Voelker, A. H. L. and de Abreu, L.: A Review of Abrupt Climate Change Events in the Northeastern
 1740 Atlantic Ocean (Iberian Margin): Latitudinal, Longitudinal, and Vertical Gradients, in: Abrupt Climate
 1741 Change: Mechanisms, Patterns, and Impacts, American Geophysical Union (AGU), 15–37,
 1742 <https://doi.org/10.1029/2010GM001021>, 2011.
- 1743 Wagner, B., Vogel, H., Francke, A., Friedrich, T., Donders, T., Lacey, J. H., Leng, M. J., Regattieri, E.,
 1744 Sadori, L., Wilke, T., Zanchetta, G., Albrecht, C., Bertini, A., Combourieu-Nebout, N., Cvetkoska, A.,
 1745 Giaccio, B., Grazhdani, A., Hauffe, T., Holtvoeth, J., Joannin, S., Jovanovska, E., Just, J., Kouli, K., Kousis,
 1746 I., Koutsodendris, A., Krastel, S., Lagos, M., Leicher, N., Levkov, Z., Lindhorst, K., Masi, A., Melles, M.,
 1747 Mercuri, A. M., Nomade, S., Nowaczyk, N., Panagiotopoulos, K., Peyron, O., Reed, J. M., Sagnotti, L.,
 1748 Sinopoli, G., Stelbrink, B., Sulpizio, R., Timmermann, A., Tofilovska, S., Torri, P., Wagner-Cremer, F.,
 1749 Wonik, T., and Zhang, X.: Mediterranean winter rainfall in phase with African monsoons during the
 1750 past 1.36 million years, *Nature*, 573, 256–260, <https://doi.org/10.1038/s41586-019-1529-0>, 2019.
- 1751 Wainer, K., Genty, D., Blamart, D., Daëron, M., Bar-Matthews, M., Vonhof, H., Dublyansky, Y., Pons-
 1752 Branchu, E., Thomas, L., Calsteren, P., Quinif, Y., and Caillon, N.: Speleothem record of the last 180 ka
 1753 in Villars cave (SW France): Investigation of a large δ 18O shift between MIS6 and MIS5, *Quaternary*
 1754 *Science Reviews - QUATERNARY SCI REV*, 30, 130–146,
 1755 <https://doi.org/10.1016/j.quascirev.2010.07.004>, 2011.
- 1756 Wainer, K., Genty, D., Blamart, D., Bar-Matthews, M., Quinif, Y., and Plagnes, V.: Millennial climatic
 1757 instability during penultimate glacial period recorded in a south-western France speleothem,
 1758 *Palaeogeography, Palaeoclimatology, Palaeoecology*, 376, 122–131,
 1759 <https://doi.org/10.1016/j.palaeo.2013.02.026>, 2013.
- 1760 Wang, Q., Wang, Y., Shao, Q., Liang, Y., Zhang, Z., and Kong, X.: Millennial-scale Asian monsoon
 1761 variability during the late Marine Isotope Stage 6 from Hulu Cave, China, *Quat. res.*, 90, 394–405,
 1762 <https://doi.org/10.1017/qua.2018.75>, 2018.
- 1763 Wang, Y. J., Cheng, H., Edwards, R. L., An, Z. S., Wu, J. Y., Shen, C. C., and Dorale, J. A.: A high-resolution
 1764 absolute-dated late Pleistocene Monsoon record from Hulu Cave, China, *Science*, 294, 2345–2348,
 1765 <https://doi.org/10.1126/science.1064618>, 2001.
- 1766 Wenzel, S.: Neanderthal presence and behaviour in central and Northwestern Europe during MIS 5e,
 1767 in: *Developments in Quaternary Sciences*, 173–193, <https://doi.org/10.13140/2.1.2747.7442>, 2007.
- 1768 White, M. J. and Pettitt, P. B.: The British Late Middle Palaeolithic: An Interpretative Synthesis of
 1769 Neanderthal Occupation at the Northwestern Edge of the Pleistocene World, *Journal of World*
 1770 *Prehistory*, 24, <https://doi.org/10.1007/s10963-011-9043-9>, 2011.
- 1771 Willis, K. J., Bennett, K. D., Walker, D., Gamble, C., Davies, W., Pettitt, P., and Richards, M.: Climate
 1772 change and evolving human diversity in Europe during the last glacial, *Philosophical Transactions of*

- 1773 the Royal Society of London. Series B: Biological Sciences, 359, 243–254,
1774 <https://doi.org/10.1098/rstb.2003.1396>, 2004.
- 1775 Wilson, G. P., Frogley, M. R., Hughes, P. D., Roucoux, K. H., Margari, V., Jones, T. D., Leng, M. J., and
1776 Tzedakis, P. C.: Persistent millennial-scale climate variability in Southern Europe during Marine Isotope
1777 Stage 6, *Quaternary Science Advances*, 3, 100016, <https://doi.org/10.1016/j.qsa.2020.100016>, 2021.
- 1778 Xue, G., Cai, Y., Ma, L., Cheng, X., Cheng, H., Edwards, R. L., Li, D., and Tan, L.: A new speleothem record
1779 of the penultimate deglacial: Insights into spatial variability and centennial-scale instabilities of East
1780 Asian monsoon, *Quaternary Science Reviews*, 210, 113–124,
1781 <https://doi.org/10.1016/j.quascirev.2019.02.023>, 2019.
- 1782 Yaworsky, P. M., Nielsen, E. S., and Nielsen, T. K.: The Neanderthal niche space of Western Eurasia 145
1783 ka to 30 ka ago, *Sci Rep*, 14, 7788, <https://doi.org/10.1038/s41598-024-57490-4>, 2024.
- 1784 Yravedra, J., Rubio-Jara, S., Panera, J., Made, J. van der, and Pérez-González, A.: Neanderthal diet in
1785 fluvial environments at the end of the Middle Pleistocene/early Late Pleistocene of PRERESA site in the
1786 Manzanares Valley (Madrid, Spain), *Quaternary International*, 520, 72–83,
1787 <https://doi.org/10.1016/j.quaint.2018.01.030>, 2019.
- 1788 Zahn, R., Comas, M. C., and Klaus, A. (Eds.): Proceedings of the Ocean Drilling Program, 161 Scientific
1789 Results, *Ocean Drilling Program*, <https://doi.org/10.2973/odp.proc.sr.161.1999>, 1999.
- 1790 Zhang, J., Zolitschka, B., Hogrefe, I., Tsukamoto, S., Binot, F., and Frechen, M.: High-resolution
1791 luminescence-dated sediment record for the last two glacial-interglacial cycles from Rodderberg,
1792 Germany, *Quaternary Geochronology*, 82, 101535, <https://doi.org/10.1016/j.quageo.2024.101535>,
1793 2024.
- 1794 Ziegler, M., Tuenter, E., and Lourens, L.: The precession phase of the boreal summer monsoon as
1795 viewed from the eastern Mediterranean (ODP Site 968), *Quaternary Science Reviews*, 29,
1796 <https://doi.org/10.1016/j.quascirev.2010.03.011>, 2010.
- 1797